Mechanistic Study of DNA Delivery from Self-Assembled Nanolayered Films

by

Sheryl Wang

B.S. Bioengineering
University of Illinois at Urbana-Champaign, 2015

Submitted to the Department of Biological Engineering
in partial fulfillment of the requirements for the degree of

Doctor of Philosophy

at the

MASSACHUSETTS INSTITUTE OF TECHNOLOGY

February 2022

Author _____
Department of Biological Engineering
January 13, 2022

Certified by _____
Paula T. Hammond
Institute Professor
David H. Koch Professor
Head, Department of Chemical Engineering
Thesis Supervisor

Certified by _____
Alan J. Grodzinsky
Professor of Biological, Mechanical, and Electrical Engineering
Thesis Supervisor

Accepted by _____
Katharina Ribbeck
Professor of Biological Engineering
Graduate Program Chair

Mechanistic Study of DNA Delivery from Self-Assembled Nanolayered Films

by

Sheryl Wang

Submitted to the Department of Biological Engineering
on January 13, 2022, in partial fulfillment of the
requirements for the degree of
Doctor of Philosophy in Biological Engineering

Abstract

The delivery of nucleic acids to modulate gene expression levels can enable highly specific and durable therapeutic effects. Formulation to protect nucleic acid cargoes and direct them to target tissues is critical to the success of these promising therapies. Delivery of nucleic acids, such as plasmid DNA, must overcome both systemic and local cellular barriers. Surface-mediated gene delivery bypasses systemic trafficking obstacles by localizing DNA release within the cellular microenvironment. Local delivery has several advantages including increased efficacy at the target site and reduced off-target effects. Layer-by-layer (LbL) self-assembly is a promising method to incorporate DNA in nanolayered thin film surface coatings for controlled, localized release. Although the potential for DNA delivery via layer-by-layer films has been reported, details in the mechanism or factors influencing the success of delivery have not been explored.

In this thesis, we designed LbL-assembled DNA multilayer films for localized gene delivery. We present a mechanistic investigation of factors impacting *in vitro* DNA transfection efficacy. Using pre-formed DNA-polymer complexes as a model system, we identified relative polymer to DNA content in polyplexes as a key driver of effective transfection. We then explored the impact of LbL assembly parameters on DNA multilayer film composition and release kinetics, and how these subsequently influence transfection efficacy *in vitro*. Finally, we characterized the film releasate to elucidate how cells interact with DNA multilayer films. Rapid release of DNA complexed with polymer was found to enable the greatest transfection efficiency. The findings described here will contribute to rational design of more effective LbL films for DNA delivery.

Thesis Co-Advisor: Paula T. Hammond, Institute Professor, David H. Koch Professor, and Department Head of Chemical Engineering, MIT

Thesis Co-Advisor: Alan J. Grodzinsky, Professor of Biological, Mechanical, and Electrical Engineering, MIT

This doctoral thesis has been examined by the following committee:

Douglas A. Lauffenburger, PhD
Chairman, Thesis Committee
Ford Foundation Professor of Biological Engineering, Chemical Engineering, and Biology, MIT

Paula T. Hammond, PhD
Thesis Co-Supervisor
Institute Professor, David H. Koch Professor, Department Head of Chemical Engineering, MIT

Alan J. Grodzinsky, ScD
Thesis Co-Supervisor
Professor of Biological, Mechanical, and Electrical Engineering, MIT

Myron Spector, PhD
Member, Thesis Committee
Professor of Orthopedic Surgery, Harvard Medical School

For my beloved family
My parents Chien-Ping Wang and Tong-Jen Fu
My sister Michelle Wang

Acknowledgements

I am grateful to the family, friends, collaborators, and mentors who have been on this graduate journey at MIT with me.

Thank you to my thesis advisor, Professor Paula Hammond for providing invaluable advice and support through scientific and personal challenges during my graduate studies. I feel so fortunate to have been a member of your lab and to have had the opportunity to learn from your scientific rigor, perseverance, and kindness.

I would also like to thank my co-advisor Professor Al Grodzinsky and my thesis committee, Professors Doug Lauffenburger and Myron Spector for their insight and positive encouragement. You encouraged me to think about fundamental principles underlying my experimental observations as well as broader implications.

I'd like to thank past and present labmates in the Hammond Group—I feel so lucky to have been a part of a supportive, fun, and brilliant group of scientists. Prof. Jouha Min, Dr. Brett Geiger, Dr. Santi Correa, and Prof. Jiahe Li, thank you for your early mentorship as I got started in the lab. Prof. John Martin and Dr. MayLin Howard, our weekly bone repair group meetings were invaluable, thank you for your friendship and advice. Adam Berger, Prof. Natalie Boehnke, and Colin Bittner, thank you for the science chats that helped me define my research "story" and for your support through challenging times. Dr. Apoorv Shanker, Dr. Joelle Straehla, and Dr. Sarah Almofty, thank you for your intellectual insights and career advice. Thank you to all my lab friends and collaborators, I've enjoyed getting to know and work with each of you: Dr. Tony Barberio, Dr. Yanpu He, Elad Deiss-Yehiely, Dr. Jonathan Chou, Brandon Johnston, Dr. Sean Smith, Ivan Pires, Dr. Stephanie Kong, Andrew Pickering, Dr. Tamara Dacoba, Dr. Nick Lamson, Dr. Simone Douglas-Green, Celestine Hong, Namita Nabar, Victoria Gomerdinger, Justin Kaskow, Sweta Roy, Dr. Sasan Jalili, Dr. Archana Boopathy, Prof. Erik Dreaden, Prof. Chibueze Amanchukwu, Dr. Connie Wu, and Dr. Wade Wang. Thank you to Liz Galoyan and Xiuyun Hou for all you do helping our lab run smoothly. To the remarkable undergraduate

researchers I mentored – Alli Abolarin and Kendreze Holland, thank you for your contributions to this work and your curiosity and enthusiasm.

So many people at MIT enhanced my graduate experience and made my research possible. Dr. Maureen Rezendes, thank you for listening with patience and empathy and for helping me reframe my thinking. I'd also like to thank members of MIT DCM and the KI Swanson Biotechnology Core, whose support and advice made this thesis possible: Dr. Jenny Haupt (DCM); Glenn Paradis and Michele Griffin (Flow Cytometry); Dr. Abigail Lytton-Jean, David Mankus, Peggy Bisher, and Dr. Dong Soo Yun (Nanomaterials); Dr. Jaime Cheah and Christian Soule (HTS); Milton Cornwall-Brady (PMIT); Jeff Wyckoff (Microscopy). Outside of MIT, I want to thank Dr. Simon Young, who performed the rabbit mandibular defect surgeries. Thank you for your help and your mentorship. I would also like to Drs. Michael Ho and Delia Danila at the UT Health Science Center at Houston for C-arm and microCT imaging advice as well as members of the Young Lab: Lindsay Wilson, Sabita Thapa, and Neeraja Dharmaraj.

To the friends who have supported me along the way: Amy Kim, Dr. Divya Tankasala, Dr. Mallika Modak, Anuradha Nandyala, thank you for your steadfast long-distance friendship. Isaac DuPree, Dr. Manu Kumar, Dr. Jacob Guggenheim, thank you for being my first friends in Cambridge and for the food adventures. Thank you Dr. Lauren Milling, Dr. Beth Pearce, Dr. Sarah Bening, Dr. Amanda Chen, Dr. Noor Momin, Meelim Lee, Dr. Miguel Reyes and everyone in BE. Thank you to friends outside of BE: Dr. Julia Zhao, Wencong Wang, Dr. Deb Ehrlich, Dr. Cameron McBride, Alex Ji, PPSM 2015, and the MIT Badminton Club. Special thank you to Julia for being the best friend, roommate, and PGSA co-president. I am so grateful for your loyal companionship, generosity, and humor.

This thesis is dedicated to my parents Chien-Ping Wang and Dr. Tong-Jen Fu, and my sister Michelle Wang. You are the inspiration and motivation for my graduate school journey and everything I do. Thank you for all you've given and for believing in me. Thank you for your endless support and love.

Table of Contents

List of Figures

Figure 4.1 Fluorescence imaging of HEK 293T cells treated with PBAE/DNA films for 48 hours (A) Blue indicates Hoechst nuclear stain, green is Rab5, Rab7, LAMP1 endolysosomal staining, and red is Cy5-DNA. White arrows indicate bright spots of DNA aggregated within endosomal compartments (B) Film-treated cells with green endolysosomal staining omitted for clarity.

Figure 4.2 DNA film treatment of HEK 293T cells with external transfection reagent (A) Schematic of cell treatment (B) Transfection efficiency of PBAE/DNA film and with added PEI or X2 in the culture medium.

Figure 4.3 PBAE/DNA and PEI-PBAE/DNA film in vitro transfection (A) Schematic of film architectures (B) Transfection efficiency of PEI-PBAE/DNA film and with added X2 (C) Side-by-side comparison of PBAE/DNA and PEI-PBAE/DNA film transfection (D) Proposed DNA release mechanisms in cell culture conditions.

Figure 4.4 Fluorescent microscope images of HEK 293T cells treated with pGFP nanolayer films Red dashed lines mark the edges of the film-coated silicon chip placed film-side down on the cell monolayer.

Figure 4.5 Agarose gel electrophoresis of DNA polyplexes and LbL film releasate (A) PBAE polyplexes and PBAE/DNA film releasate (B) PEI polyplexes and PEI-PBAE/DNA film releasate.
Figure 4.6 PicoGreen dye exclusion assay of LbL film released DNA (A) Calibration curve of fluorescence vs. PBAE:DNA mass ratio (B) pmaxGFP polymer binding curves sigmoidal curve fit, dotted lines indicate 95% confidence bands (C) Fraction of bound DNA in releasate from PBAE and PEI-PBAE films, polycation dipping concentration indicated in x-axis labels (D) Polymer:DNA mass ratio of film releasate with N/P ratio conversion indicated.

Figure 4.7 Size and charge characterization of LbL film releaseate (A) Average zeta potential measured in 0.1x PBS (B) Average diameter of film released particles measured in 1x PBS using DLS.

Figure 4.8 SEM imaging of DNA multilayer film disassembly and cell interaction (A)-(C) (PrS/SPS) (PBAE/DNA) films (D)-(F) PEI-PBAE/DNA films. A, D show films after 24 hr incubation in serum-containing media; B shows a cell grown on the film and E shows a cell after film application above the cell. C, F are higher magnification frames of B, E. Red arrows mark internalized particles and yellow arrows indicate particles adsorbed to cell surface or filopodia. Insets zoom in on filopodia-associated particles. Scale bar is 2 μm.

Figure 4.9 PBAE/DNA film release and transfection are enhanced by destabilizing baselayers (A) Cumulative DNA release over time as a fraction of total DNA loading (B) Transfection efficiency of PBAE/DNA films with and without baselayers. **$p<0.01$, ****$p<0.0001$ by one-way ANOVA with Tukey's multiple comparisons test.

Figure 4.10 (PEI/DNA) films with low or high molecular weight PBAE baselayers exhibit different release behaviors and DNA transfection efficiencies (A) Schematic of (PBAE/PAA) (PEI/DNA) film architecture (B) Cumulative DNA release over time as a fraction of total DNA loading (C) Ratio of BPEI-Atto647N to DNA-Cy3 over time (D) Transfection efficiency of fast and slow release PEI/DNA films.

Figure 5.1 Cumulative and fractional BMP-2 plasmid DNA release kinetics from DNA film-coated PCL implants (A) Cumulative DNA released in PBS at 37°C (B) DNA release profile normalized to total DNA content.

Figure 5.2 CT analysis of bone growth at 6 weeks for BMP-2 plasmid DNA and protein treatment groups (A) Isosurfaces of CT scans generated in 3DSlicer, L = lateral, M = medial face of the mandible (B) Quantification of bone volume (C) Bone volume divided by total defect volume (D) Calculated bone mineral density. *p<0.05, **p<0.01, ****p<0.0001 by ANOVA with Tukey multiple comparisons test.

Figure 5.3 12 week microCT analysis of explants from control and BMP-2 protein treatment groups (A) Isosurfaces of CT scans generated in MicroView (B) Bone volume divided by total defect volume (D) Calculated bone mineral density. *p<0.05, **p<0.01 by ANOVA with Tukey multiple comparisons test.

Figure 5.4 microCT cross-sections from control and BMP-2 protein treatment groups Yellow triangles mark bone formations within the defect volume. Red arrow/box correspond to sagittal cross-section; blue arrow/box correspond to coronal cross-sectional view (A) Empty defect (B) uncoated (blank) scaffold (C) BMP-2 protein-coated scaffold.

Figure 5.5 microCT analysis of explanted mandibles at 12 weeks (A) Isosurfaces of CT scans generated in MicroView. Red circles indicate ROI used for quantification. L = lateral, M = medial face of the mandible (B) Quantification of bone volume (C) Bone volume divided by total defect volume (D) Calculated bone mineral density.

Chapter 1. Introduction

1.1 Motivation

Nucleic acid therapies involve transport of therapeutic genes transiently or permanently into target tissues or cells to replace or modulate expression of abnormal genes. Delivery of exogenous nucleic acids to counter defective genes or to supplement beneficial pathways is attractive for enabling highly specific and durable therapeutic effects in inherited and acquired diseases.[1] Advances in understanding of molecular mechanisms of genetic diseases in the last few decades have accelerated development of enabling technologies for gene therapy. Nucleic acid therapies are promising approaches to treat a large number of genetically mediated diseases that cannot be addressed via current protein and peptide therapies.[1]

1.2 Clinical landscape of nucleic acid therapy

As of 2017, more than 2600 gene therapy clinical trials have been conducted globally to evaluate various gene-based drugs, primarily designed for treatment of cancers, monogenic diseases, cardiovascular diseases, infection, neurological diseases, and ocular diseases.[2] In particular, standout successes in gene therapy have occurred in cancer immunotherapy, specifically, using CAR T-cells to target tumor-associated cell surface antigens.[3] CAR T-cell therapy involves *ex vivo* retroviral transduction of patient-derived T-cells to express chimeric antigen receptors. Currently approved therapies include Kymriah, Yescarta, and Tecartus for treating leukemia or lymphoma.[4] Strimvelis, another clinically-approved *ex vivo* gene therapy, retrovirally transduces patient-derived CD34+ hematopoietic stem cells to express human adenosine deaminase (ADA) enzyme, treating ADA-severe combined immunodeficiency.[5]

Several *in vivo* nucleic acid therapies have also been approved, focusing on delivery of antisense oligonucleotides (ASOs) to induce exon skipping or short interfering RNAs (siRNAs) for RNA interference.[2,6] Success of these therapies is a result of years of research on methods to improve nucleic acid stability and potency *in vivo*. Nusinersen (Spinraza), approved in 2016, is a chemically-modified ASO for treating spinal muscular atrophy.[7] In addition to chemical

modifications, stabilizing and protective carriers have been developed for nucleic acids, leading to clinical approval of siRNA lipid nanoparticle patisiran (Onpattro) for treatment of hereditary transthyretin-mediated amyloidosis-associated polyneuropathy.[8,9] Nucleic acids may also be conjugated to targeting ligands to improve specificity of the therapy, for example in givosiran (Givlaari), an N-acetylgalactosamine (GalNAc) conjugated siRNA therapy for liver cell-targeted treatment of acute hepatic porphyria.[10] Most recently, approved COVID-19 vaccines containing chemically modified mRNA and lipid nanoparticles with polyethylene glycol (PEG) highlight advances due to decades of research in nucleic acid delivery.[11,12]

Development of viral and non-viral technologies have achieved some clinical success, however, low efficacy of nucleic acid delivery to cells and concerns about off-target effects remain critical barriers to clinical translation. Formulation to protect nucleic acids and direct them to their intended target cells is critical to the translatability of promising therapies. While inspiration can be drawn from delivery strategies applied to protein and small molecule delivery, approaches need to be adapted for nucleic acid specific applications.

1.3 DNA-based therapeutics

Plasmids are long, double-stranded, circular DNA constructs containing transgenes that encode target proteins. Plasmid DNA may be administered to stimulate in situ expression of proteins for disease treatment or as DNA vaccines, delivering genes encoding antigens.[4] Upon cellular internalization, plasmids utilize the cell's DNA transcription and translation machinery to synthesize the encoded therapeutic protein.[13] Gene therapy uses plasmid DNA to introduce transgenes into cells that are inherently unable to produce the encoded protein. Exogenous delivery of plasmid DNA requires cellular internalization, trafficking through the cytoplasm while avoiding nucleases, and nuclear entry.[14–19]

Most recombinant plasmids contain an antibiotic resistance gene regulated by a prokaryotic promoter, a prokaryotic origin of replication for plasmid propagation, and an expression cassette.[13] In order to achieve optimal transfection, the expression cassette typically

contains promoter and enhancer sequences to regulate gene expression, splicing and polyadenylation sites for correct mRNA processing after transcription, and elements that enhance mRNA processing and nuclear entry.[13,20,21] Promoters are crucial in initiation of transcription. In addition, strong tissue- or tumor-specific promoters can be incorporated to engineer higher expression efficiency into the plasmid DNA.[21] Plasmids are simple to construct and easily produced in large quantities. In addition, because genomic integration is highly inefficient, plasmids are associated with negligible risk of oncogenesis.[13] Plasmids can incorporate large segments of genomic DNA and are easy to handle, remaining stable at 4°C or room temperature for extended periods of time. The primary limitation of plasmid-based nucleic acid therapy is poor gene transfer efficiency on its own, spurring development of DNA carriers to improve delivery.

1.4 Delivery challenges for nucleic acids

The biggest challenge for the nucleic acid therapeutic approach is that the delivery system must bypass numerous biological and physical barriers while retaining biological activity. Systemic delivery barriers include nucleases that degrade DNA, serum proteins that mark DNA for removal by immune cells, and extracellular matrices that physically block DNA from target cells.[22] Local delivery barriers include the cell membrane, endolysosomal compartments, nucleases, and nucleic acid decomplexation to allow for transcription and translation.[23,24] Free nucleic acids are unstable in physiological conditions and are rapidly degraded by endogenous nucleases. The half-life of free plasmid DNA can be as short as 10 min in the blood circulation[25] or 1-2 hours in the cytoplasm.[19,26] Successful delivery relies on a gene carrier that protects and carries the nucleic acid through extracellular and intracellular obstacles.

Drug delivery systems are designed to modulate the interaction of nucleic acid drugs with their microenvironment.[1,4,23] Controlled release delivery systems shift pharmacokinetic parameters, including biodistribution, half-life, and total drug exposure over time.[22,27,28] Sustained release systems in particular are designed to maintain therapeutic drug

concentrations for extended periods of time.[29] There are a number of approaches that have been taken to improve efficacy of these delivery systems in the midst of the challenging microenvironment.

Tissue targeting strategies may be used to alter the biodistribution of nucleic acid therapeutics. These strategies include direct conjugation to sugars[27,30,31] or antibodies or modification of the nucleic acid carrier (lipid or polymer-based).[30] For example, patisiran (Onpattro), the first FDA approved siRNA therapy, utilizes an optimized lipid nanoparticle formulation to improve trafficking to the liver and uptake by target cells.[9] Givosiran (Givlaari) is a GalNAc-siRNA conjugate where the conjugate exhibits enhanced uptake in liver hepatocytes, which are the target cell.[10]

In addition to modulating the biodistribution of nucleic acid therapeutics, physiochemical stability of the nucleic acid and its carrier is crucial to successful delivery. Nucleic acid base modifications, polyadenylation, and capping are strategies to improve resistance to nuclease degradation,[7,13] reduce immunogenicity,[32,33] and improve interactions with target cells.[34,35] Fomivirsen (Vitravene) is an ASO that incorporates a phosphorothioate backbone modification to improve stability against nucleases.[36] Nusinersen (Spinraza), FDA-approved to treat spinal muscular atrophy, incorporates a 2'-*O*-methoxyethyl phosphorothioate modification to improve stability and reduce immunogenicity.[37] Moderna and Pfizer COVID vaccines incorporate N1-methylpseudouridine in their mRNA sequences to reduce immunogenicity and increase vaccine effectiveness.[38]

When it comes to localized delivery of nucleic acids, various strategies have been applied to encourage sufficient cellular uptake to generate a response. The cell plasma membrane is impermeable to large, hydrophilic, charged molecules such as plasmid DNA (pDNA) or a polyplex, so most enter via endocytosis.[39] The plasma membrane also has high content of anionic glycosylated membrane proteins that affect the uptake and intracellular trafficking of delivery complexes.[40–43] RNAs need to be cytosolically located to be active and

DNA needs to traffic to the nucleus. After endocytosis however, without a method to leave the endosome, nucleic acids typically end up in lysosomes and are degraded without having their intended biological effect.[44] A common approach to bypassing this barrier is inclusion of ionizable cationic lipids or polymers in the nucleic acid carrier.[24,45] These ionizable molecules typically are neutral at pH 7 and upon encountering the acidic environment of the endosome become protonated and mediate endosomal escape by buffering the endosomal pH.[46–48] Lipids can intercalate into the endosomal membrane and allow exit of the nucleic acid.[49,50] Cell-penetrating peptides have also been used to destabilize the endosomal membrane.[51–53] Nuclear import is relatively inefficient and most pDNA in the cytoplasm never reaches the nucleus.[54] Nuclear localization sequences can be included to promote nuclear delivery of DNA.[18,55,56] pDNA trafficking across the nuclear membrane occurs through nuclear pores or passive import during mitosis when the nuclear envelope temporarily breaks and reforms.[57]

1.5 DNA delivery approaches

The DNA delivery process encompasses several subprocesses to achieve effective delivery: DNA condensation, systemic circulation, targeted delivery to specific cells, cellular uptake, endosomal release, nuclear transport, unpacking of polyplexes, transcription, and translation. DNA delivery carriers or systems have been developed to help DNA progress more rapidly and efficiently through these steps. Gene delivery systems are broadly classified into recombinant viral systems and non-viral physicochemical approaches. Viral vectors are the leading DNA carrier of choice in currently approved gene therapies, due to their very high efficiency in delivering DNA, however they can trigger undesirable immune responses.[24]

Advantages of non-viral approaches include ease of chemical characterization, simplicity and reproducibility of production, larger nucleic acid packaging capacity, and reduced biosafety concerns.[58,59] Many DNA nanocarriers have been developed in the last two decades including polymeric,[31,60–63] silica-based,[64] gold nanoparticle-based,[65,66] 2D nanomaterial based,[67] and lipid-based systems.[4,11,12,68–70] However, only a few non-viral systems are currently in clinical trials,

including DOTAP-cholesterol,[71] polyethyleneimine (PEI),[72] poly(ethylene glycol)-polyethyleneimine-cholesterol (PEG-PEI-cholesterol),[73,74] and PEI-mannose-dextrose.[75] Non-viral approaches are relatively inefficient compared to recombinant viral systems and often have transient effects. Improved nucleic acid stability and potency, lipid and polymer delivery technology are rapidly advancing the field of non-viral gene delivery.[2]

Lipid-based DNA carriers

Cationic liposomes and lipid nucleic acid complexes enable encapsulation of negatively charged nucleic acids and surface charge enables cellular uptake and endosomal escape.[39,70,75,76] Toxicity, complement activation, and poor distribution[77,78] led to iterations of lipid nanoparticles incorporating PEGylated, neutral, and ionizable cationic lipids, which helped reduce toxicity and biodistribution while retaining the endosomal escape capability.[6,69,75] Cationic liposomes self-assemble and condense DNA via electrostatic interactions resulting in lipoplexes with net positive charge, which can associate with negatively charged cell surfaces. Lipoplexes enter cells via endocytosis and escape from endosomes by interacting with anionic phospholipids in the endosomal membrane, which destabilizes the endosome and allows dissociation and release of the nucleic acid from the lipoplex.[79–81]

Polymer-based DNA carriers

Polymer vectors have low immunogenicity and modular chemistry.[63] Polymeric vectors electrostatically complex nucleic acids in polyplexes, which protect the genes and mediate cellular entry. To protect from nuclease digestion and aid cellular uptake, anionic DNA is condensed with its carrier into a compact nanoparticle polyplex <200 nm diameter. DNA condensation is a reversible coil-to-globule transition driven by electrostatic interactions between the cationic carrier and DNA's negatively charged phosphate groups.[82,83] Synthetic DNA carriers balance transfection efficiency and cytotoxicity because higher surface charge correlates with stronger DNA binding, cell uptake, and transfection but also is associated with higher cytotoxicity.[54] Higher polyplex charge enables increased membrane disruption to enable

plasma membrane uptake and endosomal release, but too much membrane disruption is toxic to cells. Excess positive charge can also cause DNA carriers to associate with anionic biomolecules in the bloodstream,[28,84] marking the DNA for removal by immune cells.

Polyplexes composed of various natural, synthetic, and designer polymers have been investigated extensively for intracellular delivery of nucleic acids.[61,63,85,86] Cationic polymers, including polyethyleneimine (PEI), poly amino acids (poly-L-arginine (PLR) and poly-L-lysine (PLK)), poly(β-amino esters) (PBAEs), polycyclodextrins, and dendrimers, vary extensively in chemistry and structure.[63,87–89] They are also attractive DNA carriers due to their tunable chemistry and amenability to functionalization. Polymeric vectors may be modified with targeting moieties for receptor-mediated endocytosis.[31,63,90,91] Additionally, polymers with high density of secondary and tertiary amines, facilitate the escape of delivered genes from endosomes into the cytosol, after which DNA can continue to move toward the nucleus.[19,44,92] Polymeric vectors avoid many issues associated with viral delivery, including mutagenesis due to genome insertion and potential immunogenicity, despite their reduced gene-transfer efficiency as compared to viral vectors.[62,63,93] Intracellular trafficking of polymeric vectors remains a significant barrier to effective gene transfer and is a very active area of study. Compared with lipoplexes, polyplexes have been shown to condense DNA more efficiently and protect against enzymatic nucleic acid degradation.[42,94]

Cell uptake of DNA polyplexes has been shown to be affected by size, shape, surface charge, surface ligands, hydrophobic effect, concentration of polyplexes at the cell surface, and cell cycle stage.[16,24,61,94–99] These factors determine uptake efficiency and what pathways polyplexes follow once internalized. Endocytic pathways are the primary uptake mechanism for non-viral DNA delivery systems. During endosomal maturation, the endosomal pH drops from 7 to 5 and eventually these late stage endosomes fuse with lysosomes, in which lower pH and hydrolytic enzymes rapidly degrade DNA.[13,23,39] Several mechanisms for polyplex escape from endolysosomal pathways have been proposed, including the “proton sponge effect,” pore

formation in the endosomal membrane, and fusion with the endosomal membrane.[23,24,100] The "proton sponge effect" is a hypothesized mechanism that suggests unprotonated amines can "absorb" protons that are pumped into the endosome by ATPase during endosome maturation.[101] This "proton-sponge" activity inhibits endosomal acidification, leading to greater influx of protons and passive influx of chloride ions and water to maintain electroneutrality.[101,102] Ion influx causes osmotic swelling and polymer swelling leading to endosomal membrane rupture and release of polyplexes in to the cytosol.[102,103] Live cell imaging studies have illustrated that protonation of PEI polyplexes causes close interaction with the inner endosomal membrane, where a localized osmotic or mechanical effect causes transient membrane destabilization rather than total rupture.[104] Several alternative mechanisms have been proposed, but the proton-sponge hypothesis is currently the most widely referenced.[46,47,105–108]

Polyplexes inside endosomal vesicles may be actively transported toward the nucleus along microtubules by dynein or kinesin[109,110]. Once polyplexes are in the cytosol, they cannot utilize microtubule-mediated transport and migration through the cytoplasm by passive diffusion is very slow[58]. As a result, endosomal release ideally should occur in a perinuclear region where polyplexes have the best chance to enter the nucleus[26,44,111]. Nuclear import remains a rate-limiting step in polymer-mediated DNA delivery. Cohen et al. (2009) used quantitative PCR to estimate that only 1-5% of the initial DNA dose is delivered to the nucleus by PEI polyplexes.[112] In actively dividing cells, PEI polyplexes can enter the nucleus passively during mitosis.[16,113] In non-dividing cells, DNA must enter through the nuclear pore complex (NPC), which has an inner diameter of 9 nm and only allows passive diffusion of macromolecules < 40 kDa or DNA shorter than 350 base pairs.[14,44,114] Free or complexed DNA nuclear import is likely mediated by nuclear localization signal (NLS) sequences.[115] and some groups have attempted to mimic this activity by coupling NLS sequences to PEI or the DNA backbone with mixed success of nuclear translocation.[18,56,116–119]

Whether intact polyplexes enter the nucleus or free DNA adsorbed to cytosolic proteins enter the nucleus is unclear. Some studies indicate that polycation and DNA dissociate prior to nuclear entry[120–122] while others report intact polyplexes in the nucleus.[112,113,123–129] Dissociation of DNA and polycations may occur due to competitive binding and ion exchange with cytosolic polyanions, RNA, nuclear polyamines, or chromatin.[130–132] Released DNA likely does not remain free and rapidly associates with other polycations in the cytosol.[133] Additionally, strongly binding polycations like PEI may not dissociate from DNA in the nucleus, impacting transcriptional activity. Acellular transcription and nuclear microinjection studies have shown that the extent of DNA condensation impacted accessibility of DNA to transcription machinery.[112,127,132,134–136]

1.5.1 Polycations for DNA delivery

Polyethyleneimine (PEI) is one of the most potent cationic polymeric vectors both in branched (BPEI) and linear (LPEI) form. BPEI contains primary, secondary, and tertiary amines and possesses very high cationic charge density. The average pKa of BPEI is between 7.4 and 8.5 and BPEI buffers over a broad pH range.[137,138] Only 19% of BPEI amino nitrogens are protonated at physiological pH and 25% can be protonated during endosome acidification, enabling endosomal escape by proton sponge effect.[139] Optimal PEI molecular weight for DNA delivery is between 5 and 25 kDa because molecular weight strongly correlates with DNA binding strength and transfection efficiency, but also cytotoxicity.[140,141] PEI is non-degradable and can cause significant dose-dependent toxicity. Toxicity observed with PEI polyplex treatment has been attributed to free PEI polymer that exists in solution to stabilize the polyplexes.[136] LPEI has been described as a more efficient delivery vector than BPEI[142–144] because the lower binding stability of LPEI polyplexes may enable more facile intracellular release of DNA, enabling better transfection efficiency. Crosslinking low molecular weight LPEI with biodegradable bonds,[145] grafting PEG,[74,146–148] and shielding polyplexes with hyaluronic acid[149] have been used to reduce cytotoxicity of PEI.

Poly(beta-amino esters) (PBAEs) are biodegradable cationic polymers synthesized by conjugate addition of amines to diacrylates.[88,150,151] Vast libraries of unique PBAE structures, including branched structures, have been developed for delivery of various nucleic acids including DNA, mRNA, and short interfering RNA (siRNA).[88,150–155] PBAEs are non-cytotoxic and biodegradable via hydrolysis of ester groups into non-toxic byproducts. Top-performing polymers for DNA polyplex formation are linear PBAEs (~10 kDa) synthesized at amine:acrylate ratio of 1.2:1 with hydroxyl side chains and primary amine end groups.[155] The amine end groups facilitate endosomal escape by similar mechanisms as PEI.[88] Optimized PBAEs have 4-8 fold higher transfection efficiency with lower toxicity as compared to 25 kDa BPEI.[155]

Polyplex structure and function depend on polymer characteristics (molecular weight, branching, charge density, hydrophobicity), ratio of cationic polymer to anionic nucleic acid, and formulation method (concentration, speed and sequence of mixing, buffer components, complexation time).[24,31,143,156] Modulating these factors can change particle size, surface charge, and stability to decomplexation and as a result dramatically affect gene delivery efficacy.

1.6 Surface-mediated gene delivery

To avoid systemic barriers to gene delivery, a local reservoir of therapeutic may promote sustained, spatially defined delivery of nucleic acid therapeutics. Surface-mediated gene delivery in the context of implant-mediated drug delivery bypasses certain systemic trafficking obstacles by immobilizing DNA on a surface to increase local concentration of DNA within the cellular microenvironment[97,157–159] and reduce mass transport limitations of polyplex particle delivery.[160–164] Spatial control of gene delivery is important in tissue engineering, drug-coated medical implants, and *in vitro* cellular transfection microarrays.[165] DNA can be immobilized in polyelectrolyte multilayer films or in pre-formed polyplexes adsorbed or conjugated to a substrate. Immobilized polyplexes have been shown to effectively deliver plasmid DNA to cells grown on the substrate, although less efficiently than an equal bolus dose of polyplex delivered in solution.[97,166] The mechanism of cellular uptake of DNA from gene-activated surfaces is

unknown, but could proceed via two potential mechanisms: direct internalization of complexes from the substrate surface or release of complexes before cellular uptake.

1.7 Layer-by-layer self-assembly for controlled local drug delivery

Precise, programmable release of biologically active agents may be achieved by depositing therapeutic-loaded coatings on the surface of implants using electrostatic layer-by-layer (LbL) assembly.[167] Polymeric thin films on the order of a few hundred nanometers to tens of microns are formed through alternating adsorption of cationic and anionic multivalent species (e.g., polyelectrolytes, charged molecular drugs, proteins) at ambient conditions.[168] Recent work in the Hammond Lab has demonstrated successful incorporation and controlled release of antibiotics, anti-inflammatory drugs, chemotherapeutics, protein growth factors, and nucleic acids from LbL films.[169–177] Importantly, these therapeutics remained biologically active upon release in the target site due to the gentle, aqueous conditions of LbL assembly. Multilayer films can achieve high drug loadings due to multivalent interactions among film components. Drug loading can also be tuned by changing the number of layers. Drug release rate from LbL films can be controlled by diffusion, film dissociation, or degradation of film components.[178] Sustained release of therapeutics can be achieved by increasing the film thickness, modulating film degradation rate, covalently linking therapeutic cargo to polymers, or cross-linking the film.[179–182] Films have also been designed with enzymatically degradable moieties, allowing for more environmentally responsive film dissolution and drug release. The stratified nature of LbL films combined with physical diffusion barriers have been leveraged to enable staggered delivery of various therapeutics.[183,184] For example, Min et al. (2014) used a laponite clay-polymer composite layer[176] to form a physical diffusion barrier that enabled sequential release of gentamicin followed by bone morphogenetic protein-2, an osteogenic growth factor.

1.8 Layer-by-layer self-assembly for nucleic acid delivery

Plasmid DNA is an anionic polyelectrolyte, which makes it favorable for incorporation into thin film coatings using electrostatic LbL assembly. Incorporation of plasmid DNA directly

into LbL constructs enables precise control of DNA loading simply by controlling the number of layers deposited. Furthermore, the specific cationic polymers used in LbL assembly can be selected to facilitate intracellular DNA delivery. Lynn and colleagues[185–188] built polyelectrolyte multilayers using PBAEs and plasmid DNA on various substrates, including stents and balloon catheters, and demonstrated effective therapeutic DNA delivery in vitro and in vivo. In a rat model of arterial injury and hyperplasia, a DNA film-coated balloon catheter was shown to enable local transgene expression in the arterial wall via contact-mediated DNA transfer over a relatively short 20 min application time.[189,190] Compared to tissue treated with control pDNA films, tissue treated with therapeutic plasmid films exhibited 60% reduction in intimal hyperplasia.[190] This study demonstrated the potential of LbL-assembled films to enable localized transfection of cells and production of therapeutic protein *in vivo*. The mechanism of DNA release from LbL films and how cells uptake DNA from the films is not well understood. Atomic force microscopy (AFM) measurements suggested that DNA/polymer layers arranged themselves when immersed in cell culture media to present surface-bound condensed DNA nanoparticles.[191–193] Plasmid DNA-based LbL multilayers have also been constructed using chitosan, poly(2-aminoethyl propylene phosphate), polyethyleneimine, and reducible hyperbranched poly(amido amine).[188] As films degrade, nanoscale complexes are released, as verified by electrophoresis and transmission electron microscopy (TEM),[194] and are thought to behave similarly to pre-formed DNA polyplexes.

Pre-complexed plasmids in non-viral gene delivery vectors can also be incorporated into multilayer films. The Voegel and Jessel groups have extensively characterized LbL films to deliver PEI-condensed plasmids or pyridylaminocyclodextrin-complexed plasmids to different cell lines and primary cells.[188,195] Some studies have incorporated DNA-lipoplexes in LbL films, focusing on surface adsorption or physical incorporation or lipoplexes in pre-cast films.[97,157,161,165,196,197] Yamauchi et al. (2004) used LbL assembly to form alternating layers of DNA-lipoplexes and naked plasmid DNA on self-assembled monolayers of carboxylic acid-

terminated alkanethiol.[164] These multilayers were able to transfect HEK 293 and HUVEC endothelial cells *in vitro* with EGFP at high efficiencies (and continued EGFP expression for > 9 days).[164]

Gene delivery vectors do not diffuse readily through most LbL multilayer systems. As such, selection of polyelectrolytes that enable controlled film disassembly under physiological conditions is key. Incorporation of biodegradable chitosan (CHI) and hyaluronic acid (HA) have enhanced the DNA delivery and subsequent transfection efficiency of films containing PEI-condensed vectors.[198,199] CHI was layered with HA and Lipofectamine2000 lipoplexes were adsorbed to the films. DNA lipoplexes tended to adsorb to the multilayer surface as large aggregates of varying size. Lipoplex-embedded films achieved <14% transfection efficiency in NIH3T3 fibroblasts and 20% transfection in HEK 293 cells, although toxicity was observed with increasing DNA-lipoplex dose and cell contact time.[198,200] The Lynn and Hammond groups have incorporated hydrolysable PBAE with DNA and siRNA into LbL-assembled films and demonstrated sustained DNA release over time due to polymer degradation in physiological conditions.[173,191,201–204] The studies cited above highlight promising examples of controlled, localized gene delivery enabled by LbL self-assembly of DNA-releasing films.

1.9 Scope and Outline

Although the potential of localized DNA delivery via layer-by-layer films has been reported, details in the mechanism or factors influencing success of delivery have not been extensively explored. The primary objective of this thesis was the design and mechanistic investigation of polymer multilayer film-mediated DNA delivery, in particular factors impacting *in vitro* DNA transfection efficacy and how cells interact with LbL-assembled DNA multilayer films.

Chapter 2 discusses factors affecting gene delivery efficacy, specifically plasmid DNA delivery via pre-formed polyplexes.

Chapter 3 explores the impact of LbL assembly parameters on DNA multilayer film growth, composition, and release kinetics. Optimizing solution assembly conditions and

polycation and DNA incorporation will enable rational design of DNA multilayer films for surface-mediated nucleic acid delivery.

Chapter 4 examines the composition of DNA multilayer films and their releasate, relating these characteristics to functional assays of DNA delivery efficacy. The findings described here contribute to fundamental mechanistic understanding of how LbL film composition determines nucleic acid delivery efficacy and how cells interact with DNA multilayer films *in vitro*.

Chapter 5 details data from an *in vivo* rabbit mandible defect study of DNA multilayer film-mediated transfection for in situ growth factor expression. Plasmid DNA encoding bone morphogenetic protein-2 (BMP-2), an osteoinductive growth factor, was incorporated in a LbL-assembled polymer coating on a 3D printed scaffold. The extent of bone formation in DNA scaffold-treated groups is discussed and recommendations for future *in vivo* studies are presented.

Chapter 6 summarizes conclusions from this thesis work and discusses future outlook and research directions.

1.10 References

(1) Vargason, A. M.; Anselmo, A. C.; Mitragotri, S. The Evolution of Commercial Drug Delivery Technologies. *Nat. Biomed. Eng.* **2021**, *5*, 951–967.

(2) Ginn, S. L.; Amaya, A. K.; Alexander, I. E.; Edelstein, M.; Abedi, M. R. Gene Therapy Clinical Trials Worldwide to 2017: An Update. *J. Gene Med.* **2018**, *20*, e3015.

(3) June, C. H.; O'Connor, R. S.; Kawalekar, O. U.; Ghassemi, S.; Milone, M. C. CAR T Cell Immunotherapy for Human Cancer. *Science (80-.).* **2018**, *359*, 1361–1365.

(4) Kulkarni, J. A.; Witzigmann, D.; Thomson, S. B.; Chen, S.; Leavitt, B. R.; Cullis, P. R.; van der Meel, R. The Current Landscape of Nucleic Acid Therapeutics. *Nat. Nanotechnol.* **2021**, *16*, 630–643.

(5) Aiuti, A.; Cattaneo, F.; Galimberti, S.; Benninghoff, U.; Cassani, B.; Callegaro, L.; Scaramuzza, S.; Andolfi, G.; Mirolo, M.; Brigida, I.; *et al.* Gene Therapy for Immunodeficiency Due to Adenosine Deaminase Deficiency. *N. Engl. J. Med.* **2009**, *360*, 447–458.

(6) Akinc, A.; Maier, M. A.; Manoharan, M.; Fitzgerald, K.; Jayaraman, M.; Barros, S.; Ansell, S.; Du, X.; Hope, M. J.; Madden, T. D.; *et al.* The Onpattro Story and the Clinical Translation of Nanomedicines Containing Nucleic Acid-Based Drugs. *Nat. Nanotechnol.* **2019**, *14*, 1084–1087.

(7) Khvorova, A.; Watts, J. K. The Chemical Evolution of Oligonucleotide Therapies of Clinical Utility. *Nat. Biotechnol.* **2017**, *35*, 238–248.

(8) Whitehead, K. A.; Langer, R.; Anderson, D. G. Knocking down Barriers: Advances in SiRNA Delivery. *Nat. Rev. Drug Discov.* **2009**, *8*, 129–138.

(9) Adams, D.; Gonzalez-Duarte, A.; O'Riordan, W. D.; Yang, C.-C.; Ueda, M.; Kristen, A. V.; Tournev, I.; Schmidt, H. H.; Coelho, T.; Berk, J. L.; *et al.* Patisiran, an RNAi Therapeutic, for Hereditary Transthyretin Amyloidosis. *N. Engl. J. Med.* **2018**, *379*, 11–21.

(10) Scott, L. J. Givosiran: First Approval. *Drugs* **2020**, *80*, 335–339.

(11) Polack, F. P.; Thomas, S. J.; Kitchin, N.; Absalon, J.; Gurtman, A.; Lockhart, S.; Perez, J. L.; Pérez Marc, G.; Moreira, E. D.; Zerbini, C.; *et al.* Safety and Efficacy of the BNT162b2 MRNA Covid-19 Vaccine. *N. Engl. J. Med.* **2020**, *383*, 2603–2615.

(12) Baden, L. R.; El Sahly, H. M.; Essink, B.; Kotloff, K.; Frey, S.; Novak, R.; Diemert, D.; Spector, S. A.; Rouphael, N.; Creech, C. B.; *et al.* Efficacy and Safety of the MRNA-1273 SARS-CoV-2 Vaccine. *N. Engl. J. Med.* **2021**, *384*, 403–416.

(13) Patil, S. D.; Rhodes, D. G.; Burgess, D. J. DNA-Based Therapeutics and DNA Delivery Systems: A Comprehensive Review. *AAPS J.* **2005**, *7*, 61–77.

(14) Lam, A. P.; Dean, D. A. Progress and Prospects: Nuclear Import of Nonviral Vectors. *Gene Ther.* **2010**, *17*, 439–447.

(15) Reilly, M. J.; Larsen, J. D.; Sullivan, M. O. Polyplexes Traffic through Caveolae to the Golgi and Endoplasmic Reticulum En Route to the Nucleus. *Mol. Pharm.* **2012**, *9*, 1280–1290.

(16) Brunner, S.; Fürtbauer, E.; Sauer, T.; Kursa, M.; Wagner, E. Overcoming the Nuclear Barrier: Cell Cycle Independent Nonviral Gene Transfer with Linear Polyethylenimine or Electroporation. *Mol. Ther.* **2002**, *5*, 80–86.

(17) Rejman, J.; Bragonzi, A.; Conese, M. Role of Clathrin- and Caveolae-Mediated Endocytosis in Gene Transfer Mediated by Lipo- and Polyplexes. *Mol. Ther.* **2005**, *12*, 468–474.

(18) Ross, N. L.; Sullivan, M. O. Importin-4 Regulates Gene Delivery by Enhancing Nuclear Retention and Chromatin Deposition by Polyplexes. *Mol. Pharm.* **2015**, *12*, 4488–4497.

(19) Bai, H.; Schiralli Lester, G. M.; Petishnok, L. C.; Dean, D. A.; Lester, G. M. S.; Petishnok, L. C.; Dean, D. A. Cytoplasmic Transport and Nuclear Import of Plasmid DNA. *Biosci. Rep.* **2017**, *37*, 1–17.

(20) Young, J. L.; Benoit, J. N.; Dean, D. A. Effect of a DNA Nuclear Targeting Sequence on

Gene Transfer and Expression of Plasmids in the Intact Vasculature. *Gene Ther.* **2003**, *10*, 1465–1470.
(21) Raup, A.; Jérôme, V.; Freitag, R.; Synatschke, C. V.; Müller, A. H. E. Promoter, Transgene, and Cell Line Effects in the Transfection of Mammalian Cells Using PDMAEMA-Based Nano-Stars. *Biotechnol. Reports* **2016**, *11*, 53–61.
(22) Nelson, C. E.; Duvall, C. L.; Prokop, A.; Gersbach, C. A.; Davidson, J. M. Gene Delivery into Cells and Tissues. In *Principles of Tissue Engineering*; Elsevier, 2020; pp. 519–554.
(23) Donahue, N. D.; Acar, H.; Wilhelm, S. Concepts of Nanoparticle Cellular Uptake, Intracellular Trafficking, and Kinetics in Nanomedicine. *Adv. Drug Deliv. Rev.* **2019**, *143*, 68–96.
(24) Durymanov, M.; Reineke, J. Non-Viral Delivery of Nucleic Acids: Insight into Mechanisms of Overcoming Intracellular Barriers. *Front. Pharmacol.* **2018**, *9*, 1–15.
(25) Kawabata, K.; Takakura, Y.; Hashida, M. The Fate of Plasmid DNA after Intravenous Injection in Mice: Involvement of Scavenger Receptors in Its Hepatic Uptake. *Pharm. Res.* **1995**, *12*, 825–830.
(26) Lechardeur, D.; Sohn, K. J.; Haardt, M.; Joshi, P. B.; Monck, M.; Graham, R. W.; Beatty, B.; Squire, J.; O'Brodovich, H.; Lukacs, G. L. Metabolic Instability of Plasmid DNA in the Cytosol: A Potential Barrier to Gene Transfer. *Gene Ther.* **1999**, *6*, 482–497.
(27) Kamaly, N.; Xiao, Z.; Valencia, P. M.; Radovic-Moreno, A. F.; Farokhzad, O. C. Targeted Polymeric Therapeutic Nanoparticles : Design, Development and Clinical Translation. *Chem. Soc. Rev.* **2012**, *41*, 2971–3010.
(28) Malek, A.; Merkel, O.; Fink, L.; Czubayko, F.; Kissel, T.; Aigner, A. In Vivo Pharmacokinetics, Tissue Distribution and Underlying Mechanisms of Various PEI(–PEG)/SiRNA Complexes. *Toxicol. Appl. Pharmacol.* **2009**, *236*, 97–108.
(29) Tiwari, G.; Tiwari, R.; Sriwastawa, B.; Bhati, L.; Pandey, S.; Pandey, P.; Bannerjee, S. K. Drug Delivery Systems: An Updated Review. *Int. J. Pharm. Investig.* **2012**, *2*, 2–11.
(30) Zhao, Z.; Ukidve, A.; Kim, J.; Mitragotri, S. Targeting Strategies for Tissue-Specific Drug Delivery. *Cell* **2020**, *181*, 151–167.
(31) Wagner, E. Polymers for Nucleic Acid Transfer—An Overview. In *Advances in Genetics*; 2014; Vol. 88, pp. 231–261.
(32) Majer, O.; Liu, B.; Barton, G. M. Nucleic Acid-Sensing TLRs: Trafficking and Regulation. *Curr. Opin. Immunol.* **2017**, *44*, 26–33.
(33) Qu, M.; Kim, H.-J.; Zhou, X.; Wang, C.; Jiang, X.; Zhu, J.; Xue, Y.; Tebon, P.; Sarabi, S. A.; Ahadian, S.; *et al.* Biodegradable Microneedle Patch for Transdermal Gene Delivery. *Nanoscale* **2020**, *12*, 16724–16729.
(34) Behlke, M. A. Chemical Modification of SiRNAs for In Vivo Use. *Oligonucleotides* **2008**, *18*, 305–319.
(35) Kormann, M. S. D.; Hasenpusch, G.; Aneja, M. K.; Nica, G.; Flemmer, A. W.; Herber-Jonat, S.; Huppmann, M.; Mays, L. E.; Illenyi, M.; Schams, A.; *et al.* Expression of Therapeutic Proteins after Delivery of Chemically Modified MRNA in Mice. *Nat. Biotechnol.* **2011**, *29*, 154–157.
(36) de Smet, M. D.; Meenken, C.; Van Den Horn, G. J. Fomivirsen – a Phosphorothioate Oligonucleotide for the Treatment of CMV Retinitis. *Ocul. Immunol. Inflamm.* **2009**, *7*, 189–198.
(37) Corey, D. R. Nusinersen, an Antisense Oligonucleotide Drug for Spinal Muscular Atrophy. *Nat. Neurosci.* **2017**, *20*, 497–499.
(38) Nance, K. D.; Meier, J. L. Modifications in an Emergency: The Role of N1-Methylpseudouridine in COVID-19 Vaccines. *ACS Cent. Sci.* **2021**, *7*, 748–756.
(39) Friend, D. S.; Papahadjopoulos, D.; Debs, R. J. Endocytosis and Intracellular Processing Accompanying Transfection Mediated by Cationic Liposomes. *Biochim. Biophys. Acta* **1996**, *1278*, 41–50.

(40) Ruponen, M.; Honkakoski, P.; Tammi, M.; Urtti, A. Cell-Surface Glycosaminoglycans Inhibit Cation-Mediated Gene Transfer. *J. Gene Med.* **2004**, *6*, 405–414.
(41) Nomani, A.; Hyvönen, Z.; Pulkkinen, E.; Hiekkala, M.; Ruponen, M. Intracellular Gene Delivery Is Dependent on the Type of Non-Viral Carrier and Defined by the Cell Surface Glycosaminoglycans. *J. Control. Release* **2014**, *187*, 59–65.
(42) Ruponen, M.; Ylä-Herttuala, S.; Urtti, A. Interactions of Polymeric and Liposomal Gene Delivery Systems with Extracellular Glycosaminoglycans: Physicochemical and Transfection Studies. *Biochim. Biophys. Acta* **1999**, *1415*, 331–341.
(43) Ruponen, M.; Rönkkö, S.; Honkakoski, P.; Pelkonen, J.; Tammi, M.; Urtti, A. Extracellular Glycosaminoglycans Modify Cellular Trafficking of Lipoplexes and Polyplexes. *J. Biol. Chem.* **2001**, *276*, 33875–33880.
(44) Lechardeur, D.; Verkman, A. S.; Lukacs, G. L. Intracellular Routing of Plasmid DNA during Non-Viral Gene Transfer. *Adv. Drug Deliv. Rev.* **2005**, *57*, 755–767.
(45) Semple, S. C.; Klimuk, S. K.; Harasym, T. O.; Dos Santos, N.; Ansell, S. M.; Wong, K. F.; Maurer, N.; Stark, H.; Cullis, P. R.; Hope, M. J.; *et al.* Efficient Encapsulation of Antisense Oligonucleotides in Lipid Vesicles Using Ionizable Aminolipids: Formation of Novel Small Multilamellar Vesicle Structures. *Biochim. Biophys. Acta* **2001**, *1510*, 152–166.
(46) Rehman, Z. U.; Hoekstra, D.; Zuhorn, I. S. Mechanism of Polyplex- and Lipoplex-Mediated Delivery of Nucleic Acids: Real-Time Visualization of Transient Membrane Destabilization without Endosomal Lysis. *ACS Nano* **2013**, *7*, 3767–3777.
(47) Wojnilowicz, M.; Glab, A.; Bertucci, A.; Caruso, F.; Cavalieri, F. Super-Resolution Imaging of Proton Sponge-Triggered Rupture of Endosomes and Cytosolic Release of Small Interfering RNA. *ACS Nano* **2019**, *13*, 187–202.
(48) Lallana, E.; Rios De La Rosa, J. M.; Tirella, A.; Pelliccia, M.; Gennari, A.; Stratford, I. J.; Puri, S.; Ashford, M.; Tirelli, N. Chitosan/Hyaluronic Acid Nanoparticles: Rational Design Revisited for RNA Delivery. *Mol. Pharm.* **2017**, *14*, 2422–2436.
(49) Vaidyanathan, S.; Chen, J.; Orr, B. G.; Banaszak Holl, M. M. Cationic Polymer Intercalation into the Lipid Membrane Enables Intact Polyplex DNA Escape from Endosomes for Gene Delivery. *Mol. Pharm.* **2016**, *13*, 1967–1978.
(50) Van de Vyver, T.; Bogaert, B.; De Backer, L.; Joris, F.; Guagliardo, R.; Van Hoeck, J.; Merckx, P.; Van Calenbergh, S.; Ramishetti, S.; Peer, D.; *et al.* Cationic Amphiphilic Drugs Boost the Lysosomal Escape of Small Nucleic Acid Therapeutics in a Nanocarrier-Dependent Manner. *ACS Nano* **2020**, *14*, 4774–4791.
(51) Endoh, T.; Ohtsuki, T. Cellular SiRNA Delivery Using Cell-Penetrating Peptides Modified for Endosomal Escape. *Adv. Drug Deliv. Rev.* **2009**, *61*, 704–709.
(52) Lönn, P.; Kacsinta, A. D.; Cui, X. S.; Hamil, A. S.; Kaulich, M.; Gogoi, K.; Dowdy, S. F. Enhancing Endosomal Escape for Intracellular Delivery of Macromolecular Biologic Therapeutics. *Sci. Rep.* **2016**, *6*.
(53) Lehto, T.; Ezzat, K.; Wood, M. J. A.; EL Andaloussi, S. Peptides for Nucleic Acid Delivery. *Adv. Drug Deliv. Rev.* **2016**, *106*, 172–182.
(54) Monnery, B. D. Polycation-Mediated Transfection: Mechanisms of Internalization and Intracellular Trafficking. *Biomacromolecules* **2021**, *22*, 4060–4083.
(55) Varga, C. M.; Hong, K.; Lauffenburger, D. A. Quantitative Analysis of Synthetic Gene Delivery Vector Design Properties. *Mol. Ther.* **2001**, *4*, 438–446.
(56) Tammam, S. N.; Azzazy, H. M. E.; Lamprecht, A. The Effect of Nanoparticle Size and NLS Density on Nuclear Targeting in Cancer and Normal Cells; Impaired Nuclear Import and Aberrant Nanoparticle Intracellular Trafficking in Glioma. *J. Control. Release* **2017**, *253*, 30–36.
(57) Vaughan, E. E.; DeGiulio, J. V.; Dean, D. A. Intracellular Trafficking of Plasmids for Gene Therapy: Mechanisms of Cytoplasmic Movement and Nuclear Import. *Curr. Gene Ther.* **2006**, *6*, 671–681.

(58) Nguyen, J.; Szoka, F. C. Nucleic Acid Delivery: The Missing Pieces of the Puzzle? *Acc. Chem. Res.* **2012**, *45*, 1153–1162.
(59) Gupta, A.; Andresen, J. L.; Manan, R. S.; Langer, R. Nucleic Acid Delivery for Therapeutic Applications. *Adv. Drug Deliv. Rev.* **2021**, *178*, 113834.
(60) Rinkenauer, A. C.; Schubert, S.; Traeger, A.; Schubert, U. S. The Influence of Polymer Architecture on in Vitro PDNA Transfection. *J. Mater. Chem. B* **2015**, *3*, 7477–7493.
(61) Itaka, K.; Ishii, T.; Hasegawa, Y.; Kataoka, K. Biodegradable Polyamino Acid-Based Polycations as Safe and Effective Gene Carrier Minimizing Cumulative Toxicity. *Biomaterials* **2010**, *31*, 3707–3714.
(62) Burke, P. A.; Pun, S. H.; Reineke, T. M. Advancing Polymeric Delivery Systems Amidst a Nucleic Acid Therapy Renaissance. *ACS Macro Lett.* **2013**, *2*, 928–934.
(63) Pack, D. W.; Hoffman, A. S.; Pun, S.; Stayton, P. S. Design and Development of Polymers for Gene Delivery. *Nat. Rev. Drug Discov.* **2005**, *4*, 581–593.
(64) Song, H.; Yu, M.; Lu, Y.; Gu, Z.; Yang, Y.; Zhang, M.; Fu, J.; Yu, C. Plasmid DNA Delivery: Nanotopography Matters. *J. Am. Chem. Soc.* **2017**, *139*, 18247–18254.
(65) Lackington, W. A.; Raftery, R. M.; O'Brien, F. J. In Vitro Efficacy of a Gene-Activated Nerve Guidance Conduit Incorporating Non-Viral PEI-PDNA Nanoparticles Carrying Genes Encoding for NGF, GDNF and c-Jun. *Acta Biomater.* **2018**, *75*, 115–128.
(66) Bishop, C. J.; Liu, A. L.; Lee, D. S.; Murdock, R. J.; Green, J. J. Layer-by-Layer Inorganic / Polymeric Nanoparticles for Kinetically Controlled Multigene Delivery. *J. Biomed. Mater. Res. Part A* **2015**, *104*, 707–713.
(67) Yin, F.; Gu, B.; Lin, Y.; Panwar, N.; Tjin, S. C.; Qu, J.; Lau, S. P.; Yong, K. T. Functionalized 2D Nanomaterials for Gene Delivery Applications. *Coord. Chem. Rev.* **2017**, *347*, 77–97.
(68) Kowalski, P. S.; Rudra, A.; Miao, L.; Anderson, D. G. Delivering the Messenger: Advances in Technologies for Therapeutic MRNA Delivery. *Mol. Ther.* **2019**, *27*, 710–728.
(69) Semple, S. C.; Akinc, A.; Chen, J.; Sandhu, A. P.; Mui, B. L.; Cho, C. K.; Sah, D. W. Y.; Stebbing, D.; Crosley, E. J.; Yaworski, E.; *et al.* Rational Design of Cationic Lipids for SiRNA Delivery. *Nat. Biotechnol.* **2010**, *28*, 172–176.
(70) Buck, J.; Grossen, P.; Cullis, P. R.; Huwyler, J.; Witzigmann, D. Lipid-Based DNA Therapeutics: Hallmarks of Non-Viral Gene Delivery. *ACS Nano* **2019**, *13*, 3754–3782.
(71) Lu, C.; Stewart, D. J.; Lee, J. J.; Ji, L.; Ramesh, R.; Jayachandran, G.; Nunez, M. I.; Wistuba, I. I.; Erasmus, J. J.; Hicks, M. E.; *et al.* Phase I Clinical Trial of Systemically Administered TUSC2(FUS1)-Nanoparticles Mediating Functional Gene Transfer in Humans. *PLoS One* **2012**, *7*, 1–9.
(72) Meleshko, A. N.; Petrovskaya, N. A.; Savelyeva, N.; Vashkevich, K. P.; Doronina, S. N.; Sachivko, N. V. Phase I Clinical Trial of Idiotypic DNA Vaccine Administered as a Complex with Polyethylenimine to Patients with B-Cell Lymphoma. *Hum. Vaccin. Immunother.* **2017**, *13*, 1398–1403.
(73) Thaker, P. H.; Brady, W. E.; Lankes, H. A.; Odunsi, K.; Bradley, W. H.; Moore, K. N.; Muller, C. Y.; Anwer, K.; Schilder, R. J.; Alvarez, R. D.; *et al.* A Phase I Trial of Intraperitoneal GEN-1, an IL-12 Plasmid Formulated with PEG-PEI-Cholesterol Lipopolymer, Administered with Pegylated Liposomal Doxorubicin in Patients with Recurrent or Persistent Epithelial Ovarian, Fallopian Tube or Primary Peritoneal. *Gynecol. Oncol.* **2017**, *147*, 283–290.
(74) Alvarez, R. D.; Sill, M. W.; Davidson, S. A.; Muller, C. Y.; Bender, D. P.; Debernardo, R. L.; Behbakht, K.; Huh, W. K. A Phase II Trial of Intraperitoneal EGEN-001, An IL-12 Plasmid Formulated with PEG-PEI-Cholesterol Lipopolymer in the Treatment of Persistent or Recurrent Epithelial Ovarian, Fallopian Tube or Primary Peritoneal Cancer: A Gynecologic Oncology Group Study. *Gynecol. Oncol.* **2014**, *133*, 433–438.

(75) Beg, S.; Almalki, W. H.; Khatoon, F.; Alharbi, K. S.; Alghamdi, S.; Akhter, M. H.; Khalilullah, H.; Baothman, A. A.; Hafeez, A.; Rahman, M.; *et al.* Lipid/Polymer-Based Nanocomplexes in Nucleic Acid Delivery as Cancer Vaccines. *Drug Discov. Today* **2021**, *26*, 1891–1903.
(76) Zelphati, O.; Szoka, F. C. Intracellular Distribution and Mechanism of Delivery of Oligonucleotides Mediated by Cationic Lipids. *Pharm. Res.* **1996**, *13*, 1367–1372.
(77) Filion, M. C.; Phillips, N. C. Major Limitations in the Use of Cationic Liposomes for DNA Delivery. *Int. J. Pharm.* **1998**, *162*, 159–170.
(78) Lv, Q.; Yu, A.; Xi, Y.; Li, H.; Song, Z.; Cui, J.; Cao, F.; Zhai, G. Development and Evaluation of Penciclovir-Loaded Solid Lipid Nanoparticles for Topical Delivery. *Int. J. Pharm.* **2009**, *372*, 191–198.
(79) Xu, Y.; Szoka, F. C. Mechanism of DNA Release from Cationic Liposome/DNA Complexes Used in Cell Transfection. *Biochemistry* **1996**, *35*, 5616–5623.
(80) Östman, S.; Jin, T.; Lindfors, L.; Lindquist, J.; Sunnerhagen, P.; Valadi, H.; Maugeri, M.; Angerfors, A.; Skantze, P.; Mårtensson, I.; *et al.* Linkage between Endosomal Escape of LNP-MRNA and Loading into EVs for Transport to Other Cells. *Nat. Commun.* **2019**, *10*.
(81) Gilleron, J.; Querbes, W.; Zeigerer, A.; Borodovsky, A.; Marsico, G.; Schubert, U.; Manygoats, K.; Seifert, S.; Andree, C.; Stöter, M.; *et al.* Image-Based Analysis of Lipid Nanoparticle–Mediated SiRNA Delivery, Intracellular Trafficking and Endosomal Escape. *Nat. Biotechnol.* **2013**, *31*, 638–646.
(82) Shim, M. S.; Wang, X.; Ragan, R.; Kwon, Y. J. Dynamics of Nucleic Acid/Cationic Polymer Complexation and Disassembly under Biologically Simulated Conditions Using in Situ Atomic Force Microscopy. *Microsc. Res. Tech.* **2010**, *73*, 845–856.
(83) Rackstraw, B. J.; Martin, A. L.; Stolnik, S.; Roberts, C. J.; Garnett, M. C.; Davies, M. C.; Tendler, S. J. B. Microscopic Investigations into PEG−Cationic Polymer-Induced DNA Condensation. *Langmuir* **2001**, *17*, 3185–3193.
(84) Resina, S.; Prevot, P.; Tjierry, A. R. Physico-Chemical Characteristics of Lipoplexes Influence Cell Uptake Mechanisms and Transfection Efficacy. *PLoS One* **2009**, *4*.
(85) Lachelt, U.; Wagner, E.; Lächelt, U.; Wagner, E. Nucleic Acid Therapeutics Using Polyplexes: A Journey of 50 Years (and Beyond). *Chem. Rev.* **2015**, *115*, 11043–11078.
(86) Lazebnik, M.; Pack, D. W. Rapid and Facile Quantitation of Polyplex Endocytic Trafficking. *J. Control. Release* **2017**, *247*, 19–27.
(87) Xue, L.; Ingle, N. P.; Reineke, T. M. Highlighting the Role of Polymer Length, Carbohydrate Size, and Nucleic Acid Type in Potency of Glycopolycation Agents for PDNA and SiRNA Delivery. *Biomacromolecules* **2013**, *14*, 3903–3915.
(88) Akinc, A.; Lynn, D. M.; Anderson, D. G.; Langer, R. Parallel Synthesis and Biophysical Characterization of a Degradable Polymer Library for Gene Delivery. *J. Am. Chem. Soc.* **2003**, *125*, 5316–5323.
(89) Bishop, C. J.; Abubaker-Sharif, B.; Guiriba, T.; Tzeng, S. Y.; Green, J. J. Gene Delivery Polymer Structure–Function Relationships Elucidated via Principal Component Analysis. *Chem. Commun.* **2015**, *51*, 12134–12137.
(90) Putnam, D. Polymers for Gene Delivery across Length Scales. *Nat. Mater.* **2006**, *5*, 439–451.
(91) Raftery, R.; O'Brien, F. J.; Cryan, S. A. Chitosan for Gene Delivery and Orthopedic Tissue Engineering Applications. *Molecules* **2013**, *18*, 5611–5647.
(92) Grandinetti, G.; Reineke, T. M. Exploring the Mechanism of Plasmid DNA Nuclear Internalization with Polymer-Based Vehicles. *Mol. Pharm.* **2012**, *9*, 2256–2267.
(93) Shi, J.; Chou, B.; Choi, J. L.; Ta, A. L.; Pun, S. H. Investigation of Polyethylenimine / DNA Polyplex Transfection to Cultured Cells Using Radiolabeling and Subcellular Fractionation Methods. *Mol. Pharm.* **2013**, *10*, 2145–2156.
(94) Kumar, R.; Santa Chalarca, C. F.; Bockman, M. R.; Bruggen, C. Van; Grimme, C. J.;

Dalal, R. J.; Hanson, M. G.; Hexum, J. K.; Reineke, T. M. Polymeric Delivery of Therapeutic Nucleic Acids. *Chem. Rev.* **2021**, *121*, 11527–11652.
(95) Mäinnistö, M.; Reinisalo, M.; Ruponen, M.; Honkakoski, P.; Tammi, M.; Urtti, A. Polyplex-Mediated Gene Transfer and Cell Cycle: Effect of Carrier on Cellular Uptake and Intracellular Kinetics, and Significance of Glycosaminoglycans. *J. Gene Med.* **2007**, *9*, 479–487.
(96) Kim, J. A.; Aberg, C.; Salvati, A.; Dawson, K. A. Role of Cell Cycle on the Cellular Uptake and Dilution of Nanoparticles in a Cell Population. *Nat. Nanotechnol.* **2011**, *7*, 62–68.
(97) Bengali, Z.; Pannier, A. K.; Segura, T.; Anderson, B. C.; Jang, J. H.; Mustoe, T. A.; Shea, L. D. Gene Delivery through Cell Culture Substrate Adsorbed DNA Complexes. *Biotechnol. Bioeng.* **2005**, *90*, 290–302.
(98) Dalal, R. J.; Kumar, R.; Ohnsorg, M.; Brown, M.; Reineke, T. M. Cationic Bottlebrush Polymers Outperform Linear Polycation Analogues for PDNA Delivery and Gene Expression. *ACS Macro Lett.* **2021**, *10*, 886–893.
(99) Kumar, R.; Le, N.; Tan, Z.; Brown, M. E.; Jiang, S.; Reineke, T. M. Efficient Polymer-Mediated Delivery of Gene-Editing Ribonucleoprotein Payloads through Combinatorial Design, Parallelized Experimentation, and Machine Learning. *ACS Nano* **2020**, *14*, 17626–17639.
(100) Martens, T. F.; Remaut, K.; Demeester, J.; De Smedt, S. C.; Braeckmans, K. Intracellular Delivery of Nanomaterials: How to Catch Endosomal Escape in the Act. *Nano Today*, 2014, *9*, 344–364.
(101) Won, Y. Y.; Sharma, R.; Konieczny, S. F. Missing Pieces in Understanding the Intracellular Trafficking of Polycation/DNA Complexes. *J. Control. Release* **2009**, *139*, 88–93.
(102) Boussif, O.; Lezoualc'ht, F.; Zanta, M. A.; Mergnyt, D.; Schermant, D.; Demeneixt, B.; Behr, J.-P. A Versatile Vector for Gene and Oligonucleotide Transfer into Cells in Culture and in Vivo: Polyethylenimine. *Biochemistry* **1995**, *92*, 7297–7301.
(103) Behr, J.-P. The Proton Sponge: A Trick to Enter Cells the Viruses Did Not Exploit.
(104) Rehman, Z. U.; Hoekstra, D.; Zuhorn, I. S. Mechanism of Polyplex- and Lipoplex-Mediated Delivery of Nucleic Acids: Real-Time Visualization of Transient Membrane Destabilization without Endosomal Lysis. *ACS Nano* **2013**, *7*, 3767–3777.
(105) Akinc, A.; Thomas, M.; Klibanov, A. M.; Langer, R. Exploring Polyethylenimine-Mediated DNA Transfection and the Proton Sponge Hypothesis. *J. Gene Med.* **2005**, *7*, 657–663.
(106) Wilson, D. R.; Routkevitch, D.; Rui, Y.; Mosenia, A.; Wahlin, K. J.; Quinones-Hinojosa, A.; Zack, D. J.; Green, J. J. A Triple-Fluorophore-Labeled Nucleic Acid PH Nanosensor to Investigate Non-Viral Gene Delivery. *Mol. Ther.* **2017**, *25*, 1697–1709.
(107) Vermeulen, L. M. P.; Brans, T.; Samal, S. K.; Dubruel, P.; Demeester, J.; De Smedt, S. C.; Remaut, K.; Braeckmans, K. Endosomal Size and Membrane Leakiness Influence Proton Sponge-Based Rupture of Endosomal Vesicles. *ACS Nano* **2018**, *12*, 2332–2345.
(108) Benjaminsen, R. V.; Mattebjerg, M. A.; Henriksen, J. R.; Moghimi, S. M.; Andresen, T. L. The Possible "proton Sponge " Effect of Polyethylenimine (PEI) Does Not Include Change in Lysosomal PH. *Mol. Ther.* **2013**, *21*, 149–157.
(109) Suh, J.; Wirtz, D.; Hanes, J. Efficient Active Transport of Gene Nanocarriers to the Cell Nucleus. *Proc. Natl. Acad. Sci.* **2003**, *100*, 3878–3882.
(110) Bausinger, R.; Von Gersdorff, K.; Braeckmans, K.; Ogris, M.; Wagner, E.; Bräuchle, C.; Zumbusch, A. The Transport of Nanosized Gene Carriers Unraveled by Live-Cell Imaging. *Angew. Chemie - Int. Ed.* **2006**, *45*, 1568–1572.
(111) Dinh, A. T.; Pangarkar, C.; Theofanous, T.; Mitragotri, S. Understanding Intracellular Transport Processes Pertinent to Synthetic Gene Delivery via Stochastic Simulations and Sensitivity Analyses. *Biophys. J.* **2007**, *92*, 831.
(112) Cohen, R. N.; van der Aa, M. A. E. M.; Macaraeg, N.; Lee, A. P.; Szoka, F. C.

Quantification of Plasmid DNA Copies in the Nucleus after Lipoplex and Polyplex Transfection. *J Control Release* **2009**, *135*, 166–174.
(113) Grosse, S.; Aron, Y.; Thévenot, G.; François, D.; Monsigny, M.; Fajac, I. Potocytosis and Cellular Exit of Complexes as Cellular Pathways for Gene Delivery by Polycations. *J. Gene Med.* **2005**, *7*, 1275–1286.
(114) Pouton, C. W.; Wagstaff, K. M.; Roth, D. M.; Moseley, G. W.; Jans, D. A. Targeted Delivery to the Nucleus. *Adv. Drug Deliv. Rev.* **2007**, *59*, 698–717.
(115) Van Der Aa, M. A. E. M.; Huth, U. S.; Häfele, S. Y.; Schubert, R.; Oosting, R. S.; Mastrobattista, E.; Hennink, W. E.; Peschka-Süss, R.; Koning, G. A.; Crommelin, D. J. A. Cellular Uptake of Cationic Polymer-DNA Complexes via Caveolae Plays a Pivotal Role in Gene Transfection in COS-7 Cells. *Pharm. Res.* **2007**, *24*, 1590–1598.
(116) Tammam, S. N.; Azzazy, H. M. E.; Breitinger, H. G.; Lamprecht, A. Chitosan Nanoparticles for Nuclear Targeting: The Effect of Nanoparticle Size and Nuclear Localization Sequence Density. *Mol. Pharm.* **2015**, *12*, 4277–4289.
(117) Ogris, M.; Carlisle, R. C.; Bettinger, T.; Seymour, L. W. Melittin Enables Efficient Vesicular Escape and Enhanced Nuclear Access of Nonviral Gene Delivery Vectors. *J. Biol. Chem.* **2001**, *276*, 47550–47555.
(118) Brandén, L. J.; Mohamed, A. J.; Smith, C. I. E. A Peptide Nucleic Acid-Nuclear Localization Signal Fusion That Mediates Nuclear Transport of DNA. *Nat. Biotechnol.* **1999**, *17*, 784–787.
(119) Bitoque, D. B.; Morais, J.; Oliveira, A. V.; Sequeira, R. L.; Calado, S. M.; Fortunato, T. M.; Simão, S.; Rosa da Costa, A. M.; Silva, G. A. Human-Derived NLS Enhance the Gene Transfer Efficiency of Chitosan. *Biosci. Rep.* **2021**, *41*, 1–15.
(120) Sakai-Kato, K.; Un, K.; Nanjo, K.; Nishiyama, N.; Kusuhara, H.; Kataoka, K.; Kawanishi, T.; Goda, Y.; Okuda, H. Elucidating the Molecular Mechanism for the Intracellular Trafficking and Fate of Block Copolymer Micelles and Their Components. *Biomaterials* **2014**, *35*, 1347–1358.
(121) Chen, H. H.; Ho, Y.-P. P.; Jiang, X.; Mao, H.-Q. Q.; Wang, T.-H. H.; Leong, K. W. Quantitative Comparison of Intracellular Unpacking Kinetics of Polyplexes by a Model Constructed from Quantum Dot-FRET. *Mol. Ther.* **2008**, *16*, 324–332.
(122) van Bruggen, C.; Punihaole, D.; Keith, A. R.; Schmitz, A. J.; Tolar, J.; Frontiera, R. R.; Reineke, T. M. Quinine Copolymer Reporters Promote Efficient Intracellular DNA Delivery and Illuminate a Protein-Induced Unpackaging Mechanism. *Proc. Natl. Acad. Sci. U. S. A.* **2020**, *117*, 32919–32928.
(123) Pollard, H.; Remy, J.-S. S.; Loussouarn, G.; Demolombe, S.; Behr, J.-P. P.; Escande, D. Polyethylenimine but Not Cationic Lipids Promotes Transgene Delivery to the Nucleus in Mammalian Cells. *J. Biol. Chem.* **1998**, *273*, 7507–7511.
(124) Godbey, W. T.; Wu, K. K.; Mikos, A. G. Tracking the Intracellular Path of Poly(Ethylenimine)/DNA Complexes for Gene Delivery. *Proc. Natl. Acad. Sci. U. S. A.* **1999**, *96*, 5177–5181.
(125) Itaka, K.; Harada, A.; Yamasaki, Y.; Nakamura, K.; Kawaguchi, H.; Kataoka, K. In Situ Single Cell Observation by Fluorescence Resonance Energy Transfer Reveals Fast Intra-Cytoplasmic Delivery and Easy Release of Plasmid DNA Complexed with Linear Polyethylenimine. *J. Gene Med.* **2004**, *6*, 76–84.
(126) Männisto, M.; Rönkkö, S.; Mättö, M.; Honkakoski, P.; Hyttinen, M.; Pelkonen, J.; Urtti, A. The Role of Cell Cycle on Polyplex-Mediated Gene Transfer into a Retinal Pigment Epithelial Cell Line. *J. Gene Med.* **2005**, *7*, 466–476.
(127) Breunig, M.; Lungwitz, U.; Liebl, R.; Goepferich, A. Breaking up the Correlation between Efficacy and Toxicity for Nonviral Gene Delivery. *Proc. Natl. Acad. Sci.* **2007**, *104*, 14454–14459.
(128) Breuzard, G.; Tertil, M.; Gonçalves, C.; Cheradame, H.; Géguan, P.; Pichon, C.; Midoux,

P. Nuclear Delivery of NFκB-Assisted DNA/Polymer Complexes: Plasmid DNA Quantitation by Confocal Laser Scanning Microscopy and Evidence of Nuclear Polyplexes by FRET Imaging. *Nucleic Acids Res.* **2008**, *36*, e71.
(129) Ho, Y.-P.; Chen, H. H.; Leong, K. W.; Wang, T.-H. Evaluating the Intracellular Stability and Unpacking of DNA Nanocomplexes by Quantum Dots-FRET. *J. Control. Release* **2006**, *116*, 83–89.
(130) Schaffer, D. V.; Fidelman, N. A.; Dan, N.; Lauffenburger, D. A. Vector Unpacking as a Potential Barrier for Receptor-Mediated Polyplex Gene Delivery. *Biotechnol. Bioeng.* **2000**, *67*, 598–606.
(131) Huth, S.; Hoffmann, F.; von Gersdorff, K.; Laner, A.; Reinhardt, D.; Rosenecker, J.; Rudolph, C. Interaction of Polyamine Gene Vectors with RNA Leads to the Dissociation of Plasmid DNA-Carrier Complexes. *J. Gene Med.* **2006**, *8*, 1416–1424.
(132) Grigsby, C. L.; Leong, K. W. Balancing Protection and Release of DNA: Tools to Address a Bottleneck of Non-Viral Gene Delivery. *J. R. Soc. Interface* **2010**, *7*, 67–82.
(133) Vaughan, E. E.; Dean, D. A. Intracellular Trafficking of Plasmids during Transfection Is Mediated by Microtubules. *Mol. Ther.* **2006**, *13*, 422–428.
(134) Honoré, I.; Grosse, S.; Frison, N.; Favatier, F.; Monsigny, M.; Fajac, I. Transcription of Plasmid DNA: Influence of Plasmid DNA/Polyethylenimine Complex Formation. *J. Control. Release* **2005**, *107*, 537–546.
(135) Zhang, C.; Zhang, G.; Liu, D. Histone Deacetylase Inhibitors Reactivate Silenced Transgene in Vivo. *Gene Ther.* **2018**, *26*, 75–85.
(136) Hall, A.; Lächelt, U.; Bartek, J.; Wagner, E.; Moghimi, S. M. Polyplex Evolution: Understanding Biology, Optimizing Performance. *Mol. Ther.* **2017**, *25*, 1476–1490.
(137) Von Harpe, A.; Petersen, H.; Li, Y.; Kissel, T. Characterization of Commercially Available and Synthesized Polyethylenimines for Gene Delivery. *J. Control. Release* **2000**, *69*, 309–322.
(138) Choosakoonkriang, S.; Lobo, B. A.; Koe, G. S.; Koe, J. G.; Middaugh, C. R. Biophysical Characterization of PEI/DNA Complexes. *J. Pharm. Sci.* **2003**, *92*, 1710–1722.
(139) Boussif, O.; LezoualC'H, F.; Zanta, M. A.; Mergny, M. D.; Scherman, D.; Demeneix, B.; Behr, J. P. A Versatile Vector for Gene and Oligonucleotide Transfer into Cells in Culture and in Vivo: Polyethylenimine. *Proc. Natl. Acad. Sci. U. S. A.* **1995**, *92*, 7297–7301.
(140) Neu, M.; Fischer, D.; Kissel, T. Recent Advances in Rational Gene Transfer Vector Design Based on Poly(Ethylene Imine) and Its Derivatives. *J. Gene Med.* **2005**, *7*, 992–1009.
(141) Boeckle, S.; Gersdorff, K. von; Piepen, S. van der; Culmsee, C.; Wagner, E.; Ogris, M.; von Gersdorff, K.; van der Piepen, S.; Culmsee, C.; Wagner, E.; *et al.* Purification of Polyethylenimine Polyplexes Highlights the Role of Free Polycations in Gene Transfer. *J. Gene Med.* **2004**, *6*, 1102–1111.
(142) Wightman, L.; Kircheis, R.; Rössler, V.; Garotta, S.; Ruzicka, R.; Kursa, M.; Wagner, E. Different Behavior of Branched and Linear Polyethylenimine for Gene Delivery in Vitro and in Vivo. *J. Gene Med.* **2001**, *3*, 362–372.
(143) Kircheis, R.; Èller, S. S.; Brunner, S.; Ogris, M.; Heider, K.-H.; Zauner, W.; Wagner, E. Polycation-Based DNA Complexes for Tumor-Targeted Gene Delivery in Vivo. *J. Gene Med.* **1999**, *1*, 111–120.
(144) Bragonzi, A.; Dina, G.; Villa, A.; Calori, G.; Biffi, A.; Bordignon, C.; Assael, B. M.; Conese, M. Biodistribution and Transgene Expression with Nonviral Cationic Vector/DNA Complexes in the Lungs. *Gene Ther.* **2000**, *7*, 1753–1760.
(145) Bonner, D. K.; Zhao, X.; Buss, H.; Langer, R.; Hammond, P. T. Crosslinked Linear Polyethyleneimine Enhances Delivery of DNA to the Cytoplasm. *J. Control. Release* **2013**, *167*, 101–107.
(146) Ulasov, A. V; Khramtsov, Y. V; Trusov, G. A.; Rosenkranz, A. A.; Sverdlov, E. D.;

Sobolev, A. S. Properties of PEI-Based Polyplex Nanoparticles That Correlate With Their Transfection Efficacy. *Mol. Ther.* **2011**, *19*, 103–112.
(147) Malek, A.; Czubayko, F.; Aigner, A. PEG Grafting of Polyethylenimine (PEI) Exerts Different Effects on DNA Transfection and SiRNA-Induced Gene Targeting Efficacy. *J. Drug Target.* **2008**, *16*, 124–139.
(148) Levacic, A. K.; Morys, S.; Kempter, S.; Lächelt, U.; Wagner, E. Minicircle Versus Plasmid DNA Delivery by Receptor-Targeted Polyplexes. *Hum. Gene Ther.* **2017**, *28*, 862–874.
(149) Jain, S.; Kumar, S.; Agrawal, A. K.; Thanki, K.; Banerjee, U. C. Hyaluronic Acid–PEI–Cyclodextrin Polyplexes: Implications for in Vitro and in Vivo Transfection Efficiency and Toxicity. *RSC Adv.* **2015**, *5*, 41144–41154.
(150) Lynn, D. M.; Langer, R. Degradable Poly(Beta-Amino Esters): Synthesis, Characterization, and Self-Assembly with Plasmid DNA. *J. Am. Chem. Soc.* **2000**, *122*, 10761–10768.
(151) Anderson, D. G.; Akinc, A.; Hossain, N.; Langer, R. Structure/Property Studies of Polymeric Gene Delivery Using a Library of Poly(β-Amino Esters). *Mol. Ther.* **2005**, *11*, 426–434.
(152) Zamboni, C. G.; Kozielski, K. L.; Vaughan, H. J.; Nakata, M. M.; Kim, J.; Higgins, L. J.; Pomper, M. G.; Green, J. J. Polymeric Nanoparticles as Cancer-Specific DNA Delivery Vectors to Human Hepatocellular Carcinoma. *J. Control. Release* **2017**, *263*, 18–28.
(153) Karlsson, J.; Rhodes, K. R.; Green, J. J.; Tzeng, S. Y. Poly(Beta-Amino Ester)s as Gene Delivery Vehicles: Challenges and Opportunities. *Expert Opin. Drug Deliv.* **2020**, *17*, 1395–1410.
(154) Eltoukhy, A. A.; Siegwart, D. J.; Alabi, C. A.; Rajan, J. S.; Langer, R.; Anderson, D. G. Effect of Molecular Weight of Amine End-Modified Poly(β-Amino Ester)s on Gene Delivery Efficiency and Toxicity. *Biomaterials* **2012**, *33*, 3594–3603.
(155) Green, J. J.; Langer, R.; Anderson, D. G. A Combinatorial Polymer Library Approach Yields Insight into Nonviral Gene Delivery. *Acc. Chem. Res.* **2008**, *41*, 749–759.
(156) Monnery, B. D. Polycation-Mediated Transfection: Mechanisms of Internalization and Intracellular Trafficking. *Biomacromolecules* **2021**, *22*, 4060–4083.
(157) Pannier, A. K.; Anderson, B. C.; Shea, L. D. Substrate-Mediated Delivery from Self-Assembled Monolayers: Effect of Surface Ionization, Hydrophilicity, and Patterning. *Acta Biomater.* **2005**, *1*, 511–522.
(158) Segura, T.; Volk, M. J.; Shea, L. D. Substrate-Mediated DNA Delivery: Role of the Cationic Polymer Structure and Extent of Modification. *J. Control. Release* **2003**, *93*, 69–84.
(159) Bengali, Z.; Pannier, A. K.; Segura, T.; Anderson, B. C.; Jang, J.; Mustoe, T. A.; Shea, L. D. Gene Delivery through Cell Culture Substrate Adsorbed DNA Complexes. *Biotechnol. Bioeng.* **2005**, *90*, 290–302.
(160) Pannier, A. K.; Shea, L. D. Controlled Release Systems for DNA Delivery. *Mol. Ther.* **2004**, *10*, 19–26.
(161) Segura, T.; Shea, L. D. Surface-Tethered DNA Complexes for Enhanced Gene Delivery. *Bioconjug. Chem.* **2002**, *13*, 621–629.
(162) Varga, C. M.; Tedford, N. C.; Thomas, M.; Klibanov, A. M.; Griffith, L. G.; Lauffenburger, D. A. Quantitative Comparison of Polyethylenimine Formulations and Adenoviral Vectors in Terms of Intracellular Gene Delivery Processes. *Gene Ther.* **2005**, *12*, 1023–1032.
(163) Barretina, J.; Caponigro, G.; Stransky, N.; Venkatesan, K.; Margolin, A. A.; Kim, S.; Wilson, C. J.; Lehár, J.; Kryukov, G. V.; Sonkin, D.; *et al.* The Cancer Cell Line Encyclopedia Enables Predictive Modelling of Anticancer Drug Sensitivity. *Nature* **2012**, *483*, 603–607.
(164) Yamauchi, F.; Kato, K.; Iwata, H. Micropatterned, Self-Assembled Monolayers for Fabrication of Transfected Cell Microarrays. *Biochim. Biophys. Acta - Gen. Subj.* **2004**,

1672, 138–147.
(165) Gower, R. M.; Shea, L. D. Biomaterial Scaffolds for Controlled, Localized Gene Delivery of Regenerative Factors. *Adv. Wound Care* **2013**, *2*, 100–106.
(166) Bengali, Z.; Rea, J. C.; Gibly, R. F.; Shea, L. D. Efficacy of Immobilized Polyplexes and Lipoplexes for Substrate-Mediated Gene Delivery. *Biotechnol. Bioeng.* **2009**, *102*, 1679–1691.
(167) Hammond, P. T. Form and Function in Multilayer Assembly: New Applications at the Nanoscale. *Adv. Mater.* **2004**, *16*, 1271–1293.
(168) Decher, G. Fuzzy Nanoassemblies: Toward Layered Polymeric Multicomposites. *Science (80-.).* **1997**, *277*, 1232–1237.
(169) Shah, N. J.; Hong, J.; Hyder, M. N.; Hammond, P. T. Osteophilic Multilayer Coatings for Accelerated Bone Tissue Growth. *Adv. Mater.* **2012**, *24*, 1445–1450.
(170) Shukla, A.; Fleming, K. E.; Chuang, H. F.; Chau, T. M.; Loose, C. R.; Stephanopoulos, G. N.; Hammond, P. T. Controlling the Release of Peptide Antimicrobial Agents from Surfaces. *Biomaterials* **2010**, *31*, 2348–2357.
(171) Moskowitz, J. S.; Blaisse, M. R.; Samuel, R. E.; Hsu, H.-P.; Harris, M. B.; Martin, S. D.; Lee, J. C.; Spector, M.; Hammond, P. T. The Effectiveness of the Controlled Release of Gentamicin from Polyelectrolyte Multilayers in the Treatment of Staphylococcus Aureus Infection in a Rabbit Bone Model. *Biomaterials* **2010**, *31*, 6019–6030.
(172) Shukla, A.; Fuller, R. C.; Hammond, P. T. Design of Multi-Drug Release Coatings Targeting Infection and Inflammation. *J. Control. Release* **2011**, *155*, 159–166.
(173) DeMuth, P. C.; Su, X.; Samuel, R. E.; Hammond, P. T.; Irvine, D. J. Nano-Layered Microneedles for Transcutaneous Delivery of Polymer Nanoparticles and Plasmid DNA. *Adv. Mater.* **2010**, *22*, 4851–4856.
(174) Macdonald, M. L.; Samuel, R. E.; Shah, N. J.; Padera, R. F.; Beben, Y. M.; Hammond, P. T. Tissue Integration of Growth Factor-Eluting Layer-by-Layer Polyelectrolyte Multilayer Coated Implants. *Biomaterials* **2011**, *32*, 1446–1453.
(175) Samuel, R. E.; Shukla, A.; Paik, D. H.; Wang, M. X.; Fang, J. C.; Schmidt, D. J.; Hammond, P. T. Osteoconductive Protamine-Based Polyelectrolyte Multilayer Functionalized Surfaces. *Biomaterials* **2011**, *32*, 7491–7502.
(176) Min, J.; Braatz, R. D.; Hammond, P. T. Tunable Staged Release of Therapeutics from Layer-by-Layer Coatings with Clay Interlayer Barrier. *Biomaterials* **2014**, *35*, 2507–2517.
(177) Min, J.; Choi, K. Y.; Dreaden, E. C.; Padera, R. F.; Braatz, R. D.; Spector, M.; Hammond, P. T. Designer Dual Therapy Nanolayered Implant Coatings Eradicate Biofilms and Accelerate Bone Tissue Repair. *ACS Nano* **2016**, *10*, 4441–4450.
(178) Alkekhia, D.; Hammond, P. T.; Shukla, A. Layer-by-Layer Biomaterials for Drug Delivery. *Annu. Rev. Biomed. Eng.* **2020**, *22*, 1–24.
(179) Mansouri, S.; Winnik, F. M.; Tabrizian, M. Modulating the Release Kinetics through the Control of the Permeability of the Layer-by-Layer Assembly: A Review. *Expert Opin. Drug Deliv.* **2009**, *6*, 585–597.
(180) Hsu, B. B.; Hagerman, S. R.; Jamieson, K.; Veselinovic, J.; O'Neill, N.; Holler, E.; Ljubimova, J. Y.; Hammond, P. T. Multilayer Films Assembled from Naturally-Derived Materials for Controlled Protein Release. *Biomacromolecules* **2014**, *15*, 2049–2057.
(181) Wood, K. C.; Boedicker, J. Q.; Lynn, D. M.; Hammond, P. T. Tunable Drug Release from Hydrolytically Degradable Layer-by-Layer Thin Films. *Langmuir* **2005**, *21*, 1603–1609.
(182) Ghiorghita, C. A.; Bucatariu, F.; Dragan, E. S. Influence of Cross-Linking in Loading/Release Applications of Polyelectrolyte Multilayer Assemblies. A Review. *Mater. Sci. Eng. C* **2019**, *105*, 1–20.
(183) Shah, N. J.; Hsu, B. B.; Dreaden, E. C.; Hammond, P. T. Engineering Layer-by-Layer Thin Films for Multiscale and Multidrug Delivery Applications. In *Layer-by-Layer Films for Biomedical Applications*; 2015; pp. 131–170.

(184) Hsu, B. B.; Jamieson, K. S.; Hagerman, S. R.; Holler, E.; Ljubimova, J. Y.; Hammond, P. T. Ordered and Kinetically Discrete Sequential Protein Release from Biodegradable Thin Films. *Angew. Chemie - Int. Ed.* **2014**, *53*, 8093–8098.
(185) Jewell, C. M.; Lynn, D. M. Multilayered Polyelectrolyte Assemblies as Platforms for the Delivery of DNA and Other Nucleic Acid-Based Therapeutics. *Adv. Drug Deliv. Rev.* **2008**, *60*, 979–999.
(186) Jewell, C. M.; Zhang, J.; Fredin, N. J.; Wolff, M. R.; Hacker, T. A.; Lynn, D. M. Release of Plasmid DNA from Intravascular Stents Coated with Ultrathin Multilayered Polyelectrolyte Films. *Biomacromolecules* **2006**, *7*, 2483–2491.
(187) Saurer, E. M.; Jewell, C. M.; Roenneburg, D. A.; Bechler, S. L.; Torrealba, J. R.; Hacker, T. A.; Lynn, D. M. Polyelectrolyte Multilayers Promote Stent-Mediated Delivery of DNA to Vascular Tissue. *Biomacromolecules* **2013**, *14*, 1696–1704.
(188) Ogier, J. LbL-Based Gene Delivery: Challenges and Promises. In *Layer-by-Layer Films for Biomedical Applications*; Wiley-VCH Verlag GmbH & Co. KGaA: Weinheim, Germany, 2015; pp. 195–206.
(189) Bechler, S. L.; Si, Y.; Yu, Y.; Ren, J.; Liu, B.; Lynn, D. M. Reduction of Intimal Hyperplasia in Injured Rat Arteries Promoted by Catheter Balloons Coated with Polyelectrolyte Multilayers That Contain Plasmid DNA Encoding PKCδ. *Biomaterials* **2013**, *34*, 226–236.
(190) Yu, Y.; Si, Y.; Bechler, S. L.; Liu, B.; Lynn, D. M. Polymer Multilayers That Promote the Rapid Release and Contact Transfer of DNA. *Biomacromolecules* **2015**, *16*, 2998–3007.
(191) Jewell, C. M.; Zhang, J.; Fredin, N. J.; Lynn, D. M. Multilayered Polyelectrolyte Films Promote the Direct and Localized Delivery of DNA to Cells. *J. Control. Release* **2005**, *106*, 214–223.
(192) Jingtao Zhang; Sara I. Montañez; Christopher M. Jewell, and; Lynn*, D. M.; Zhang, J.; Montañez, S. I.; Jewell, C. M.; Lynn, D. M. Multilayered Films Fabricated from Plasmid DNA and a Side-Chain Functionalized Poly(β-Amino Ester): Surface-Type Erosion and Sequential Release of Multiple Plasmid Constructs from Surfaces. *Langmuir* **2007**, *23*, 11139–11146.
(193) Casdorff, K.; Keplinger, T.; Bellanger, H.; Michen, B.; Schön, S.; Burgert, I. High-Resolution Adhesion Mapping of the Odd–Even Effect on a Layer-by-Layer Coated Biomaterial by Atomic-Force-Microscopy. *ACS Appl. Mater. Interfaces* **2017**, *9*, 13793–13800.
(194) Wang, X.; Sun, J.; Ji, J. PH Modulated Layer-by-Layer Assembly as a New Approach to Tunable Formulating of DNA within Multilayer Coating. *React. Funct. Polym.* **2011**, *71*, 254–260.
(195) Meyer, F.; Ball, V.; Schaaf, P.; Voegel, J. C.; Ogier, J. Polyplex-Embedding in Polyelectrolyte Multilayers for Gene Delivery. *Biochim. Biophys. Acta - Biomembr.* **2006**, *1758*, 419–422.
(196) Segura, T.; Shea, L. D. Materials for Non-Viral Gene Delivery. *Annu. Rev. Mater. Res.* **2001**, *31*, 25–46.
(197) Rea, J. C.; Gibly, R. F.; Barron, A. E.; Shea, L. D. Self-Assembling Peptide–Lipoplexes for Substrate-Mediated Gene Delivery. *Acta Biomater.* **2009**, *5*, 903–912.
(198) Holmes, C. A.; Tabrizian, M. Substrate-Mediated Gene Delivery from Glycol-Chitosan/Hyaluronic Acid Polyelectrolyte Multilayer Films. *ACS Appl. Mater. Interfaces* **2013**, *5*, 524–531.
(199) Husteden, C.; Doberenz, F.; Goergen, N.; Pinnapireddy, S. R.; Janich, C.; Langner, A.; Syrowatka, F.; Repanas, A.; Erdmann, F.; Jedelská, J.; *et al.* Contact-Triggered Lipofection from Multilayer Films Designed as Surfaces for in Situ Transfection Strategies in Tissue Engineering. *ACS Appl. Mater. Interfaces* **2020**, *12*, 8963–8977.
(200) Holmes, C.; Daoud, J.; Bagnaninchi, P. O.; Tabrizian, M. Polyelectrolyte Multilayer

Coating of 3D Scaffolds Enhances Tissue Growth and Gene Delivery: Non-Invasive and Label-Free Assessment. *Adv. Healthc. Mater.* **2014**, *3*, 572–580.
(201) Bechler, S. L.; Si, Y.; Yu, Y.; Ren, J.; Liu, B.; Lynn, D. M. Reduction of Intimal Hyperplasia in Injured Rat Arteries Promoted by Catheter Balloons Coated with Polyelectrolyte Multilayers That Contain Plasmid DNA Encoding PKCδ. *Biomaterials* **2013**, *34*, 226–236.
(202) Castleberry, S. A.; Almquist, B. D.; Li, W.; Reis, T.; Chow, J.; Mayner, S.; Hammond, P. T. Self-Assembled Wound Dressings Silence MMP-9 and Improve Diabetic Wound Healing in Vivo. *Adv. Mater.* **2016**, *28*, 1809–1817.
(203) DeMuth, P. C.; Min, Y.; Huang, B.; Kramer, J. A.; Miller, A. D.; Barouch, D. H.; Hammond, P. T.; Irvine, D. J. Polymer Multilayer Tattooing for Enhanced DNA Vaccination. *Nat. Mater.* **2013**, *12*, 367–376.
(204) Chou, J. J.; Berger, A. G.; Jalili-Firoozinezhad, S.; Hammond, P. T. A Design Approach for Layer-by-Layer Surface-Mediated SiRNA Delivery. *Acta Biomater.* **2021**, *135*, 331–341.

Chapter 2. Understanding key factors in cationic polymer-assisted DNA delivery using polyplexes as a model system

2.1 Introduction

Cationic polymers of diverse physicochemical characteristics (e.g., degradability and charge density) have been developed for non-viral gene delivery applications, particularly in the form of pre-formed polyplexes delivered in solution. These complexes interact electrostatically with cells and facilitate endocytosis of DNA in cationic polymer-assisted transfection.[1] Cellular uptake of DNA usually relies on positively charged transfection agents that compensate the charge of DNA and greatly reduce the hydrodynamic size of DNA, allowing it to pass the negatively charged cell membrane.[2] The ratio of polycation to DNA, in particular the ratio of protonated amines to phosphates (N/P ratio), is a key factor in formation of stable polyplexes.

In order to form stable polyplexes, an excess of polycation is typically required, which can cause cytotoxicity. Careful selection and modification of polycation components is needed to maintain charge stability of polyplexes while minimizing cytotoxicity. Cellular uptake of DNA polyplexes has been shown to be impacted by size, shape, surface charge, surface ligands, concentration of polyplexes at the cell surface, and cell cycle stage.[3–11] After internalization, the DNA must traffic to the nucleus where polyplex unpacking needs to occur before transcription can begin. As such, the strength of DNA binding and complexation by cationic polymers can also affect delivery and transfection outcomes. Weak binding of DNA during polyplex formation results in insufficiently protected DNA while overly strong binding slows or prevents DNA release from the polymer and hinders transcription.[12] Polyelectrolytes including poly(beta-amino esters), polyethylenimine, poly amino acids, and chitosan have been chemically modified to modulate DNA binding and unbinding and to preserve DNA condensation capacity while diminishing impact on cell viability.

Layer-by-layer (LbL) self-assembled DNA nanolayers are hypothesized to leverage similar cellular association and uptake mechanisms as polyplexes. Studies have shown that

degradable DNA multilayers rearrange in physiological solution to present nanoparticles at the film surface,[13–15] which are thought to mediate cellular uptake of DNA. The structure, composition, and behavior of these film-released particles are not well understood. Investigating pre-formed polyplexes assembled from the same components could elucidate key factors and mechanisms of action generalizable to LbL film releasates. Here, we study poly(beta-amino ester) and polyethyleneimine polyplex complexation and delivery of plasmid DNA and discuss implications for the function of electrostatically-assembled DNA multilayer films.

Chapter scope: This study examined factors affecting gene delivery efficacy, specifically plasmid DNA delivery via pre-formed polyplexes. The effect of plasmid size, polymer degradability, polymer molecular weight, and relative polymer/DNA content on cellular uptake of DNA, transfection efficiency, and cell viability were investigated in four model cell lines.

2.2 Methods

2.2.1 Materials

All materials were obtained from Millipore Sigma (St. Louis, MO) unless otherwise specified. Linear polyethyleneimine (25 kDa LPEI) was obtained from Polysciences (Warrington, PA). 1,4-butanediol diacrylate and 1,6-hexanediol diacrylate were purchased from Alfa Aesar (Ward Hill, MA). Phosphate buffered saline (PBS) was purchased from Lonza (Morristown, NJ). Accublue Broad and High Sensitivity dsDNA Quantitation kits were obtained from Biotium (Fremont, CA). Precast 0.8% and EX 1% agarose E-gels were obtained from ThermoFisher Scientific (Waltham, MA).

2.2.2 Cell culture

Human epithelial kidney 293T (HEK 293T) cells were a gift from Dr. Jiahe Li at Northeastern University. U2OS human osteosarcoma cells were a gift from Dr. Michael Yaffe's Lab at MIT. MC3T3-E1 murine pre-osteoblast subclone 4 were purchased from ATCC. HEK and U2OS cells were cultured in Dulbecco's Modified Eagle Medium (DMEM, Corning, NY), supplemented with 10% Fetal Bovine Serum (FBS) and 1% penicillin-streptomycin. MC3T3-E1

cells were cultured in α Minimum Essential Medium (αMEM, ThermoFisher, MA) supplemented with 10% FBS and 1% penicillin-streptomycin. These cells tested negative for mycoplasma after thawing from storage and monthly during culture using Lonza MycoAlert kit (Morristown, NJ).

2.2.3 Polymer synthesis

Poly (beta-amino ester) (PBAE) hereafter called Poly 1 or Poly 2, was prepared as following procedures described previously.[16,17] Briefly, diacrylate (butanediol diacrylate for Poly 1 and hexanediol diacrylate for Poly 2) and dipiperidine small molecule monomers were dissolved in anhydrous tetrahydrofuran (THF) with excess dipiperidine (1.02:1 molar ratio) and were allowed to react for 24 hours at 50°C, stirring at 200 rpm under nitrogen. The polymer was precipitated into ice cold hexane and isolated by centrifugation. Polymer was dialyzed in THF for 24 hours to remove remaining unreacted monomer. Molecular weight was quantified using gel permeation chromatography. Polymer was dried and stored in a vacuum desiccator.

2.2.4 Bacterial culture and plasmid purification

Plasmid DNA (pHIV-eGFP, 7.8 kb; pmaxGFP, 3.5 kb) was transformed into competent *E. coli* (New England Biolabs) per manufacturer instruction. Starter cultures were initiated by directly transferring cells from frozen stocks into 50 mL of Luria-Bertani (LB) medium with 100 μg/mL ampicillin (pHIV-eGFP) or 50 μg/mL kanamycin (pmaxGFP). Starter cultures were incubated overnight at 37°C with shaking at 220 rpm. Starter cultures were then transferred into 2 L of LB media with ampicillin or kanamycin and incubated for 24 hours at 37°C in a shaking incubator (220 rpm). Overnight cultures were centrifuged at 3700 rpm for 15 min to harvest cells. GFP plasmid DNA (pGFP) was purified from cells using the endotoxin-free ZymoPURE II Plasmid Gigaprep Kit per manufacturer instructions (Zymo Research, Irvine, CA). Purified DNA was eluted at high concentrations (1-3 mg/mL) in TE buffer and frozen at -20°C until use.

2.2.5 Fluorescent labelling of plasmid DNA

Plasmid DNA was fluorescently tagged to determine cellular association and uptake via flow cytometry and to visualize cellular localization via fluorescence microscopy. DNA was

labelled with Cy5 using Label IT Intracellular Nucleic Acid Localization Kit (Mirus Bio LLC, Madison, WI). The labelling density was approximately 1 dye molecule per 300 basepairs.

2.2.6 DNA polyplex formation

Pre-formed polyplexes were prepared by mixing cationic polymers and pGFP in 20 mM sodium acetate to allow electrostatic complexation. Polyplexes were assembled by mixing equal volumes of polycation dissolved in 40 mM sodium acetate and pGFP in water at the appropriate polymer:DNA mass ratios (5:1, 10:1, 20:1, 30:1). For example, 20 µL each of polycation and pGFP stock were mixed to obtain a 40 µL master treatment mix containing 400 ng pGFP, 4000 ng PBAE (10:1 ratio), and 20 mM sodium acetate. For 96-well plates, 10 µL of each master mix was distributed to each treatment well. Polyplexes were assembled just prior to transfection studies and used immediately. Polyplexes prepared with commercial transfection reagents LT1 or TransIT-X2 (Mirus Bio LLC, Madison, WI) at a ratio of 3 µl reagent:1 µg DNA were used as positive transfection controls.

2.2.7 In vitro polyplex transfection

HEK 293T cells were grown in complete growth medium (DMEM supplemented with 10% fetal bovine serum and 1% penicillin-streptomycin) in a humidified incubator at 37°C with 5% CO_2. Culture medium was replaced every 2 days and cells were subcultured when near 100% confluence using 0.25% trypsin-EDTA. Cells used were less than passage 20. For analysis of DNA polyplex transfection, cells were seeded at 10,000 cells/well in 96-well tissue culture plates the day before transfection such that cells were 70% confluent at the time of transfection. Culture medium was changed to 90 µL transfection medium (5% FBS) prior to treatment. Cells were incubated with DNA polyplexes (100 ng of DNA in 10 µL of treatment per well) for 8 hours before replacing media with complete media. Cells were then maintained at 37°C and 5% CO_2 for 48 hours before analysis by flow cytometry.

2.2.8 Measuring transfection efficiency via flow cytometry

The transfection efficiency of the DNA polyplexes or DNA films was quantified by measuring the fraction of treated cells that successfully took up and expressed the delivered GFP plasmid. For DNA polyplex transfection studies, 48 hours after treatment, cells were harvested and resuspended in PBS containing 1:500 diluted ZombieViolet Viability Dye and incubated in the dark for 15 minutes. Resuspended cells were loaded in 96-well V bottom plates, centrifuged again, and resuspended in PBS with 1% FBS. Cells were analyzed using a BD FACSCelesta unit with the high throughput sampler attachment in the Koch Institute Swanson Biotechnology Center Flow Cytometry Facility. ZombieViolet was read with a 405nm laser and 450/40 filter set, GFP fluorescence with a 488nm laser and 530/30 filter set, and Cy3 or Cy5 labelled DNA with a 561nm laser and either 586/15 or 670/30 filter set. Flow cytometry data was analyzed using Flow Jo. Live single cell populations were analyzed for DNA fluorescence, indicating cellular association or uptake, and GFP expression, indicating expression of the delivered plasmid DNA. The fraction of single cells that were GFP positive (% GFP positive) was taken as a measure of transfection efficiency.

2.2.9 Polyplex characterization

DNA polyplex were characterized using dynamic light scattering. A Malvern ZS90 Particle Analyzer was used for size and zeta potential measurements. 40 µL containing 100 ng/µL DNA with increasing polycation concentrations to obtain polymer:DNA mass ratios of 5, 10, 20, 30, 40, and 60 were used for DLS measurements. Samples were diluted ten-fold (0.1X PBS final buffer concentration) with molecular biology grade water for zeta potential measurements. Results from the Malvern are reported using the SD of three measurements.

2.2.10 Statistical analysis

Statistical analysis was performed using GraphPad Prism 9 software (San Diego, CA). Data are reported as mean ± standard deviation of a minimum of 3 samples. Each polyplex

formulation was tested in triplicate and in two separate trials. Statistical significance was evaluated using one-way ANOVA with Tukey's multiple comparisons test or Student's t-test.

2.3 Results and Discussion

2.3.1 Effect of molecular weight on PBAE polyplex transfection efficiency

We first examined polyplex delivery of plasmid DNA to identify key factors impacting polycation-mediated DNA transfection that could also impact polyelectrolyte multilayer film-based DNA delivery. In polycation-assisted gene delivery, polycation molecular weight and overall positive particle charge are key for effectively condensing DNA and facilitating cellular uptake. In this study, GFP plasmid was selected for a fluorescent indicator of gene expression, amenable to microscopy and flow cytometry. The polycations examined in this study are shown in **Figure 2.1A.** Poly 2 is a poly (beta-amino ester) (PBAE) that hydrolytically degrades in physiological buffers into biocompatible subunits and has been applied for both DNA and RNA gene delivery.[18–22] Linear and branched polyethyleneimine are positively charged synthetic polycations well-known for their gene delivery ability via endosomal pH buffering activity.[23–28] HEK 293T cells were selected as a model cell line for their reliable growth and relative ease of transfection. It is important to note that HEK 293T cells are engineered cell lines that have high propensity for transfection and produce proteins at higher levels and for longer durations than primary cells and many other cell lines.[29,30] HEK 293T cells were treated with polyplexes containing pHIV-eGFP plasmid (7.8 kb) and a synthetic polycation or a commercial transfection reagent, TransIT-X2. After 48 hours incubation with polyplexes, cells were harvested for flow analysis of green fluorescence on a FACS Celesta flow cytometer. The percent GFP positive cells of all single cells analyzed is reported as a measure of transfection efficiency.

PBAE polyplex transfection efficiency as a function of polycation molecular weight and polymer:DNA mass ratio is shown in **Figure 2.1B**. Of the PBAE molecular weights tested, all enabled polyplex transfection efficiencies between 15 and 35% in HEK 293T cells. No particular trend was observed in % GFP positive cells with increasing PBAE molecular weight. For LPEI

and BPEI, polyplex transfection efficacy increased with increasing polymer molecular weight, except for 70 kDa BPEI, which caused substantial cytotoxicity (**Figure 2.1C**). For all polycations tested, decreased cell viability was observed in the presence of the highest molecular weight polymers. Increased transfection activity and increased toxicity with higher polymer molecular weights can both be attributed to increased positive charge per polymer molecule, which results in greater cellular membrane disruption activity.[31] Similarly, increasing the amount of polymer relative to DNA in a polyplex can modulate the efficacy and toxicity of polyplex delivery. The polymer:DNA mass ratio or the nitrogen:phosphate (N/P) ratio denotes the polyplex composition. No GFP expression was detected in cells treated with PBAE:DNA mass ratios less than 10:1 (N/P = 15) and transfection efficiency trended up with increasing polymer dose (**Figure 2.1B**). The number of GFP positive cells also increased with increasing PEI:DNA mass ratio (**Figure 2.1C**). Transfection efficiencies between 15% and 40% were achieved at PEI:DNA mass ratio 3:1 (N/P = 23). Higher mass ratios were examined, but resulted in unacceptable cytotoxicity and are thus not presented here.

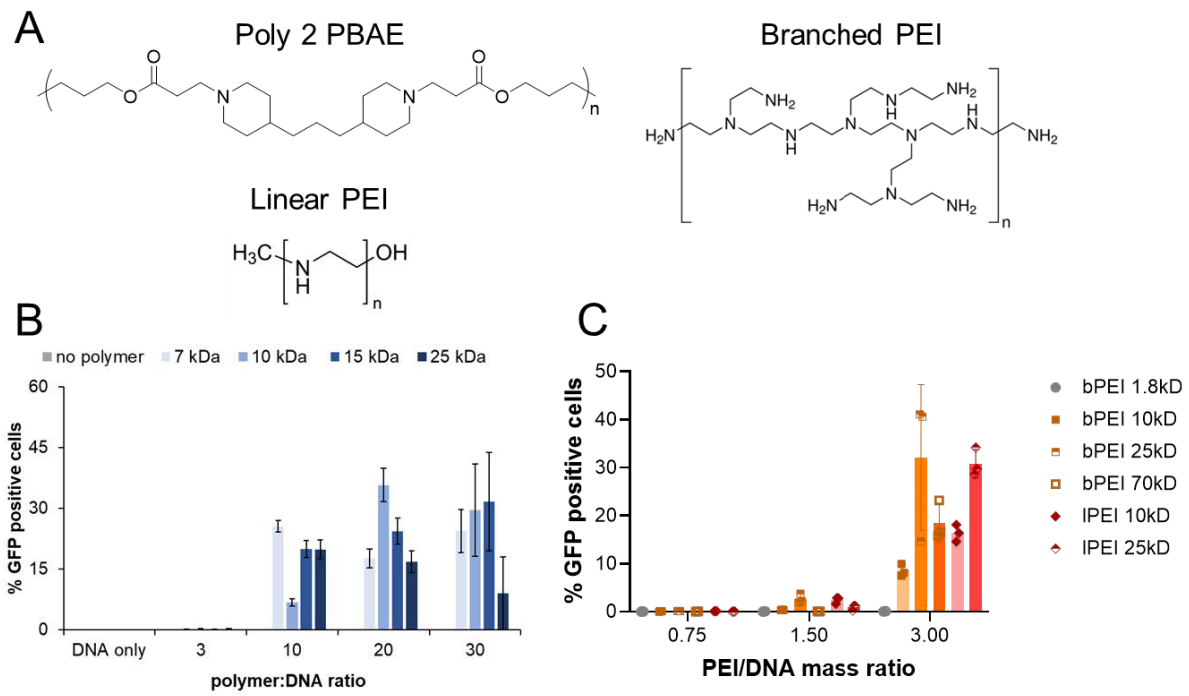

Figure 2.1 Effect of polycation molecular weight and polymer:DNA ratio on Poly 2 and PEI polyplex transfection efficiency *(A) Chemical structure of poly(beta-amino ester) Poly 2, branched polyethyleneimine and linear polyethyleneimine (B) Percent GFP positive HEK 293T cells treated with Poly 2 polyplexes (C) Percent GFP positive cells treated with branched or linear PEI polyplexes.*

2.3.2 Size and charge characterization of PBAE/DNA polyplexes

Polyplex size and surface charge (zeta potential) are key design parameters for effective DNA condensation and intracellular delivery. We formulated PBAE/DNA polyplexes using 7 kDa PBAE and pHIV-eGFP plasmid (7.8 kb) with varying polycation doses to examine the effect of polyplex composition on PBAE polyplex size, charge, and transfection efficiency (**Figure 2.3**). At polymer:DNA mass ratio 5:1, polyplexes were approximately 120 nm in diameter with a high polydispersity index (PDI) around 0.6 (**Figure 2.3A**). Increasing the polymer:DNA ratio beyond 5:1 resulted in a slight increase in polyplex diameter and a drop in PDI, implying that at mass ratio 10:1, DNA charge had been compensated and additional polycation was present to stabilize the complex**.** Further increasing the amount of polycation resulted in increased polyplex size with constant PDI of 0.2. Between 10:1 and 60:1, additional PBAE likely contributes to the

free polycation shell surrounding the core PBAE/DNA complex, stabilizing it against aggregation.

Surface charge reversal from negative to positive occurs between polymer:DNA mass ratios 5:1 and 10:1 (**Figure 2.3B**). At low polymer:DNA ratios, the PBAE complexes were negatively charged due to insufficient DNA shielding. PBAE/DNA polyplexes exhibited a constant +40 mV zeta potential for polymer:DNA ratios greater than 10:1. This suggests that a core polyplex forms and additional polycation chains do not contribute to the surface charge of the complex. A strikingly similar trend in polyplex transfection efficiency with polymer:DNA ratio was observed (**Figure 2.3C**).These results highlight the importance of a sufficient polymer:DNA mass ratio or N/P ratio to compensate DNA's high negative charge. Additionally, the presence of excess free polycation is important both for polyplex stabilization and effective transfection.

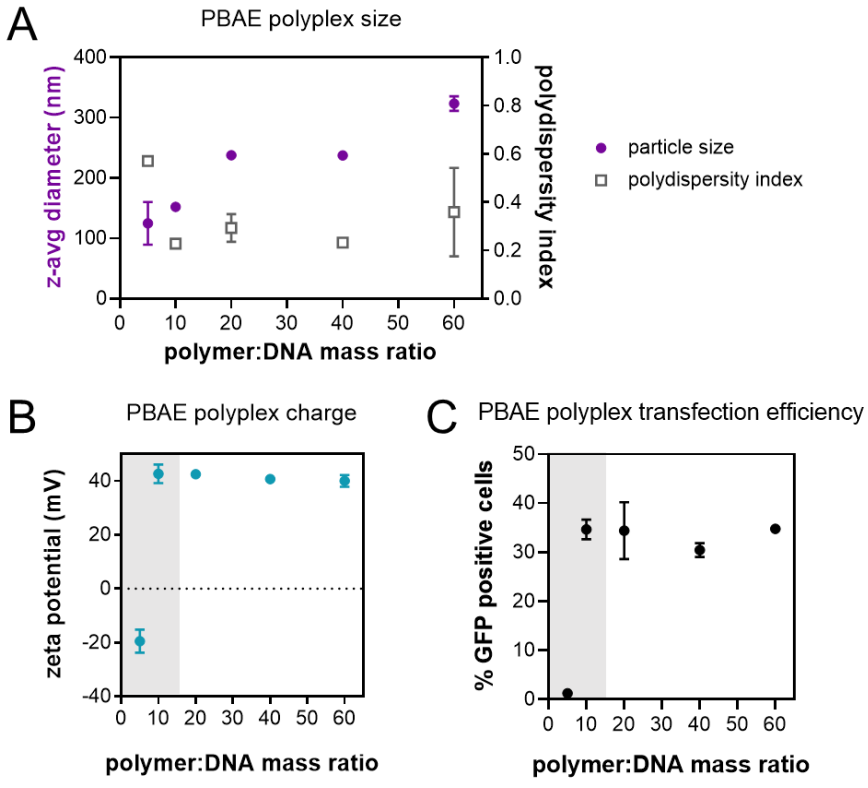

Figure 2.2 Characterization of PBAE/DNA polyplexes with varying polymer:DNA mass ratios *(A) Z-average diameter and polydispersity index (B) Zeta potential (C) Transfection efficiency in HEK 293T cells.*

The core-shell model for positively charged DNA complexes describes a hydrophobic core consisting of net neutral complexed polycation/DNA chains surrounded by a hydrophilic shell composed of excess polycation chains.[32–34] At low N/P ratios, polyplexes are characterized by incomplete DNA condensation. Complete condensation occurs at around N/P 2, forming neutral polyplex cores that are unstable and tend to aggregate.[34–37] At high concentrations of polymer, excess polymer forms a shell around the core and stabilizes polyplexes against aggregation. Polycation chains in the polyplex core primarily act to condense and protect nucleic acids during cell uptake and intracellular trafficking while free polycation chains promote gene transfection.

High efficiency polyplex-mediated DNA delivery has been observed with polyplexes formed at high N/P ratios with a large excess of polycation. Cationic polymers, however, bind DNA only up to a certain N/P ratio sufficient to neutralize the negative charge and any additional polymer remains free and weakly associated.[36] The presence of excess polymer has been shown to play an important role in transfection studies *in vitro,* although the precise mechanism remains unclear. Free polymer has been demonstrated to promote gene transfection even when added to cells after polyplex treatment,[36,38] suggesting that the free polymer chains may aid with endosomal release and later steps of delivery.

Ketola et al. (2011) separated free PEI chains from PEI polyplexes using size exclusion chromatography.[39] These particles were similar charge and size before and after purification. They posited that free PEI helps decrease inhibitory polyplex interactions with cell-surface glycosaminoglycans (GAGs), whose presence varies by cell type.[39] Negatively-charged GAGs can bind to and destabilize polyplexes, causing premature release of DNA and a decrease in transfection activity.[40,41] As such, free excess polycation can bind anionic GAGs and reduce undesirable destabilizing interactions with polyplexes. However, free PEI has also been shown to compete with polyplexes for cellular association and does not enhance cellular uptake of polyplexes.[36,42,43] Instead, free PEI was found to enhance the transfection efficiency of already

internalized polyplexes,[36,44] suggesting that the free polycations' positive effect on transfection efficiency is due primarily to intracellular mechanisms, i.e. enhancing endosomal escape of already internalized polyplexes. Internalized PEI polyplexes have been shown to co-localize with GAGs in endosomal vesicles.[45] Binding of endosomal GAGs and polyplexes may reduce the proton-buffering capacity of PEI[1] or reduce osmotic swelling, thus inhibiting endosomal escape. The presence of free PEI has been proposed to facilitate endosomal escape by providing extra proton buffering[46] or by adsorbing on the inner cell membrane and interfering with SNARE signal proteins and trafficking of endosomal polyplexes.[43,47] Overall, the polymer:DNA mass ratio-dependent changes in polyplex size, charge, and transfection efficiency highlight the importance of both DNA-condensing polycation and free polycation for effective polyplex-mediated DNA delivery.

2.3.3 Plasmid size affects efficacy of polycation-mediated transfection

Two different sized plasmids were tested to examine the impact of polycation chemistry and charge density on transfection efficiency. A 3.5 kb plasmid (pmaxGFP) and 7.8 kb plasmid (pHIV-eGFP) were examined in polyplex transfection of cells. The cationic carriers evaluated included Mirus TransIT-X2 commercial reagent (X2), 7 kDa Poly 2 (PBAE), and 10 kDa branched PEI (BPEI). The DNA dose was held constant for each polyplex formation. Greater transfection was observed in cells treated with pre-formed polyplexes of the smaller plasmid, regardless of polymer chemistry (**Figure 2.3**). X2 complexes achieved 75% transfection for both plasmid sizes. PBAE complexes achieved 21% ± 1.6% transfection efficiency for the larger pGFP plasmid and 45% ± 1.2% for the smaller plasmid. BPEI complexes enabled 32% ± 4.7% transfection for the larger plasmid and 49% ± 3.2% for the smaller plasmid.

Polycation chemistry did not affect transfection efficiency with the small GFP plasmid, while non-degradable BPEI polyplexes achieved higher transfection ($p<0.01$) with the large plasmid (**Figure 2.3**). PBAE is a much less charge dense polycation than X2 and branched polyethyleneimine. These results affirm that sufficient positive charge must be supplied to

package plasmid DNA for cellular delivery. TransIT-X2 achieved higher transfection efficiency for both plasmids than the polycations tested. While X2 includes a polycationic component, it also includes an amphiphilic lipid-like component that could drive its high transfection activity. Systematic studies of polymer characteristics that drive improved DNA transfer efficacy have found that in addition to cationic character and titratable amines, hydrophobicity also has an effect on DNA condensation, polyplex stability, and cellular uptake.[3]

For both PBAE and PEI polyplexes, greater transfection efficiency was achieved with the small pGFP plasmid than with the large plasmid (**Figure 2.3**). Transgene expression has been shown to increase with the number of intracellular plasmid copies, but the plasmid molarity was matched in the treatment groups, thus differences in transfection could not be accounted for by plasmid copy number. It has been previously reported that optimized PEI and inactivated adenovirus were required to achieve similar transfection efficiencies of a >100 kb plasmid and a 7 kb plasmid, and the results were attributed to intracellular processes that limit efficiency of large DNA molecule expression.[48] Both plasmids evaluated in this study have molecular weights in the millions of Da and the larger plasmid is approximately twice the size of the smaller plasmid. It is possible that the smaller plasmid is more rapidly transported through the cytoplasm or more likely to pass through nuclear pores;[49,50] however, the plasmids are relatively similar in size and these two mechanisms are likely not responsible for plasmid size-dependence of transfection efficiency.

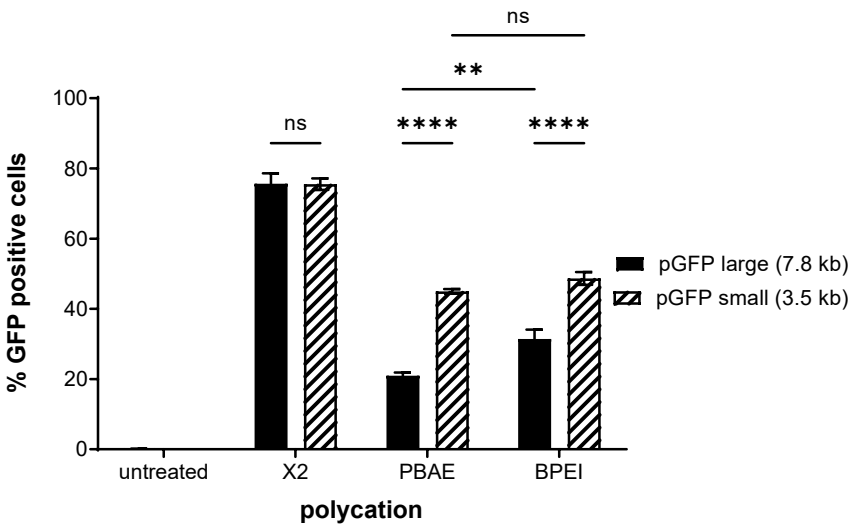

Figure 2.3 Effect of plasmid DNA size on polyplex transfection efficiency with different polycations. *DNA complex compositions were as follows: X2, 2 µL reagent: 1 µg DNA; PBAE (7 kDa), 20:1 mass ratio; BPEI (10 kDa), 3:1 mass ratio. Significance was evaluated using two-way ANOVA with Tukey multiple comparisons test. ns = not significant, *p<0.05, **p<0.01, ****p<0.0001, where the horizontal lines indicate groups being compared.*

2.3.4 Cell-type dependence of DNA transfer efficiency and transgene expression

Transfection efficiency (percent of cells that can uptake plasmid DNA) and transgene expression efficiency (extent to which target cells express the transgene) were found to be cell-type dependent (**Figure 2.4**). Previously, we used HEK 293T cells as the *in vitro* model system due their reliable growth and ease of transfection. However, HEK 293T cells are highly modified immortalized cancer cells engineered specifically to overproduce target proteins. To explore cell-type dependence of transfection efficiency, we selected several bone lineage cell lines to test, motivated by potential applications of transient DNA transfection to stimulate in situ growth factor expression in bone repair. More metabolically active osteosarcoma cell lines U2OS and MG63 were selected as bone lineage cell lines that have been used in nucleic acid delivery settings previously.[51–53] We also selected MC3T3-E1 murine pre-osteoblast cells, which are used in cell culture models of osteogenic differentiation and mineralization.[54,55] Compared to HEK 293T cells, U2OS, MG63, and MC3T3-E1 cells generally divide more slowly and have

limited expansion capacity.[52,56] In addition, transgene expression was expected to be lower in these cells because HEK 293T cells are modified to express proteins at very high levels.

U2OS, MG63, and E1 cells were transfected with DNA polyplexes containing increasing doses of BPEI or PBAE. Subsequent studies proceeded with the smaller pmaxGFP (3.5 kb) plasmid, due to its greater ease of cell transfection compared to the larger pHIV-EGFP plasmid (**Figure 2.3**). Polycation dose dependent increases in percent GFP positive cells and toxicity were observed for both U2OS and MG63 cells (**Figure 2.4A, B**). BPEI polyplexes achieved up to 70% transfection in both cell lines, while PBAE polyplexes achieved up to 25% transfection in both cells lines. BPEI polyplexes were very cytotoxic in MC3T3-E1 cells while PBAE polyplexes were less toxic, enabling 30% transfection at 30:1 mass ratio (**Figure 2.4C**).

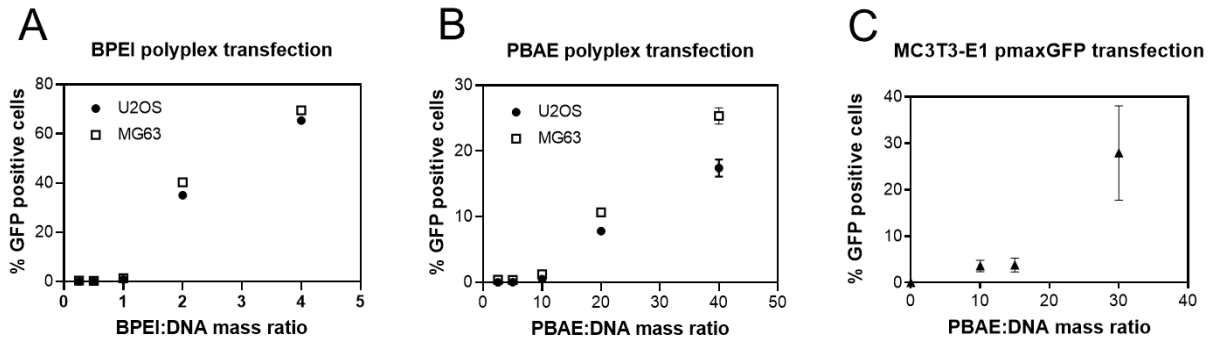

Figure 2.4 Polyplex transfection efficiency in various bone lineage cell lines *(A) BPEI polyplex transfection with increasing mass ratio in U2OS and MG63 cells (B) PBAE polyplex transfection of U2OS and MG63 cells (C) PBAE polyplex transfection of MC3T3-E1 cells.*

HEK 293T cells more frequently divide (doubling time 18-24 hours) than MC3T3-E1 cells (doubling time 38 hours),[57] MG63 cells (doubling time 38 hours),[58] and U2OS cells (doubling time 25-30 hours).[59] DNA that has been internalized can passively enter the nucleus during cell division, and as a result, mitotically active cells are more likely to express delivered plasmid DNA. Cell cycle also has a strong influence on transfection efficiency. Brunner et al. (2002) fractionated cell populations by size and density into fractions of discrete cell cycle phases and transfected cells at different phases with various non-viral and viral methods.[8] Luciferase activity

from cells transfected with polycation or lipid-based systems was 30- to 500-fold higher when transfection was performed during S or G2 phase compared with during G1 phase. This effect was less pronounced with recombinant adenovirus.[8] These results suggested that mitosis enhances non-viral transfection and that DNA complexes deposited in G1 cells are likely cleared or that S phase is inhibitory. Cell cycle and mitosis-dependence of transfection efficiency could explain why more rapidly dividing HEK 293T and U2OS cells are easier to transfect than MG63 and MC3T3-E1 cells.

2.4 Conclusions

This study investigated the effect of polycation molecular weight and chemistry, polyplex composition and polycation chemistry on *in vitro* DNA transfection efficacy. Polymer:DNA ratio was found to be a key determining factor for polyplex size, charge, and transfection efficiency, consistent with previously reported studies of polycation-mediated DNA delivery. The importance of free polycation chains for stabilizing polyplexes and for enhancing DNA delivery efficacy was discussed. Plasmid size and cell type were found to impact DNA polyplex transfection efficiency, with more effective delivery and expression of shorter plasmids and greater transfection achieved in rapidly dividing cells. Key factors discussed in this chapter, in particular polymer:DNA ratio, plasmid size, and cell type, are expected to impact DNA multilayer film transfection efficiency.

2.5 References

(1) Won, Y. Y.; Sharma, R.; Konieczny, S. F. Missing Pieces in Understanding the Intracellular Trafficking of Polycation/DNA Complexes. *J. Control. Release* **2009**, *139*, 88–93.

(2) Midoux, P.; Breuzard, G.; Gomez, J.; Pichon, C. Polymer-Based Gene Delivery: A Current Review on the Uptake and Intracellular Trafficking of Polyplexes. *Curr. Gene Ther.* **2008**, *8*, 335–352.

(3) Kumar, R.; Le, N.; Tan, Z.; Brown, M. E.; Jiang, S.; Reineke, T. M. Efficient Polymer-Mediated Delivery of Gene-Editing Ribonucleoprotein Payloads through Combinatorial Design, Parallelized Experimentation, and Machine Learning. *ACS Nano* **2020**, *14*, 17626–17639.

(4) Bengali, Z.; Pannier, A. K.; Segura, T.; Anderson, B. C.; Jang, J. H.; Mustoe, T. A.; Shea, L. D. Gene Delivery through Cell Culture Substrate Adsorbed DNA Complexes. *Biotechnol. Bioeng.* **2005**, *90*, 290–302.

(5) Dalal, R. J.; Kumar, R.; Ohnsorg, M.; Brown, M.; Reineke, T. M. Cationic Bottlebrush Polymers Outperform Linear Polycation Analogues for PDNA Delivery and Gene Expression. *ACS Macro Lett.* **2021**, *10*, 886–893.

(6) Itaka, K.; Ishii, T.; Hasegawa, Y.; Kataoka, K. Biodegradable Polyamino Acid-Based Polycations as Safe and Effective Gene Carrier Minimizing Cumulative Toxicity. *Biomaterials* **2010**, *31*, 3707–3714.

(7) Durymanov, M.; Reineke, J. Non-Viral Delivery of Nucleic Acids: Insight into Mechanisms of Overcoming Intracellular Barriers. *Front. Pharmacol.* **2018**, *9*, 1–15.

(8) Brunner, S.; Fürtbauer, E.; Sauer, T.; Kursa, M.; Wagner, E. Overcoming the Nuclear Barrier: Cell Cycle Independent Nonviral Gene Transfer with Linear Polyethylenimine or Electroporation. *Mol. Ther.* **2002**, *5*, 80–86.

(9) Kumar, R.; Santa Chalarca, C. F.; Bockman, M. R.; Bruggen, C. Van; Grimme, C. J.; Dalal, R. J.; Hanson, M. G.; Hexum, J. K.; Reineke, T. M. Polymeric Delivery of Therapeutic Nucleic Acids. *Chem. Rev.* **2021**, *121*, 11527–11652.

(10) Mäinnistö, M.; Reinisalo, M.; Ruponen, M.; Honkakoski, P.; Tammi, M.; Urtti, A. Polyplex-Mediated Gene Transfer and Cell Cycle: Effect of Carrier on Cellular Uptake and Intracellular Kinetics, and Significance of Glycosaminoglycans. *J. Gene Med.* **2007**, *9*, 479–487.

(11) Kim, J. A.; Aberg, C.; Salvati, A.; Dawson, K. A. Role of Cell Cycle on the Cellular Uptake and Dilution of Nanoparticles in a Cell Population. *Nat. Nanotechnol.* **2011**, *7*, 62–68.

(12) Schaffer, D. V.; Fidelman, N. A.; Dan, N.; Lauffenburger, D. A. Vector Unpacking as a Potential Barrier for Receptor-Mediated Polyplex Gene Delivery. *Biotechnol. Bioeng.* **2000**, *67*, 598–606.

(13) Zhang, J.; Fredin, N. J.; Janz, J. F.; Sun, B.; Lynn, D. M. Structure/Property Relationships in Erodible Multilayered Films: Influence of Polycation Structure on Erosion Profiles and the Release of Anionic Polyelectrolytes. *Langmuir* **2006**, *22*, 239–245.

(14) Jewell, C. M.; Zhang, J.; Fredin, N. J.; Lynn, D. M. Multilayered Polyelectrolyte Films Promote the Direct and Localized Delivery of DNA to Cells. *J. Control. Release* **2005**, *106*, 214–223.

(15) DeMuth, P. C.; Su, X.; Samuel, R. E.; Hammond, P. T.; Irvine, D. J. Nano-Layered Microneedles for Transcutaneous Delivery of Polymer Nanoparticles and Plasmid DNA. *Adv. Mater.* **2010**, *22*, 4851–4856.

(16) Lynn, D. M.; Langer, R. Degradable Poly(Beta-Amino Esters): Synthesis, Characterization, and Self-Assembly with Plasmid DNA. *J. Am. Chem. Soc.* **2000**, *122*, 10761–10768.

(17) Chou, J. J.; Berger, A. G.; Jalili-Firoozinezhad, S.; Hammond, P. T. A Design Approach for Layer-by-Layer Surface-Mediated SiRNA Delivery. *Acta Biomater.* **2021**, *135*, 331–

341.
(18) Akinc, A.; Anderson, D. G.; Lynn, D. M.; Langer, R. Synthesis of Poly(β-Amino Ester)s Optimized for Highly Effective Gene Delivery. *Bioconjug. Chem.* **2003**, *14*, 979–988.
(19) Green, J. J.; Langer, R.; Anderson, D. G. A Combinatorial Polymer Library Approach Yields Insight into Nonviral Gene Delivery. *Acc. Chem. Res.* **2008**, *41*, 749–759.
(20) Green, J. J. J.; Zugates, G. T. G. T.; Tedford, N. C. N. C.; Huang, Y. H. Y.-H.; Griffith, L. G. L. G.; Lauffenburger, D. A. D. A.; Sawicki, J. A. J. A.; Langer, R.; Anderson, D. G. D. G. Combinatorial Modification of Degradable Polymers Enables Transfection of Human Cells Comparable to Adenovirus. *Adv. Mater.* **2007**, *19*, 2836–2842.
(21) Castleberry, S. A.; Almquist, B. D.; Li, W.; Reis, T.; Chow, J.; Mayner, S.; Hammond, P. T. Self-Assembled Wound Dressings Silence MMP-9 and Improve Diabetic Wound Healing in Vivo. *Adv. Mater.* **2016**, *28*, 1809–1817.
(22) DeMuth, P. C.; Min, Y.; Huang, B.; Kramer, J. A.; Miller, A. D.; Barouch, D. H.; Hammond, P. T.; Irvine, D. J. Polymer Multilayer Tattooing for Enhanced DNA Vaccination. *Nat. Mater.* **2013**, *12*, 367–376.
(23) Pack, D. W.; Hoffman, A. S.; Pun, S.; Stayton, P. S. Design and Development of Polymers for Gene Delivery. *Nat. Rev. Drug Discov.* **2005**, *4*, 581–593.
(24) Van Der Aa, M. A. E. M.; Huth, U. S.; Häfele, S. Y.; Schubert, R.; Oosting, R. S.; Mastrobattista, E.; Hennink, W. E.; Peschka-Süss, R.; Koning, G. A.; Crommelin, D. J. A. Cellular Uptake of Cationic Polymer-DNA Complexes via Caveolae Plays a Pivotal Role in Gene Transfection in COS-7 Cells. *Pharm. Res.* **2007**, *24*, 1590–1598.
(25) Varga, C. M.; Tedford, N. C.; Thomas, M.; Klibanov, A. M.; Griffith, L. G.; Lauffenburger, D. A. Quantitative Comparison of Polyethylenimine Formulations and Adenoviral Vectors in Terms of Intracellular Gene Delivery Processes. *Gene Ther.* **2005**, *12*, 1023–1032.
(26) Boussif, O.; Lezoualc'ht, F.; Zanta, M. A.; Mergnyt, D.; Schermant, D.; Demeneixt, B.; Behr, J.-P. A Versatile Vector for Gene and Oligonucleotide Transfer into Cells in Culture and in Vivo: Polyethylenimine. *Biochemistry* **1995**, *92*, 7297–7301.
(27) Oh, Y. K.; Suh, D.; Kim, J. M.; Choi, H. G.; Shin, K.; Ko, J. J. Polyethylenimine-Mediated Cellular Uptake, Nucleus Trafficking and Expression of Cytokine Plasmid DNA. *Gene Ther.* **2002**, *9*, 1627–1632.
(28) Gallops, C.; Ziebarth, J.; Wang, Y. A Polymer Physics Perspective on Why PEI Is an Effective Nonviral Gene Delivery Vector. *ACS Symp. Ser.* **2020**, *1350*, 1–12.
(29) Pear, W. S.; Nolan, G. P.; Scott, M. L.; Baltimore, D. Production of High-Titer Helper-Free Retroviruses by Transient Transfection. *Proc. Natl. Acad. Sci. U. S. A.* **1993**, *90*, 8392–8396.
(30) Lin, Y. C.; Boone, M.; Meuris, L.; Lemmens, I.; Van Roy, N.; Soete, A.; Reumers, J.; Moisse, M.; Plaisance, S.; Drmanac, R.; *et al.* Genome Dynamics of the Human Embryonic Kidney 293 Lineage in Response to Cell Biology Manipulations. *Nat. Commun.* **2014**, *5*, 1–12.
(31) Monnery, B. D.; Wright, M.; Cavill, R.; Hoogenboom, R.; Shaunak, S.; Steinke, J. H. G.; Thanou, M. Cytotoxicity of Polycations: Relationship of Molecular Weight and the Hydrolytic Theory of the Mechanism of Toxicity. *Int. J. Pharm.* **2017**, *521*, 249–258.
(32) Fliervoet, L. A. L.; Lisitsyna, E. S.; Durandin, N. A.; Kotsis, I.; Maas-Bakker, R. F. M.; Yliperttula, M.; Hennink, W. E.; Vuorimaa-Laukkanen, E.; Vermonden, T. Structure and Dynamics of Thermosensitive PDNA Polyplexes Studied by Time-Resolved Fluorescence Spectroscopy. *Biomacromolecules* **2019**, *21*, 73–88.
(33) Ketola, T. M.; Hanzlíková, M.; Leppänen, L.; Raviña, M.; Bishop, C. J.; Green, J. J.; Urtti, A.; Lemmetyinen, H.; Yliperttula, M.; Vuorimaa-Laukkanen, E. Independent versus Cooperative Binding in Polyethylenimine-DNA and Poly(l-Lysine)-DNA Polyplexes. *J. Phys. Chem. B* **2013**, *117*, 10405–10413.
(34) Monnery, B. D. Polycation-Mediated Transfection: Mechanisms of Internalization and

Intracellular Trafficking. *Biomacromolecules* **2021**, *22*, 4060–4083.
(35) Clamme, J. P.; Azoulay, J.; Mély, Y. Monitoring of the Formation and Dissociation of Polyethylenimine/DNA Complexes by Two Photon Fluorescence Correlation Spectroscopy. *Biophys. J.* **2003**, *84*, 1960–1968.
(36) Boeckle, S.; Gersdorff, K. von; Piepen, S. van der; Culmsee, C.; Wagner, E.; Ogris, M.; von Gersdorff, K.; van der Piepen, S.; Culmsee, C.; Wagner, E.; *et al.* Purification of Polyethylenimine Polyplexes Highlights the Role of Free Polycations in Gene Transfer. *J. Gene Med.* **2004**, *6*, 1102–1111.
(37) Yue, Z. G.; Wei, W.; Lv, P. P.; Yue, H.; Wang, L. Y.; Su, Z. G.; Ma, G. H. Surface Charge Affects Cellular Uptake and Intracellular Trafficking of Chitosan-Based Nanoparticles. *Biomacromolecules* **2011**, *12*, 2440–2446.
(38) Thibault, M.; Nimesh, S.; Lavertu, M.; Buschmann, M. D. Intracellular Trafficking and Decondensation Kinetics of Chitosan–PDNA Polyplexes. *Mol. Ther.* **2010**, *18*, 1787–1795.
(39) Ketola, T.-M.; Hanzlíková, M.; Urtti, A.; Lemmetyinen, H.; Yliperttula, M.; Vuorimaa, E. Role of Polyplex Intermediate Species on Gene Transfer Efficiency: Polyethylenimine−DNA Complexes and Time-Resolved Fluorescence Spectroscopy. *J. Phys. Chem. B* **2011**, *115*, 1895–1902.
(40) Ruponen, M.; Rönkkö, S.; Honkakoski, P.; Pelkonen, J.; Tammi, M.; Urtti, A. Extracellular Glycosaminoglycans Modify Cellular Trafficking of Lipoplexes and Polyplexes. *J. Biol. Chem.* **2001**, *276*, 33875–33880.
(41) Ruponen, M.; Honkakoski, P.; Tammi, M.; Urtti, A. Cell-Surface Glycosaminoglycans Inhibit Cation-Mediated Gene Transfer. *J. Gene Med.* **2004**, *6*, 405–414.
(42) Bausinger, R.; Von Gersdorff, K.; Braeckmans, K.; Ogris, M.; Wagner, E.; Bräuchle, C.; Zumbusch, A. The Transport of Nanosized Gene Carriers Unraveled by Live-Cell Imaging. *Angew. Chem. Int. Ed. Engl.* **2006**, *45*, 1568–1572.
(43) Klauber, T. C. B.; Søndergaard, R. V.; Sawant, R. R.; Torchilin, V. P.; Andresen, T. L. Elucidating the Role of Free Polycations in Gene Knockdown by SiRNA Polyplexes. *Acta Biomater.* **2016**, *35*, 248–259.
(44) Dai, Z.; Gjetting, T.; Mattebjerg, M. A.; Wu, C.; Andresen, T. L. Elucidating the Interplay between DNA-Condensing and Free Polycations in Gene Transfection through a Mechanistic Study of Linear and Branched PEI. *Biomaterials* **2011**, *32*, 8626–8634.
(45) Payne, C. K.; Jones, S. A.; Chen, C.; Zhuang, X. Internalization and Trafficking of Cell Surface Proteoglycans and Proteoglycan-Binding Ligands. *Traffic* **2007**, *8*, 389–401.
(46) Vaidyanathan, S.; Chen, J.; Orr, B. G.; Banaszak Holl, M. M. Cationic Polymer Intercalation into the Lipid Membrane Enables Intact Polyplex DNA Escape from Endosomes for Gene Delivery. *Mol. Pharm.* **2016**, *13*, 1967–1978.
(47) Cai, J.; Yue, Y.; Wang, Y.; Jin, Z.; Jin, F.; Wu, C. Quantitative Study of Effects of Free Cationic Chains on Gene Transfection in Different Intracellular Stages. *J. Control. Release* **2016**, *238*, 71–79.
(48) Baker, A.; Cotten, M. Delivery of Bacterial Artificial Chromosomes into Mammalian Cells with Psoralen-Inactivated Adenovirus Carrier. *Nucleic Acids Res.* **1997**, *25*, 1950–1956.
(49) Vaughan, E. E.; Dean, D. A. Intracellular Trafficking of Plasmids during Transfection Is Mediated by Microtubules. *Mol. Ther.* **2006**, *13*, 422–428.
(50) Friend, D. S.; Papahadjopoulos, D.; Debs, R. J. Endocytosis and Intracellular Processing Accompanying Transfection Mediated by Cationic Liposomes. *Biochim. Biophys. Acta* **1996**, *1278*, 41–50.
(51) Wang, Y.; Li, J.; Oupický, D. Polymeric Plerixafor: Effect of PEGylation on CXCR4 Antagonism, Cancer Cell Invasion, and DNA Transfection. *Pharm. Res.* **2014**, *31*, 3538–3548.
(52) Corsi, K.; Chellat, F.; Yahia, L.; Fernandes, J. C. Mesenchymal Stem Cells, MG63 and

HEK293 Transfection Using Chitosan-DNA Nanoparticles. *Biomaterials* **2003**, *24*, 1255–1264.
(53) Fouriki, A.; Clements, M. A.; Farrow, N.; Dobson, J. Efficient Transfection of MG-63 Osteoblasts Using Magnetic Nanoparticles and Oscillating Magnetic Fields. *Ann. Am. Thorac. Soc.* **2012**, *8*, 169–175.
(54) Yamano, S.; Dai, J.; Moursi, A. M. Comparison of Transfection Efficiency of Nonviral Gene Transfer Reagents. *Mol. Biotechnol.* **2010**, *46*, 287–300.
(55) Jiang, Q. H.; Liu, L.; Peel, S.; Yang, G. L.; Zhao, S. F.; He, F. M. Bone Response to the Multilayer BMP-2 Gene Coated Porous Titanium Implant Surface. *Clin. Oral Implants Res.* **2013**, *24*, 853–861.
(56) Yang, H. Y.; Vonk, L. A.; Licht, R.; Van Boxtel, A. M. G.; Bekkers, J. E. J.; Kragten, A. H. M.; Hein, S.; Varghese, O. P.; Howard, K. A.; Cumhur Öner, F.; *et al.* Cell Type and Transfection Reagent-Dependent Effects on Viability, Cell Content, Cell Cycle and Inflammation of RNAi in Human Primary Mesenchymal Cells. *Eur. J. Pharm. Sci.* **2014**, *53*, 35–44.
(57) MC3T3-E1 Subclone 4 | ATCC https://www.atcc.org/products/crl-2593 (accessed Jan 4, 2022).
(58) MG-63 | ATCC https://www.atcc.org/products/crl-1427 (accessed Jan 4, 2022).
(59) U-2 OS | ATCC https://www.atcc.org/products/htb-96 (accessed Jan 4, 2022).

Chapter 3. Solution conditions for layer-by-layer assembly of DNA multilayer films with high loading and sustained release behavior

3.1 Introduction

Layer-by-layer (LbL) self-assembly is a versatile method that has been applied broadly to fabricate nano- to micrometer scale thin films. Electrostatic LbL involves alternating deposition of oppositely charged polymers to form a multilayer thin film coating. Other intermolecular interactions, including hydrophobic, hydrogen bonding, host-guest, covalent bonding, and receptor-ligand interactions may also be leveraged to form LbL multilayers.[1–5] LbL self-assembly has been applied to conformally coat various substrate materials and geometries, including bandages, sutures, stents, and orthopedic implants,[6–13] providing a means of modulating tissue-material interactions or delivering therapeutics. Polymer multilayer films have been successfully constructed with precise control of drug loading and release kinetics for antibiotics, anti-inflammatory drugs, chemotherapeutics, protein growth factors, and nucleic acids.[6,11,14–19] Importantly, these therapeutics remained biologically active upon release in the target site due to the gentle, aqueous conditions of LbL assembly.

Temperature, ionic strength, and pH affect physicochemical properties of polyelectrolytes and their interactions. Polyelectrolyte self-assembly involves charged polymer segments replacing associated counterions driven by the entropy gain from release of counterions and water molecules.[5,20] Increasing salt concentration increases ionic shielding in polyelectrolytes, allowing formation of thicker films. Ionic shielding along the backbone of polyelectrolytes allows adsorption in loopy conformations, resulting in greater polymer mass and thicker layers deposited per surface area. Above a threshold salt concentration, however, interactions between film components are abrogated, preventing film growth. The amount of polymer adsorbed per layer is capped due to self-electrostatic repulsion and surface charge reversal.[5] Polymer molecular weight, polyelectrolyte concentration, adsorption time, and assembly method also affect LbL assembly.

LbL incorporation of DNA enables sustained delivery of nucleic acid and creates opportunity to co-release transfection enhancing polymers.[21] Plasmid DNA is an anionic polyelectrolyte, which makes it favorable for incorporation in electrostatic LbL assemblies. Incorporation of DNA as an LbL component can enable precise control of DNA loading simply by controlling the number of layers deposited. Furthermore, the specific cationic polymers used in LbL assembly can be selected to facilitate intracellular pDNA delivery.

Several groups have successfully incorporated DNA and other nucleic acids in polymer multilayer films of diverse architectures and compositions for *in vitro* and *in vivo* therapies.[6,10,17,21–23] However, there remains a need to elucidate fundamental LbL assembly conditions that enable efficient DNA multilayer assembly for transfection. An effective DNA delivery system must satisfy several design criteria: tunable loading, sustained release, and delivery of biologically active plasmid DNA. Key to this approach is temporal control. Robust drug loading and controlled release behavior of LbL films is highly dependent on the specific components used and assembly parameters require optimization for DNA incorporation.

Chapter scope: The work described in this chapter explores the impact of different LbL assembly parameters on DNA multilayer film growth, composition, and release kinetics. The parameters studied included pH, ionic strength, DNA concentration, and number of PBAE/DNA bilayers. Understanding and optimizing these solution conditions for robust film growth and predictable polycation and DNA incorporation will enable rational design of DNA multilayer films for surface-mediated nucleic acid delivery.

3.2 Methods

3.2.1 Materials

NaCl powder was purchased from Macron Fine Chemicals. Plasmid DNAs encoding green fluorescent protein pmaxGFP (gift from Dr. Robert Weinberg's lab at MIT) and pHIV-eGFP (gift from Dr. Jiahe Li's lab at Northeastern University) were produced in *E. coli* DH5α and purified using ZymoPURE II Plasmid Gigaprep kits (Zymo Research, Irvine, CA) or produced

commercially by GenScript (Piscataway, NJ). HyClone molecular biological grade water was purchased from Fisher Scientific. Silicon wafers were obtained from WaferPro (Santa Clara, CA). PBAE was synthesized as previously described.[7,24] Linear polyethyleneimine (25 kDa) was obtained from Polysciences (Warrington, PA). Phosphate buffered saline (PBS) was purchased from Lonza (Morristown, NJ). Accublue Broad and High Sensitivity dsDNA Quantitation kits were obtained from Biotium (Fremont, CA). MicroBCA Protein Assay Kit was purchased from ThermoFisher Scientific (Waltham, MA). All other materials were obtained from Millipore Sigma (St. Louis, MO). Chemicals were stored per manufacturer's instructions.

3.2.2 Cell culture

Human epithelial kidney 293T (HEK 293T) cells were a gift from Dr. Jiahe Li's Lab at Northeastern University. U2OS human osteosarcoma cells were a gift from Dr. Michael Yaffe's Lab at MIT. MC3T3-E1 murine pre-osteoblast subclone 4 were purchased from ATCC. HEK and U2OS cells were cultured in Dulbecco's Modified Eagle Medium (DMEM, Corning, NY), supplemented with 10% Fetal Bovine Serum (FBS) and 1% penicillin-streptomycin. MC3T3-E1 cells were cultured in α Minimum Essential Medium (αMEM, ThermoFisher, MA) supplemented with 10% FBS and 1% penicillin-streptomycin. These cells tested negative for mycoplasma after thawing from storage and monthly during culture using Lonza MycoAlert kit (Morristown, NJ).

3.2.3 Layer-by-layer film assembly

LbL films were deposited on plasma-treated silicon substrates. Silicon substrates were cleaned with methanol, ethanol, and ultra-pure water and then dried under nitrogen. Cleaned silicon substrates approximately 0.5 x 2.0 cm^2 were oxygen plasma treated at high RF power for 90 seconds using a Harrick PDC-32G plasma cleaner. The treated silicon substrates were immediately immersed in the first cationic solution for at least 30 minutes. A Carl Zeiss HMS-DS50 automated slide stainer (Oberkochen, Germany) was used to assemble the LbL films. Completed films were allowed to air dry and stored in a vacuum desiccator at room temperature until analysis.

The PBAE (Poly 2) was dissolved for 1 hour on a rotating mixer at 1 mg/mL in 100 mM sodium acetate buffer (pH 5.2). The PBAE solution was then filtered through a sterile 0.2 μm cellulose acetate syringe filter. PBAE was dissolved fresh daily due to its hydrolysable nature. Plasmid DNA was diluted from 1-3 mg/mL stocks to the desired concentration in MilliQ (18 mΩ) water or 10 mM sodium acetate (pH 5.2). DNA solutions were not filtered to minimize loss of plasmid. For experiments varying buffer pH and ionic strength, PBAE was dissolved in 100 mM or 1 M sodium acetate and the pH was adjusted to 5, 5.5, 6, 6.5 with 0.1 M sodium hydroxide (NaOH). Plasmid DNA was dissolved in MilliQ water (pH 4.5) or 100 mM sodium acetate, which was then adjusted to pH 5 or pH 6.5 with 0.1 M hydrochloric acid (HCl) or NaOH. PBAE/DNA bilayer films were constructed by alternate dipping in the polycation solution for 10 minutes followed by two consecutive 30 second rinse steps in 10 mM sodium acetate (pH 5.2), and then into the polyanion solution for 10 minutes followed by two 30 second rinses in 10 mM sodium acetate. This cycle was repeated until the desired number of bilayers was deposited.

For films containing a baselayer, protamine sulfate (PrS) was dissolved at 2 mg/mL and poly(4-styrene-sulfonate) (SPS) at 5 mM with respect to the repeat unit (3.7 mg/mL) in 100 mM sodium acetate, pH 5.2. Baselayers were deposited by alternating immersion in PrS and SPS solutions for 10 minutes, separated by two 1 min 100 mM sodium acetate rinses.

3.2.4 Characterization of DNA nanolayer film thickness and roughness

Film thickness and surface roughness were measured using a Dektak Stylus profilometer (Veeco Instruments Inc, Plainview, NY). Dry films were scored with a razor blade and film thickness and roughness were measured at four locations on the film. The measurements at the four locations were averaged.

3.2.5 Quantification of total DNA and PBAE content

DNA nanolayered films were completely disrupted by incubating films in high salt solution (1X PBS with 2M NaCl) overnight with agitation. The total amount of DNA released into solution was analyzed using Accublue DNA Quantitation kits (Biotium) per manufacturer

instructions and by NanoDrop. Total DNA loading was normalized by film surface area and reported as nanograms or micrograms of DNA per cm^2. The Pierce MicroBCA Protein Assay Kit (ThermoFisher Scientific, Waltham, MA) was repurposed to quantify PBAE polycation in the releasate,[7] taking advantage of polymer backbone amide groups to chelate and reduce copper in the BCA reaction.

3.2.6 Quantification of DNA release kinetics

Films constructed on silicon chips were cut into 0.5 cm x 0.5 cm pieces and immersed in 500 µL PBS, pH 7.4 at 37°C in a shaking incubator. At each timepoint, the silicon chip was transferred to a fresh PBS aliquot and returned to the incubator. DNA release into PBS from film constructs was quantified using the Accublue DNA Quantitation kit or by comparing fluorescently tagged DNA signal to a standard curve of tagged DNA concentrations.

3.2.7 In vitro transfection

For analysis of DNA polyplex transfection, cells were seeded at 10,000 cells/well in 96-well tissue culture plates the day before transfection such that cells were 70% confluent at the time of transfection. Culture medium was changed to transfection medium (7% FBS) prior to treatment. Cells were incubated with DNA polyplexes for 8 hours before replacing media with complete media. Cells were then maintained at 37°C and 5% CO_2 for 48 hours before analysis by flow cytometry.

For analysis of DNA film transfection, cells were seeded at 10,000 cells/well in 96-well, 20,000 cells/well in 48-well, or 40,000 cells/well in 24-well tissue culture plates the day before transfection. Culture medium was changed to fresh complete media prior to treatment. DNA films were placed directly in the cell culture wells, with the film in contact with the cell layer. Media was changed every 2 days until analysis. As a positive transfection control, Mirus TransIT-X2 (X2) or LT1 was mixed with pGFP diluted in OptiMEM at a 2:1 ratio (X2 µL:DNA µg) and incubated at room temperature for 20 minutes. X2 complexes were delivered to cells at the same DNA dosages as the polyplex formulations (200 ng DNA per well).

3.2.8 Measuring GFP transfection efficiency via flow cytometry

Transfection efficiency was quantified by measuring the fraction of treated cells that successfully took up and expressed the delivered GFP plasmid. 2 days after polyplex treatment or 4 or 7 days after film treatment was initiated, cells were trypsinized and resuspended in warm media before centrifuging at 300 rcf for 5 minutes. Harvested cells were resuspended in PBS with NucBlue Live Cell Stain (ThermoFisher) or ZombieViolet Viability Dye diluted 1:500 and incubated protected from light for 15 minutes. Resuspended cells were transferred to 96-well V bottom plates, centrifuged at 300 rcf for 5 minutes, and resuspended in PBS with 1% FBS. Cells were analyzed on a BD FACSCelesta Cell Analyzer. NucBlue or ZombieViolet was read with a 405nm laser and 450/40 filter set, GFP fluorescence with a 488nm laser and 530/30 filter set, and Cy3 or Cy5 labelled DNA with a 561nm laser and 586/15 or 670/30 filter set. Flow cytometry data was analyzed using Flow Jo (BD, Ashland, OR). Data was first gated to isolate single cells negative for the viability stain and then gated for DNA fluorescence, indicating cellular association or uptake of DNA and for GFP expression, indicating expression of delivered plasmid DNA. The fraction of single cells that were GFP positive (% GFP positive) was taken as a measure of transfection efficiency.

3.2.9 Statistical analysis

Statistical analysis was performed using GraphPad Prism 9 software (San Diego, CA). Data are reported as mean ± standard deviation of a minimum of 3 samples. Each LbL film formulation was tested in triplicate and in two separate trials. Statistical significance was evaluated using ANOVA with Tukey's multiple comparisons test. Significance levels are indicated as follows: *$p \leq 0.05$, **$p \leq 0.01$, ***$p \leq 0.001$, ****$p \leq 0.0001$.

3.3 Results and Discussion

3.3.1 Impact of DNA dipping concentration on LbL assembly and release

LbL films were assembled on silicon substrates. The poly(beta-amino ester) (PBAE) Poly 2 was selected as the polycation partner for plasmid DNA for its high transfection activity,

biodegradability, and longer degradation half-life as compared with Poly 1.[16,25,26] A two-component bilayer architecture is denoted (polycation/polyanion)n, where n is the number of polycation/polyanion bilayers. The plasmid DNA used encoded green fluorescent protein (GFP).

Solution conditions including polyelectrolyte concentration, pH, and ionic strength have a dramatic impact on the molecular scale interactions that drive LbL self-assembly. Previously developed DNA multilayers from the Lynn Lab and the Hammond Lab incorporated PBAE at 2 mg/mL and plasmid DNA at 1 mg/mL with different baselayers separating the substrate and the DNA layer.[10,17,27] Although LbL self-assembly enables high weight % loading of DNA, a large amount of DNA is lost to the dipping solutions and rinse baths.[28] The potential to use lower DNA dipping concentrations for (PBAE/DNA) multilayer assembly was explored here. Driving assembly conditions further from equilibrium strengthens kinetic control of LbL assembly, amplifying the impact of dip adsorption time and solution concentration on film composition.

PBAE and plasmid DNA solutions of different concentrations were alternately adsorbed to silicon chips and film thickness and total DNA content were quantified. Below 50 μg/mL of DNA, films formed poorly and incorporated very little plasmid (**Figure 3.1A**). Profilometer measurements indicated the multilayer film thickness increased linearly with the number of bilayers deposited. The amount of material adsorbed per bilayer increased with increasing DNA concentration, based on film thickness and total DNA loading. Increasing the adsorption time from 5 to 15 minutes also increased total DNA loading at all DNA concentrations (**Figure 3.1B**). These time-dependent and concentration-dependent trends reflect kinetically controlled electrostatic assembly of the multilayer films.[29] The linear increase of film total DNA content with the number of bilayers deposited offers a method to precisely tune DNA loading.

To examine the kinetics of plasmid DNA release from the bilayer films, 40 bilayer films were constructed with 50, 100, and 500 μg/mL DNA. **Figure 3.1C** shows the cumulative release of DNA into PBS as a percentage of total DNA loading in the film. Fractional DNA release is the cumulative amount of DNA released over time scaled by the total DNA loading of each sample.

Sustained release of plasmid DNA was achieved over at least two weeks, with 50% of DNA released in 1-2 days, 70% released in 5 days, and 100% released in 10-12 days (**Figure 3.1C**). No particular trend was observed in the relative rate of DNA release from films with an increasing concentration of DNA in the LbL assembly solution. Gradual film erosion resulting in slow DNA release is consistent with previous studies of DNA release from (PBAE/DNA) films and suggests that DNA release is driven by hydrolysis of PBAE ester bonds at or close to the film surface.[30–32]

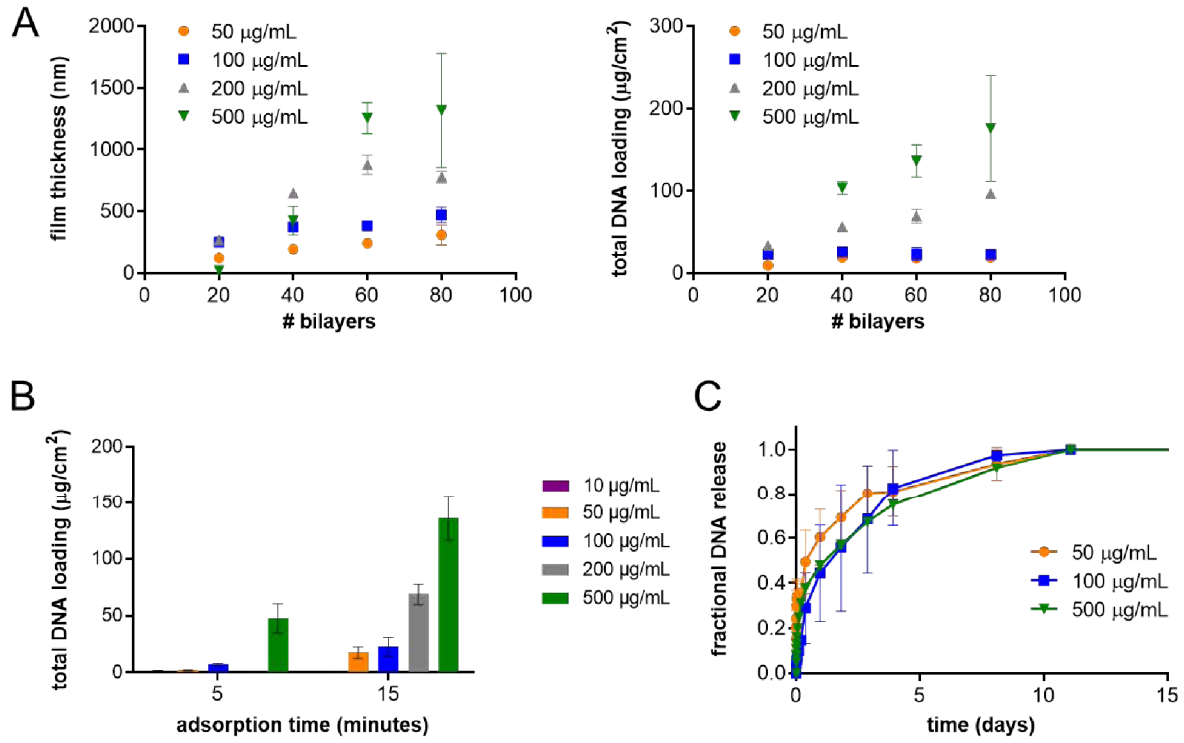

Figure 3.1 Impact of DNA dipping concentration on LbL assembly and release *(A) (PBAE/DNA) film thickness and total DNA loading per film surface area as function of DNA dipping concentration and number of bilayers (B) Total DNA loading dependence on adsorption time and DNA concentration (C) Cumulative fractional DNA release kinetics from (PBAE/DNA) films.*

3.3.2 Solution pH and ionic strength-dependent changes in film growth and DNA release behavior

To investigate the effect of pH during film assembly on LbL film composition and DNA release, Poly 2 and DNA bilayer films were constructed at fixed pH of 5, 5.5, and 6. At lower pH,

more tertiary amines in the Poly 2 backbone are protonated and the polymer is more positively charged.[7] In this narrow range of pH, the charge on the phosphate groups in the DNA backbone is unaffected. While the overall film thickness did not vary with pH, the total DNA content in films was lower in films constructed at pH 6 than in films made at pH 5 (**Figure 3.2A**). This could indicate that films assembled at pH 6 had relatively lower DNA content and relatively greater PBAE content than films assembled at pH 5. Chou and Berger et al. (2021) similarly observed that increasing the assembly pH of (PBAE/siRNA) films towards the polymer pKa resulted in increased polymer loading and decreased siRNA loading.[7] Less charged polymer chains deposit on a charged surface in a more globular, loopy conformation than more charged polymer chains, which would deposit in a more extended conformation.[33] Because the PBAE layer is less densely charged at pH 6 than at pH 5, the amount of plasmid DNA that can adsorb per layer to neutralize the charge is decreased. The total DNA loading increased with increasing bilayers of films assembled at pH 5 and pH 5.5, while total DNA loading appeared to plateau in film assembled at pH 6 (**Figure 3.2B**). This could indicate that in pH 6 conditions, above 20 bilayers, the adsorbed PBAE layer was not sufficiently positively charged to adsorb more plasmid DNA and continue multilayer growth.

Films constructed at pH 6 released DNA more slowly than films constructed at pH 5.5 and pH 5, releasing 100% of DNA content over two weeks, while films constructed at pH 5 released 100% of DNA after 5 days (**Figure 3.2C-D**). The time to release 50% of total DNA when immersed in pH 7.4 PBS also varied with film assembly pH: 5.5 days for films made at pH 6, 3.4 days for films made at pH 5.5, and 0.51 days for films made at pH 5 (**Figure 3.2D**). A potential explanation for this observation could be the difference in PBAE conformation at the different LbL assembly pHs. Klitzing and Mohwald (1996) found that transport of a rhodamine dye molecule was faster through flat polyelectrolyte multilayer films constructed at low ionic strength than through loopy films assembled at high ionic strength.[34] They attribute this to the less tightly packed structure within a polycation or a polyanion layer, due to increased repulsion

between same charged polyelectrolyte chains. Although DNA is several orders of magnitude larger than rhodamine, a similar theory could be applied to films assembled with highly charged PBAE (pH 5), where the less tightly packed polyelectrolytes enable more rapid film dissolution and DNA release, while weakly charged PBAE at pH 6 results in closer packing of PBAE chains and can slow DNA release kinetics.

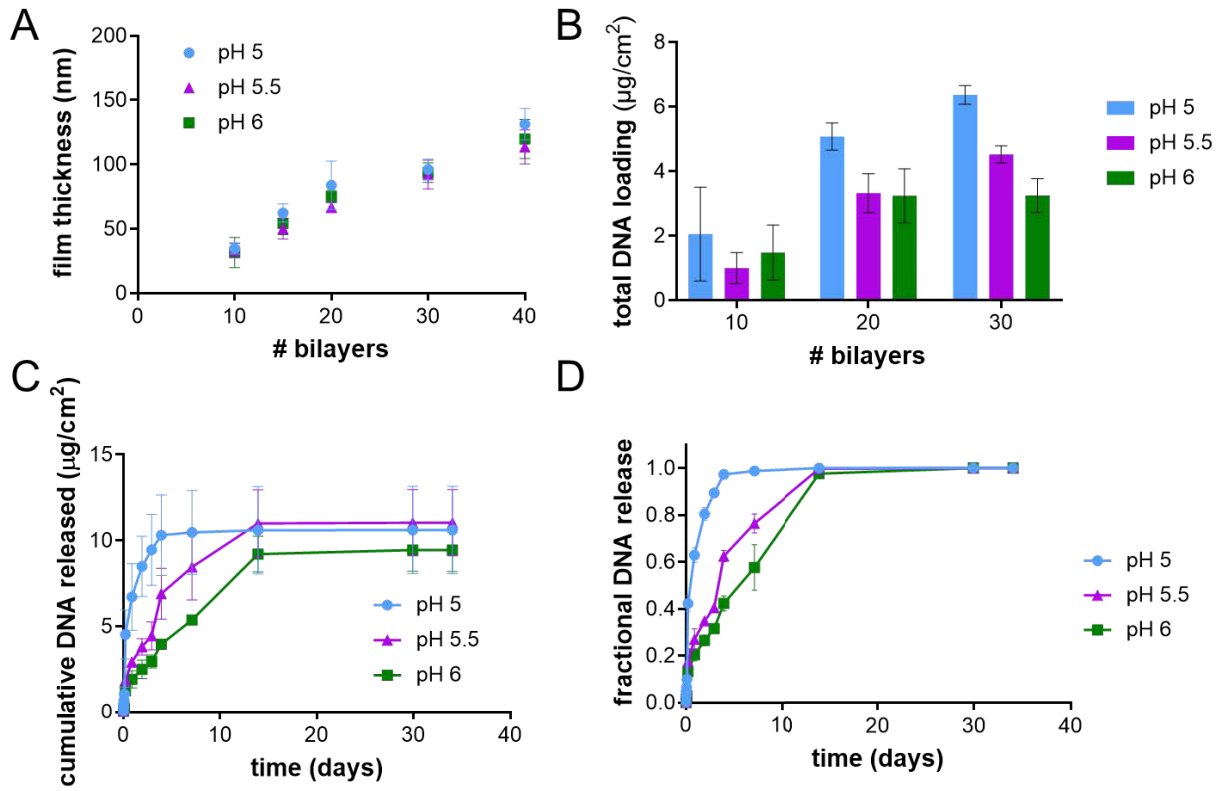

Figure 3.2 Impact of LbL assembly pH on film growth, DNA loading and release kinetics *(A) (PBAE/DNA) bilayer film thickness increases at similar rates regardless of assembly pH. (B) Less DNA is incorporated as assembly pH approaches the pKa of the PBAE, due to decreased ionization of the polycation. (C-D) DNA release rate at pH 7.4 changes depending on film assembly pH.*

3.3.3 Increasing (PBAE/DNA) bilayers slows DNA release kinetics from LbL films

To explore the impact of film thickness on DNA release kinetics, PBAE/DNA films were constructed with 0.05 or 0.2 mg/mL DNA and 40, 60, 80, and 100 bilayers. The cumulative mass of DNA released and fraction of total DNA loading released over time are depicted in **Figure 3.3A** for films constructed at 0.05 mg/mL DNA and **Figure 3.3B** for films constructed at

0.2 mg/mL DNA. Generally, increasing the number of PBAE/DNA layers increased total DNA content and slowed DNA release rate over time. For 0.05 mg/mL DNA films, the time to release 50% of the film total DNA content ($t_{50\%}$) for 40, 60, 80 bilayers were around 1.8 days, while 100 bilayers increased $t_{50\%}$ to 8.3 days (**Figure 3.3A**). For 0.2 mg/mL DNA films, doubling the number of film bilayers from 40 to 80 bilayers slowed DNA release substantially, increasing $t_{50\%}$ from 1.6 days to 7.9 days (**Figure 3.3B**). Similar fractional DNA release profiles between films assembled at different DNA concentrations is consistent with data presented in **Figure 3.1C**. The burst-like release of 90% of DNA in 2-5 days for 40 and 60 bilayer films reflects diffusion or bulk dissociation-based release.[26] Due to the high molecular weight of plasmid DNA (3-4 MDa) and the multivalent electrostatic interactions between DNA and PBAE, the burst occurs over a longer timescale than for low molar mass drugs, which rapidly release within a few hours.

The permeability of LbL assembled polyelectrolyte multilayer films has also been shown to decrease with film thickness and increasing layer number.[35] Additionally, interlayer penetration of polyelectrolyte components and entanglement of polymer chains both increase with more layers deposited and can contribute to slowing of film dissolution. These results are consistent with studies of other linearly growing LbL systems (e.g., PBAE and dextran sulfate),[36] demonstrating that the rate and duration of DNA release can be tuned simply by changing the number of deposited layers.

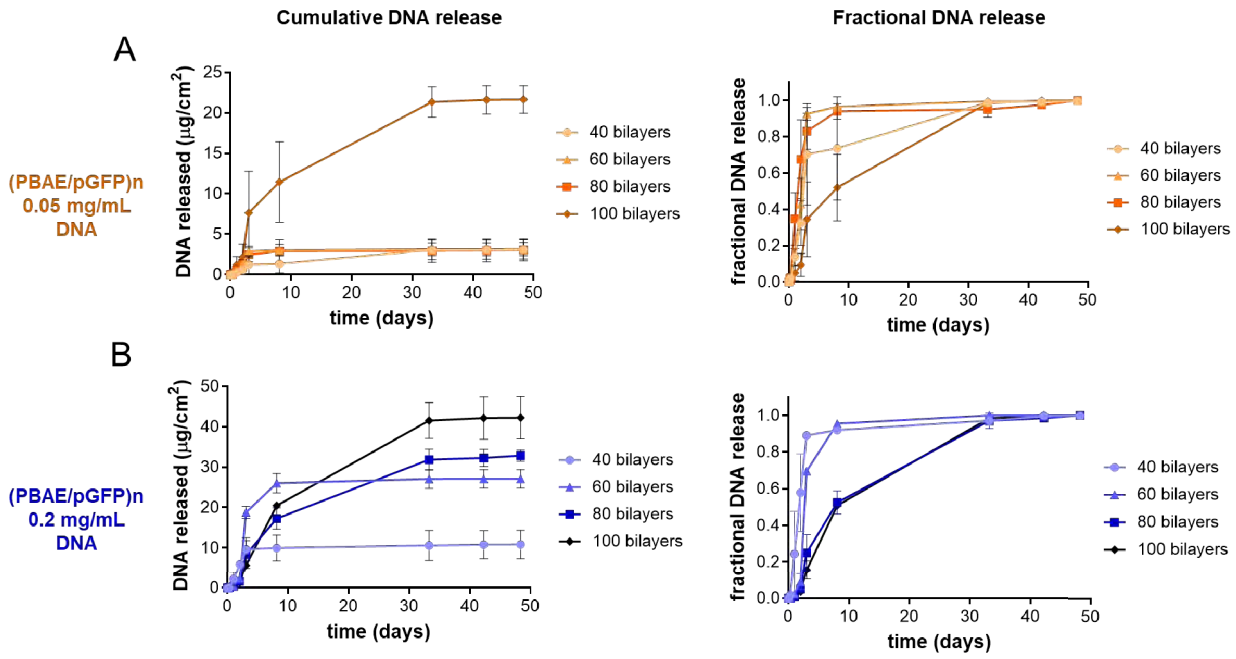

Figure 3.3 Increasing (PBAE/DNA) film thickness slows DNA release kinetics *(A) Cumulative mass of DNA released per film surface area and fraction of total DNA content released over time for films constructed with 0.05 mg/mL DNA (B) Cumulative mass of DNA released and fractional DNA released over time for films constructed with 0.2 mg/mL DNA.*

3.3.4 Calculating total polymer and DNA incorporated into LbL bilayer films

As described in Chapter 2, the relative polymer and DNA content in polyplexes is a critical determinant of successful DNA condensation and polycation-mediated transfection. We hypothesized that polymer:DNA ratio would also be important in film-mediated DNA delivery and sought to quantify the overall polymer:DNA mass ratio incorporated in (PBAE/DNA) films. MicroBCA assay and Accublue DNA quantitation assay were used to quantify total PBAE and DNA content in disrupted films. The microBCA assay was previously validated in the Hammond Lab for quantification of PBAE in solution.[7] The impact of DNA concentration and dissolving plasmid DNA in water or 100 mM sodium acetate (pH 5.2) during LbL assembly on overall film composition was explored. The rinse baths were either water or 100 mM sodium acetate, matching the DNA solution. PBAE solutions were consistently in 100 mM sodium acetate buffer.

The ionic strength of the LbL assembly solutions impacts charge shielding along the backbone of polyelectrolytes during deposition. Increasing ionic strength of the buffer increases charge shielding of polymers in solution and allows polymers to adsorb in loopy conformations, resulting in greater polymer mass and thicker layers deposited per surface area. Accordingly, we observed that depositing DNA layers in 100 mM sodium acetate buffer enhanced both DNA and PBAE loading in (PBAE/DNA)40 films (**Figure 3.4A, B**). The concentration of DNA during LbL assembly also impacted both the DNA and PBAE content of the film (**Figure 3.4A, B**). Increased DNA deposition per layer resulted results in a corresponding increasing in the amount of PBAE adsorbed to achieve surface charge overcompensation, causing enhanced PBAE loading. The total polymer:DNA ratio was calculated by dividing PBAE loading by the DNA loading (**Figure 3.4C**). (PBAE/DNA) films assembled with 0.2 and 1 mg/mL of DNA in water had total polymer:DNA mass ratios of 3.0 ± 1.1 and 5.6 ± 1.6, respectively. Introducing 100 mM sodium acetate to the DNA assembly solutions resulted in films of polymer:DNA mass ratio 3.2 ± 2.1 (0.2 mg/mL DNA) and 2.3 ± 0.43 (1 mg/mL DNA).

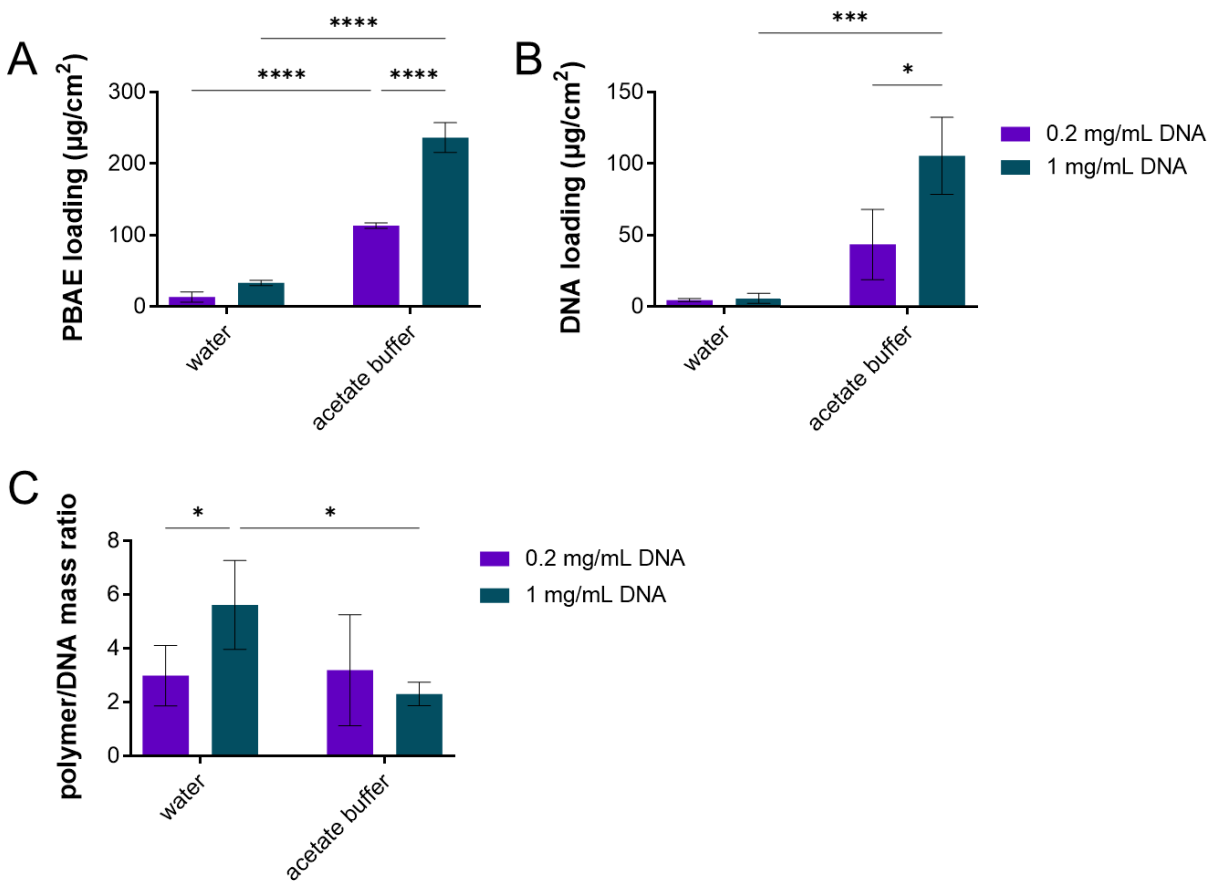

Figure 3.4 Impact of LbL buffer ionic strength and DNA concentration on overall PBAE/DNA film composition *(A) Total PBAE loading quantified by microBCA assay (B) Total film DNA loading quantified by Accublue assay (C) Total film polymer:DNA mass ratio.*

The stoichiometry of polyelectrolytes in LbL films depends on the fraction of charged segments along the adsorbing polymer chains and the surface charge density of the previously adsorbed layer.[37] To achieve electroneutrality within the LbL film, polycation and polyanion charges should either exactly compensate each other at a 1:1 stoichiometry or counterions may intrinsically or extrinsically compensate some of the charges, with the latter occurring more commonly.[37–39] For fixed solution conditions, the number of electrostatic binding sites within the film and the charge states of DNA and PBAE remain constant, which could explain the similar polymer:DNA mass ratios observed in the different film conditions studied here (**Figure 3.4C**). Additionally, the slightly lower polymer:DNA mass ratio calculated for films constructed with

DNA in sodium acetate buffer could be due to sodium counterions compensating a fraction of DNA negative charges, resulting in a lower relative incorporation of PBAE than in the absence of sodium acetate buffer. Overall, the total polymer:DNA mass ratio observed in (PBAE/DNA) films was between 2 and 5 and addition of sodium acetate buffer in DNA solutions and rinse baths enhanced polymer and DNA loading in the films. However, based on transfection efficiency results obtained with PBAE-DNA polyplexes in Chapter 2, a polymer:DNA mass ratio of at least 5:1 was required to successively condense DNA and achieve detectable DNA transfection. Further increasing the ionic strength of the PBAE buffer or increasing the assembly pH closer to the PBAE pKa could increase PBAE adsorption per layer and thus increase the overall polymer:DNA ratio of the film.

3.3.5 In vitro transfection with (PBAE/DNA) films

The transfection efficiency of (PBAE/DNA) films carrying GFP plasmid DNA was tested *in vitro* using HEK 293T cells as depicted in **Figure 3.5A**. The 4-day film treatment time was selected after observing that the peak transfection efficiency occurred at 4 days rather than 2 days, which is the standard *in vitro* transfection time frame for DNA polyplexes. Films constructed at 0.05 and 0.2 mg/mL DNA were placed in direct contact with cells before analysis of GFP expression using flow cytometry. As shown in **Figure 3.5B**, only films constructed with 0.2 mg/mL DNA were able to transfect cells. 20 bilayers films did not stimulate detectable GFP expression (not depicted). Films with increasing number of bilayers achieved the following transfection efficiencies: 40 bilayers 9.1% ± 5.6%, 60 bilayers 4.7% ± 3.8%, 80 bilayers 6.5% ± 2.9%, and 100 bilayers 0.84% ± 0.55% GFP positive cells. Increasing the number of (PBAE/DNA) layers in a polymer multilayer film results in a corresponding increase in the total DNA content of the film, as discussed in Section 3.3.3. The decreasing trend in transfection efficiency with increasing film bilayers was unexpected and led us to quantify the DNA dose released from the (PBAE/DNA) films during the 4-day treatment period **(Figure 3.5C**). As film thickness increased, the instantaneous DNA dose released was relatively constant and actually

decreased slightly for the greatest number of film bilayers. Additionally, the dotted horizontal line drawn on **Figure 3.5C** indicates the minimum DNA dose (0.1 μg) required to see DNA polyplex transfection activity in this setting. All films constructed with 0.05 mg/mL DNA released doses below this threshold dose, which could explain the lack of transfection activity from these films.

Films constructed with 0.2 mg/mL DNA released sufficient DNA dose, but in contrast to the total film DNA loading, the amount of DNA released at a given time did not increase with film thickness (**Figure 3.5C**). This could be explained by the surface-eroding behavior of (PBAE/DNA) films, where film dissolution and DNA release proceeds in a top-down, layer by layer fashion.[23,32,36,40] Due to the linear growth behavior of (PBAE/DNA) films discussed in Section 3.3.1, the DNA loading per bilayer of film should be the same regardless of the number of film bilayers if the assembly conditions, such as DNA concentration, are kept constant. As a result, it could be expected that the number of disassembled layers and amount of DNA released in 4 days should be the same for DNA nanolayer films that differ only by the number of bilayers. While the 40 and 60 bilayer films had respectively released 90% and 60% of their total DNA loading by 4 days, the 80 and 100 bilayer films had released 20% and 10% of their total DNA content (**Figure 3.3B**). Examining the actual mass of DNA released in 4 days, although the fraction of total released decreased with more bilayers, the instantaneous dose of DNA was relatively similar for all films. This release behavior is consistent with surface erosion of films, releasing equivalent amounts of material instantaneously regardless of total film thickness.

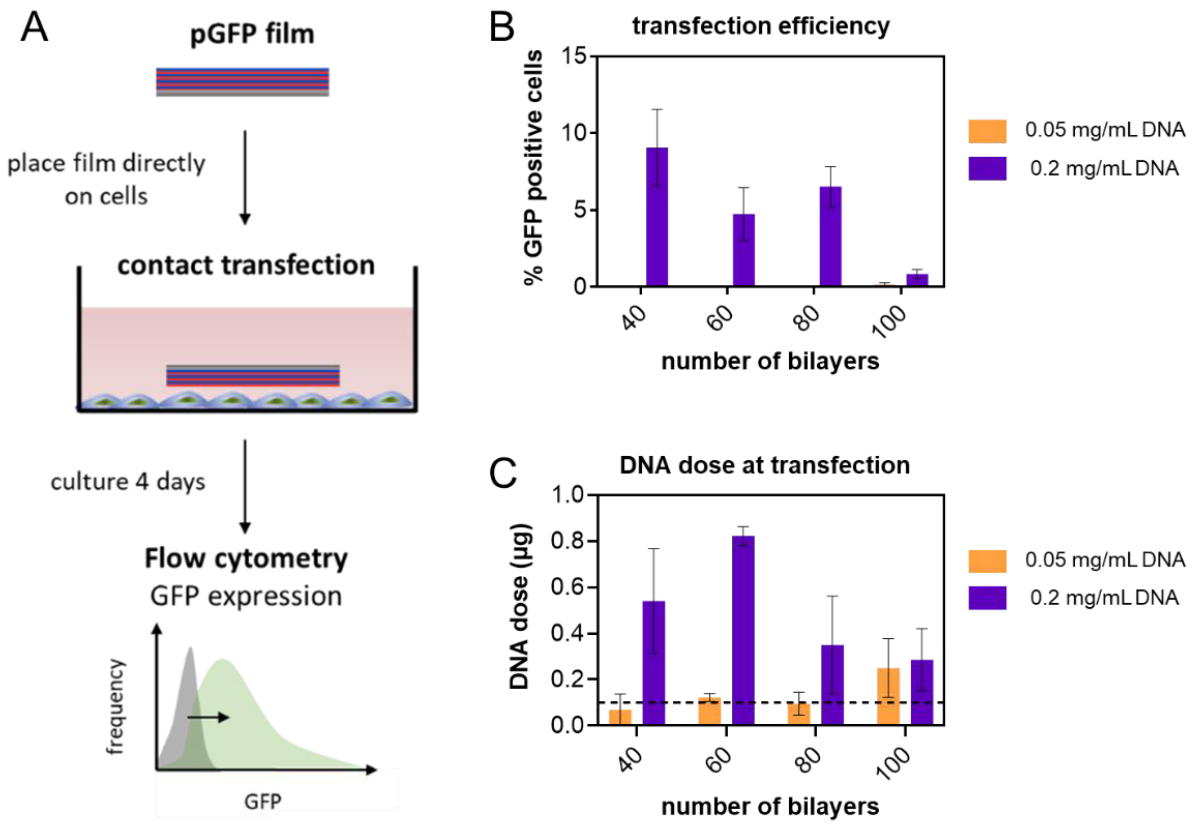

Figure 3.5 In vitro DNA transfection with LbL films assembled at different DNA concentrations *(A) Workflow and schematic of DNA nanolayer contact transfection of HEK 293T cells (B) Transfection efficiency of (PBAE/pGFP) films constructed with 0.05 or 0.2 mg/mL DNA with varying numbers of bilayers (C) Total dose of DNA released from (PBAE/pGFP) films after 4 days of incubation in PBS.*

Having observed that increasing the DNA assembly concentration from 0.05 to 0.2 mg/mL improved transfection efficiency, we further tested (PBAE/DNA)35 films assembled with 0.5 and 1 mg/mL DNA for transfection (**Figure 3.6A**), PBAE and DNA content (**Figure 3.6B**), and overall polymer:DNA mass ratio (**Figure 3.6.C**). Transfection efficiency slightly increased with increasing DNA assembly concentration, but the differences were not statistically significant and transfection efficiency was less than 1% for all films tested (**Figure 3.6A**). As expected, increasing the DNA assembly concentration resulted in greater DNA loading and correspondingly greater PBAE loading to compensate the anionic charge (**Figure 3.6B**). When we divide each formulation/s PBAE content by its DNA content, average polymer:DNA mass

ratios of 5.2 ± 0.88, 1.7 ± 0.23, 1.4 ± 0.30, 2.3 ± 0.48 were obtained for films constructed with 0.05, 0.2, 0.5, 1 mg/mL DNA, respectively (**Figure 3.6C**). These values are similar to those previously discussed in Section 3.3.4, determined by the fraction of charged segments in PBAE and DNA at these assembly conditions and by the requirement of electroneutrality in the bulk of the film.[37,39] The 0.05 mg/mL DNA formulation achieved the highest polymer:DNA ratio, but likely driven by very low DNA incorporation rather than a large excess of polycation compensating incorporated DNA. Overall, increasing DNA concentration during adsorption increased DNA loading, but did not affect the polymer:DNA ratio or transfection efficiency.

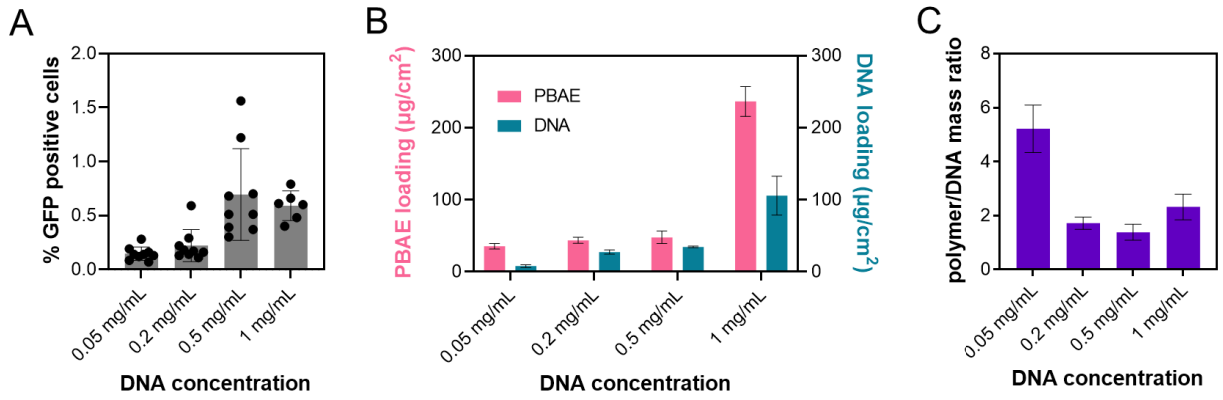

Figure 3.6 Varying DNA assembly concentration to tune transfection and film composition *(A) Transfection efficiency of PBAE/DNA films constructed with different DNA concentrations (B) Total PBAE and DNA loading (C) Mass ratio of PBAE and DNA in films.*

3.4 Conclusions

This chapter investigated the impact of LbL assembly solution conditions on robust DNA loading, release kinetics, and polymer/DNA composition in (PBAE/DNA) bilayer architecture films. We determined the effects of DNA concentration, assembly pH, ionic strength, and number of film bilayers on the composition and release behavior of DNA nanolayer films assembled on silicon chips. The film growth behavior and solution condition-dependence of film thickness and composition are consistent with theory and findings from past studies of weak polyelectrolyte LbL assembled films. (PBAE/DNA) films release DNA slowly, following a surface

erosion pattern, and the duration of the release can be simply tuned by varying the number of bilayers. We also demonstrated that assembly conditions could be used to tune the polymer:DNA ratio in films, a key factor determining pre-formed polyplex DNA delivery efficacy. The (PBAE/DNA) two-component architecture is a tunable and effective local DNA delivery system that could be further modulated for desired DNA release kinetics or sequential release of multiple DNAs by introducing diffusion barrier layers, as has been applied for staged protein and antibiotic delivery.[15,36,41] Further studies could modulate pH and ionic strength to maximize polymer:DNA mass ratio of the films and examine the resulting transfection efficiency. However, increasing DNA loading or modulating polymer:DNA mass ratio alone was not accompanied by corresponding improvements in transfection efficiency, highlighting the need for more in depth, structural investigations of how self-assembled DNA nanolayers disassemble and how cells interact with the films to achieve transfection.

3.5 References

(1) Dubas, S. T.; Farhat, T. R.; Schlenoff, J. B. Multiple Membranes from “True” Polyelectrolyte Multilayers. *J. Am. Chem. Soc.* **2001**, *123*, 5368–5369.

(2) Zhijie Sui; David Salloum, and; Schlenoff*, J. B.; Sui, Z.; Salloum, D.; Schlenoff, J. B. Effect of Molecular Weight on the Construction of Polyelectrolyte Multilayers: Stripping versus Sticking. *Langmuir* **2003**, *19*, 2491–2495.

(3) Schoeler, B.; Kumaraswamy, G.; Caruso, F. Investigation of the Influence of Polyelectrolyte Charge Density on the Growth of Multilayer Thin Films Prepared by the Layer-by-Layer Technique. *Macromolecules* **2002**, *35*, 889–897.

(4) Sukhishvili, S. A.; Granick, S. Layered, Erasable Polymer Multilayers Formed by Hydrogen-Bonded Sequential Self-Assembly. *Macromolecules* **2001**, *35*, 301–310.

(5) Alkekhia, D.; Hammond, P. T.; Shukla, A. Layer-by-Layer Biomaterials for Drug Delivery. *Annu. Rev. Biomed. Eng.* **2020**, *22*, 1–24.

(6) Castleberry, S. A.; Almquist, B. D.; Li, W.; Reis, T.; Chow, J.; Mayner, S.; Hammond, P. T. Self-Assembled Wound Dressings Silence MMP-9 and Improve Diabetic Wound Healing in Vivo. *Adv. Mater.* **2016**, *28*, 1809–1817.

(7) Chou, J. J.; Berger, A. G.; Jalili-Firoozinezhad, S.; Hammond, P. T. A Design Approach for Layer-by-Layer Surface-Mediated SiRNA Delivery. *Acta Biomater.* **2021**, *135*, 331–341.

(8) Jewell, C. M.; Zhang, J.; Fredin, N. J.; Wolff, M. R.; Hacker, T. A.; Lynn, D. M. Release of Plasmid DNA from Intravascular Stents Coated with Ultrathin Multilayered Polyelectrolyte Films. *Biomacromolecules* **2006**, *7*, 2483–2491.

(9) Saurer, E. M.; Jewell, C. M.; Roenneburg, D. A.; Bechler, S. L.; Torrealba, J. R.; Hacker, T. A.; Lynn, D. M. Polyelectrolyte Multilayers Promote Stent-Mediated Delivery of DNA to Vascular Tissue. *Biomacromolecules* **2013**, *14*, 1696–1704.

(10) Yu, Y.; Si, Y.; Bechler, S. L.; Liu, B.; Lynn, D. M. Polymer Multilayers That Promote the Rapid Release and Contact Transfer of DNA. *Biomacromolecules* **2015**, *16*, 2998–3007.

(11) Moskowitz, J. S.; Blaisse, M. R.; Samuel, R. E.; Hsu, H.-P.; Harris, M. B.; Martin, S. D.; Lee, J. C.; Spector, M.; Hammond, P. T. The Effectiveness of the Controlled Release of Gentamicin from Polyelectrolyte Multilayers in the Treatment of Staphylococcus Aureus Infection in a Rabbit Bone Model. *Biomaterials* **2010**, *31*, 6019–6030.

(12) Min, J.; Choi, K. Y.; Dreaden, E. C.; Padera, R. F.; Braatz, R. D.; Spector, M.; Hammond, P. T. Designer Dual Therapy Nanolayered Implant Coatings Eradicate Biofilms and Accelerate Bone Tissue Repair. *ACS Nano* **2016**, *10*, 4441–4450.

(13) Shah, N. J.; Hong, J.; Hyder, M. N.; Hammond, P. T. Osteophilic Multilayer Coatings for Accelerated Bone Tissue Growth. *Adv. Mater.* **2012**, *24*, 1445–1450.

(14) Hsu, B. B.; Hagerman, S. R.; Jamieson, K.; Veselinovic, J.; O’Neill, N.; Holler, E.; Ljubimova, J. Y.; Hammond, P. T. Multilayer Films Assembled from Naturally-Derived Materials for Controlled Protein Release. *Biomacromolecules* **2014**, *15*, 2049–2057.

(15) Min, J.; Braatz, R. D.; Hammond, P. T. Tunable Staged Release of Therapeutics from Layer-by-Layer Coatings with Clay Interlayer Barrier. *Biomaterials* **2014**, *35*, 2507–2517.

(16) Shah, N. J.; Macdonald, M. L.; Beben, Y. M.; Padera, R. F.; Samuel, R. E.; Hammond, P. T. Tunable Dual Growth Factor Delivery from Polyelectrolyte Multilayer Films. *Biomaterials* **2011**, *32*, 6183–6193.

(17) DeMuth, P. C.; Min, Y.; Huang, B.; Kramer, J. A.; Miller, A. D.; Barouch, D. H.; Hammond, P. T.; Irvine, D. J. Polymer Multilayer Tattooing for Enhanced DNA Vaccination. *Nat. Mater.* **2013**, *12*, 367–376.

(18) Dallas, A.; Trotsyuk, A.; Ilves, H.; Bonham, C. A.; Rodrigues, M.; Engel, K.; Barrera, J. A.; Kosaric, N.; Stern-Buchbinder, Z. A.; White, A.; *et al.* Acceleration of Diabetic Wound Healing with PHD2- and MiR-210-Targeting Oligonucleotides. *Tissue Eng. - Part A* **2019**, *25*, 44–54.

(19) Alkekhia, D.; Hammond, P. T.; Shukla, A. Layer-by-Layer Biomaterials for Drug Delivery. *Annu. Rev. Biomed. Eng.* **2020**, *22*, 1–24.
(20) Ladam, G.; Schaad, P.; Voegel, J. C.; Schaaf, P.; Decher, G.; Cuisinier, F. In Situ Determination of the Structural Properties of Initially Deposited Polyelectrolyte Multilayers. *Langmuir* **1999**, *16*, 1249–1255.
(21) Ogier, J. LbL-Based Gene Delivery: Challenges and Promises. In *Layer-by-Layer Films for Biomedical Applications*; Wiley-VCH Verlag GmbH & Co. KGaA: Weinheim, Germany, 2015; pp. 195–206.
(22) Bechler, S. L.; Si, Y.; Yu, Y.; Ren, J.; Liu, B.; Lynn, D. M. Reduction of Intimal Hyperplasia in Injured Rat Arteries Promoted by Catheter Balloons Coated with Polyelectrolyte Multilayers That Contain Plasmid DNA Encoding PKCδ. *Biomaterials* **2013**, *34*, 226–236.
(23) Liu, X.; Zhang, J.; Lynn, D. M. Ultrathin Multilayered Films That Promote the Release of Two DNA Constructs with Separate and Distinct Release Profiles. *Adv. Mater.* **2008**, *20*, 4148–4153.
(24) Lynn, D. M.; Langer, R. Degradable Poly(Beta-Amino Esters): Synthesis, Characterization, and Self-Assembly with Plasmid DNA. *J. Am. Chem. Soc.* **2000**, *122*, 10761–10768.
(25) Anderson, D. G.; Akinc, A.; Hossain, N.; Langer, R. Structure/Property Studies of Polymeric Gene Delivery Using a Library of Poly(β-Amino Esters). *Mol. Ther.* **2005**, *11*, 426–434.
(26) Macdonald, M. L.; Rodriquez, N. M.; Smith, R. C.; Hammond, P. T. Release of a Model Protein from Biodegradable Self Assembled Films for Surface Delivery Applications. *J Control Release* **2008**, *131*, 228–234.
(27) Flessner, R. M.; Yu, Y.; Lynn, D. M. Rapid Release of Plasmid DNA from Polyelectrolyte Multilayers: A Weak Poly(Acid) Approach. *Chem. Commun.* **2011**, *47*, 550–552.
(28) Richardson, J. J.; Cui, J.; Björnmalm, M.; Braunger, J. A.; Ejima, H.; Caruso, F. Innovation in Layer-by-Layer Assembly. *Chem. Rev.* **2016**, *116*, 14828–14867.
(29) Ferreira, M.; Rubner, M. F. Molecular-Level Processing of Conjugated Polymers. 1. Layer-by-Layer Manipulation of Conjugated Polyions. *Macromolecules* **1995**, *28*, 7107–7114.
(30) Vázquez, E.; Dewitt, D. M.; Hammond, P. T.; Lynn, D. M. Construction of Hydrolytically-Degradable Thin Films via Layer-by-Layer Deposition of Degradable Polyelectrolytes. *J. Am. Chem. Soc.* **2002**, *124*, 13992–13993.
(31) Zhang, J.; Chua, L. S.; Lynn, D. M. Multilayered Thin Films That Sustain the Release of Functional DNA under Physiological Conditions. *Langmuir* **2004**, *20*, 8015–8021.
(32) Zhang, J.; Fredin, N. J.; Janz, J. F.; Sun, B.; Lynn, D. M. Structure/Property Relationships in Erodible Multilayered Films: Influence of Polycation Structure on Erosion Profiles and the Release of Anionic Polyelectrolytes. *Langmuir* **2006**, *22*, 239–245.
(33) Shiratori, S. S.; Rubner, M. F. PH-Dependent Thickness Behavior of Sequentially Adsorbed Layers of Weak Polyelectrolytes. *Macromolecules* **2000**, *33*, 4213–4219.
(34) Klitzing, R. V.; Möhwald, H. A Realistic Diffusion Model for Ultrathin Polyelectrolyte Films. *Macromolecules* **1996**, *29*, 6901–6906.
(35) Mansouri, S.; Winnik, F. M.; Tabrizian, M. Modulating the Release Kinetics through the Control of the Permeability of the Layer-by-Layer Assembly: A Review. *Expert Opin. Drug Deliv.* **2009**, *6*, 585–597.
(36) Wood, K. C.; Chuang, H. F.; Batten, R. D.; Lynn, D. M.; Hammond, P. T. Controlling Interlayer Diffusion to Achieve Sustained, Multiagent Delivery from Layer-by-Layer Thin Films. *Proc. Natl. Acad. Sci. U. S. A.* **2006**, *103*, 10207–10212.
(37) Schönhoff, M.; Bieker, P. Linear and Exponential Growth Regimes of Multilayers of Weak Polyelectrolytes in Dependence on PH. *Macromolecules* **2010**, *43*, 5052–5059.

(38) Oh, Y. K.; Suh, D.; Kim, J. M.; Choi, H. G.; Shin, K.; Ko, J. J. Polyethylenimine-Mediated Cellular Uptake, Nucleus Trafficking and Expression of Cytokine Plasmid DNA. *Gene Ther.* **2002**, *9*, 1627–1632.
(39) Voigt, U.; Khrenov, V.; Tauer, K.; Hahn, M.; Jaeger, W.; Von Klitzing, R. The Effect of Polymer Charge Density and Charge Distribution on the Formation of Multilayers. *J. Phys. Condens. Matter* **2003**, *15*, 213–218.
(40) Jewell, C. M.; Zhang, J.; Fredin, N. J.; Lynn, D. M. Multilayered Polyelectrolyte Films Promote the Direct and Localized Delivery of DNA to Cells. *J. Control. Release* **2005**, *106*, 214–223.
(41) Hsu, B. B.; Jamieson, K. S.; Hagerman, S. R.; Holler, E.; Ljubimova, J. Y.; Hammond, P. T. Ordered and Kinetically Discrete Sequential Protein Release from Biodegradable Thin Films. *Angew. Chemie - Int. Ed.* **2014**, *53*, 8093–8098.

Chapter 4. Mechanistic investigation of LbL film-mediated DNA release and cellular delivery *in vitro*

4.1 Introduction

LbL incorporation of DNA enables sustained delivery of nucleic acid and creates opportunity to co-release transfection enhancing polymers. Various polyelectrolytes and film architectures to enable nucleic acid delivery from LbL-assembled nanolayered films have been explored, with successful application *in vitro* and *in vivo* for DNA vaccination, treatment of intimal hyperplasia, and modulation of wound healing.[1–4] Proposed mechanisms for LbL film-mediated DNA delivery draw from extensive literature describing polyplex and nanoparticle-mediated delivery. Films are thought to release polymer and DNA particles that mediate cellular uptake and intracellular processing of DNA. Previous work has suggested that DNA multilayer films shed positively-charged particles into solution that have an average diameter between 100 and 1000 nm.[1,5] However, both the size and charge distributions are very broad and how cells interact with the particles, via uptake from solution or active remodeling of the LbL film, is not well understood.

In vivo biodistribution and intracellular trafficking of nucleic acid vehicles have been rigorously studied;[6–10] however, the initial interactions between nucleic acid vehicles and the cell surface before internalization are not well understood. A recent study by Ingle et al. (2020) investigated mechanisms of cellular internalization and trafficking of polyplexes by HeLa cells using live and fixed cell confocal imaging.[11] They proposed that filopodia, thin actin projections from the cell surface, actively sense and explore their environment and mediate internalization of polyplexes into clathrin- and caveolae-rich vesicles. Rehman et al. (2012) also examined lipo- and polyplex uptake, observing that complexes are captured by actin-rich filopodia and interact with syndecans, causing local clustering, which in turn stimulates retraction of the filopodia into the cell body.[12] Inhibition of actin polymerization and syndecan recruitment weakened polyplex binding to filopodia, prevented transport of polyplexes along filopodia, and strongly reduced

transfection efficiency.[12] These findings outline a syndecan-mediated cellular mechanism for polyplex attachment to cells preceding endocytosis, presenting an alternative to random electrostatic adsorption of polyplexes to the cell membrane.

Polyplex composition, defined by polymer:DNA mass ratio or N/P ratio, is a key determining factor for efficiency of polyplex transfection. Insufficient polycation results in poorly complexed DNA that either cannot enter cells or is unable to escape endosomes. Too much polycation can result in significant toxicity. Polymer:DNA ratio could also play an important role in determining LbL film transfection efficacy. While methodologies exist to probe the total ratio of polymers in the bulk film, the composition of the material released from LbL films upon immersion in physiological conditions is largely unknown.[13–15] Investigation of how film composition and architecture affect releasate composition and structure and the subsequent impact on DNA delivery has not been explored. LbL self-assembly of DNA nanolayers is highly tunable, presenting a huge parameter space to be optimized. Identification of general principles and film structure-function relationships guiding LbL film-mediated DNA transfection would enable rational design and more efficient optimization of future LbL films for DNA delivery.

Chapter scope: This chapter describes work to elucidate the composition of DNA multilayer films and their corresponding releasate and relates these characteristics to functional assays of DNA delivery efficacy. The findings described here contribute to fundamental mechanistic understanding of how LbL film composition relates to film-mediated nucleic acid delivery efficacy and how cells interact with DNA multilayer films *in vitro*.

4.2 Methods

4.2.1 Materials

Plasmid DNA encoding green fluorescent protein (pmaxGFP) was produced at research-grade by GenScript and stored at 20°C in 1 mg/mL aliquots in TE buffer. Tissue culture plates, black 96-well plates, glass microscope slides, and DNA LoBind Eppendorf tubes were purchased from VWR. Endosomal marker primary antibody sampler kit, anti-rabbit F(ab')2

fragment Alexa Fluor 647 conjugate, and Hoechst 33342 nuclear stain were purchased from Cell Signaling Technologies (Danvers, MA). LAMP1 rabbit polyclonal primary antibody was purchased from Abcam (Cambridge, UK). MatTek No 1.5 coverslips and Prolong Antifade Diamond Mountant were purchased from ThermoFisher (Waltham, MA). HyClone molecular biological grade water was purchased from Fisher Scientific. MicroBCA Protein Assay Kit, 5M bioreagent grade NaCl solution, and precast 0.8% and EX 1% agarose E-gels were obtained from ThermoFisher Scientific (Waltham, MA). Silicon wafers were obtained from WaferPro (Santa Clara, CA). PBAE was synthesized according to previously published procedures.[16,17] Linear polyethyleneimine (LPEI, 25 kDa) and polyacrylic acid (PAA, 50 kDa), 25% solution in water were obtained from Polysciences (Warrington, PA). Branched polyethyleneimine (BPEI), protamine sulfate (PrS), poly (4-styrene sulfate) (SPS, 70 kDa) sodium salt, 3 M sodium acetate (pH 5.2), dimethyl sulfoxide, and Atto 647N NHS were purchased from Millipore Sigma. Phosphate buffered saline (PBS) was purchased from Lonza (Morristown, NJ). Accublue Broad and High Sensitivity dsDNA Quantitation kits were obtained from Biotium (Fremont, CA). Polystyrene semimicro cuvettes for the Malvern Zetasizer were purchased from VWR, and DTS1070 folded capillary cells were purchased directly from Malvern. All other materials were obtained from Millipore Sigma (St. Louis, MO). Chemicals were stored per manufacturer's instructions.

4.2.2 Cell culture

Human epithelial kidney 293T (HEK 293T) cells were a gift from Dr. Jiahe Li at Northeastern University. U2OS human osteosarcoma cells were a gift from Dr. Michael Yaffe's Lab at MIT. MC3T3-E1 murine pre-osteoblast subclone 4 were purchased from ATCC. HEK and U2OS cells were cultured in Dulbecco's Modified Eagle Medium (DMEM, Corning, NY), supplemented with 10% Fetal Bovine Serum (FBS) and 1% penicillin-streptomycin. MC3T3-E1 cells were cultured in α Minimum Essential Medium (αMEM, ThermoFisher, MA) supplemented

with 10% FBS and 1% penicillin-streptomycin. These cells tested negative for mycoplasma after thawing from storage and monthly during culture using Lonza MycoAlert kit (Morristown, NJ).

4.2.3 Fluorescent dye labelling of plasmid DNA and polyethyleneimine

Plasmid DNA was fluorescently tagged to determine cellular association and uptake via flow cytometry and to track release into PBS. DNA was labelled with Cy3 or Cy5 using Label IT Nucleic Acid Labeling Kit (Mirus Bio LLC, Madison, WI). The labelling reaction was performed at a ratio of 1 µL dye reagent: 3 µg DNA following manufacturer instructions.

Branched polyethyleneimine (M_n 10 kDa, M_w 25 kDa) was conjugated to the fluorescent dye Atto 647N NHS ester (Millipore Sigma). Atto 647N NHS was dissolved in dimethyl sulfoxide at 5 mg/mL. BPEI was dissolved in 0.2 M sodium bicarbonate (pH 8.5) at 5 mg/mL. Atto 647N NHS stock was added to the BPEI solution at a molar ratio of 3:1 (dye to primary amine) and reacted at room temperature for 18 hours with stirring, protected from light. Atto 647N-conjugated BPEI (BPEI-Atto647N) was separated from free dye by dialysis against deionized water, changing the water after 8 hours and 24 hours. After 48 hours of dialysis, BPEI-Atto647N was lyophilized for 48 hours. The amount of conjugated dye was estimated to be 0.02 mol dye per mol BPEI via NanoDrop.

4.2.4 Polymer-DNA complex preparation

Pre-formed polyplexes were prepared by mixing cationic polymers and pGFP in 20 mM sodium acetate to allow electrostatic complexation. Polyplexes were assembled by mixing equal volumes of polycation dissolved in 40 mM sodium acetate and pGFP in water at the appropriate polymer:DNA mass ratios (5:1, 10:1, 20:1, 30:1). For example, 20 µL of polycation and pGFP stock were mixed to obtain a 40 µL master treatment mix containing 400 ng pGFP, 4000 ng PBAE (10:1 ratio), and 20 mM sodium acetate. For 96-well plates, 10 µL of each master mix was distributed to each treatment well. Polyplexes were assembled just prior to transfection studies and used immediately. Polyplexes prepared with commercial transfection reagents

TransIT-X2 (Mirus Bio LLC, Madison, WI) at a ratio of 3 µl reagent:1 µg DNA were used as positive transfection controls.

4.2.5 Layer-by-layer film assembly

LbL films were deposited on plasma-treated silicon substrates. Silicon substrates were cleaned with methanol, ethanol, and ultra-pure water and then dried under nitrogen. Cleaned silicon substrates approximately 0.5 x 2.0 cm^2 were oxygen plasma treated at high RF power for 90 seconds using a Harrick PDC-32G plasma cleaner. The treated silicon substrates were immediately immersed in the first cationic solution for at least 30 minutes. A Carl Zeiss HMS-DS50 automated slide stainer (Oberkochen, Germany) was used to assemble the LbL films. Completed films were allowed to air dry and stored in a vacuum desiccator at room temperature until analysis.

PBAE, BPEI, LPEI, and PrS were dissolved at 2 mg/mL in 100 mM sodium acetate buffer (pH 5.2). BPEI and LPEI solutions were further diluted to 1, 0.5, 0.25 mg/mL with 100 mM sodium acetate. BPEI dipping solutions for fluorescent tracking of release contained 5 or 25 wt% BPEI-Atto 647N mixed with unlabeled BPEI. SPS was dissolved at 5 mM with respect to the repeat unit (3.7 mg/mL) and PAA was dissolved at 1 mg/mL in 100 mM sodium acetate (pH 5.2). Synthetic polyelectrolyte solutions were then filtered through a sterile 0.2 µm cellulose acetate syringe filter. PBAE was dissolved fresh daily due to its hydrolysable nature. Plasmid DNA was diluted from 1-3 mg/mL stocks in TE buffer to the desired concentration in MilliQ(18 mΩ) water or 10 mM sodium acetate (pH 5.2). DNA dipping solutions for fluorescent tracking of release contained 10 wt% Cy3-labelled pmaxGFP and 90 wt% unlabeled. DNA solutions were not filtered to minimize loss of plasmid. All dipping solutions were changed after 12-16 hours to maintain the desired polyelectrolyte concentration.

Bilayer films were constructed by alternate dipping in the polycation solution for 10 minutes (PBAE, PrS) or 5 minutes (BPEI, LPEI) followed by two consecutive 30 second rinse steps in 10 mM sodium acetate, and then into the polyanion solution for 10 minutes followed by

two 30 second rinses in 10 mM sodium acetate. This cycle was repeated until the desired number of bilayers was deposited.

PrS and SPS baselayer films were assembled by alternate dipping in PrS (2 mg/mL) and SPS (3.7 mg/mL) solutions for 10 minutes, separated by two 1 min 10 mM sodium acetate rinses. This cycle was repeat 20 times. PBAE (1 mg/mL) and PAA (1 mg/mL) baselayers were deposited by alternating immersion in PBAE and PAA solutions for 5 minutes, separated by two 1 min MilliQ water rinses.

4.2.6 BPEI and DNA release kinetics quantification

Films constructed on silicon chips were cut into 0.5 cm x 0.5 cm pieces and immersed in 300 µL PBS, pH 7.4 at 37°C in a shaking incubator. At each timepoint, the silicon chip was transferred to a fresh PBS aliquot and returned to the incubator. DNA release into PBS from film constructs was quantified using the Accublue DNA Quantitation kit or by comparing fluorescently tagged DNA signal to a standard curve of tagged DNA concentrations. BPEI release into PBS was quantified by comparing releasate signal to a standard curve of BPEI-Atto 647N concentrations. Each timepoint was quantified in duplicate.

Release studies were continued until no more DNA-Cy3 or BPEI-Atto647N could be detected in the release supernatant. The amount of DNA or BPEI released from films was standardized by the surface area of the film and reported as mass per unit area.[18] The cumulative DNA or BPEI released from the film at a given time point i can by calculated by

$$m_i = C_i V_i + \sum_{j=1}^{i-1} C_j V_j$$

Where m_i (µg) is the total cumulative mass of DNA or BPEI released at time point (i), C_i (µg/ml) is the concentration of sample i, V_i (ml) is the total volume of the release supernatant, and the summation term adds up the total mass of from each of the previous timepoints.
Fractional DNA release at each timepoint was calculated as follows:

$$f_i = \frac{C_i V_i}{\sum_{j=1}^{i} C_j V_j}$$

Where f_i is the fraction of the total DNA or BPIE content of the film that was released at timepoint (i) and the summation term represents the total cumulative mass released from the film, which was taken as total DNA or BPEI content of the film.

4.2.7 Polyplex and LbL film releasate characterization

Film-released material in PBS was characterized using dynamic light scattering. Malvern ZS90 Particle Analyzer was used for size and zeta potential measurements. 0.5 x 0.5 cm^2 pieces of each film were immersed in 300 µL PBS for 1 or 3 days in a 37°C shaking incubator. 40 µL of undiluted releasate was used for DLS measurements. Samples were diluted ten-fold (0.1X PBS final buffer concentration) with molecular biology grade water for zeta potential measurements. Results from the Malvern are reported using the SD of three measurements.

4.2.8 Determination of complexation state: DNA gel electrophoresis and PicoGreen dye exclusion assay

Agarose gels were used to determine the complexation state of film-released DNA. 20 µL of the releasate (used as is or diluted to <20 ng/µL with PBS) were added to the wells of a precast 0.8% or EX 1% agarose E-gel. The gel was run using the E-gel system (ThermoFisher) for 10 min and the visualized using a Bio-Rad ChemiDoc imager.

PicoGreen dye exclusion assay was used to determine DNA complexation state. The extent of fluorescence quenching relative to free DNA signal was used to determine the fraction of bound DNA in film release and to estimate a polymer:DNA mass ratio and N/P ratio. A standard curve of fluorescence signal vs. polycation concentration was constructed using pre-formed DNA polyplexes with a fixed DNA concentration of 2 ng/µL and increasing amounts of PBAE or BPEI. 25 µL of 2 ng/uL free DNA in PBS was added to each well of a black 96-well plate. Two-fold serial dilutions of PBAE (starting from 20 ng/µL, polymer:DNA ratio of 10:1) and BPEI (starting from 8 ng/µL, polymer:DNA ratio of 4:1) were performed in 10 mM sodium

acetate. 25 µL of each dilution aliquot was added in triplicate. The plate was placed on a shaker at 300 RPM for at least 30 minutes to allow complexation. PicoGreen reagent stock was diluted 200x into PBS and 50 µL was added to each well (final PicoGreen dilution 400x, final buffer composition 0.75X PBS with 2.5 mM sodium acetate). The plate was immediately read at excitation 480 nm and emission 520 nm. A binding curve was constructed by plotting fluorescence vs. log(polymer:DNA mass ratio) and performing a nonlinear regression in GraphPad Prism 9. The sigmoidal, 4PL, X is log(concentration) equation was selected using default settings and no parameter constraints. This standard curve was used to back-calculate an estimated polymer:DNA mass ratio based on the fluorescence of the film releasate sample.

The DNA concentration in film release samples was determined via NanoDrop and Cy3-DNA fluorescence. Samples were diluted with PBS to 2 ng/µL and 25 µL was transferred in triplicate to two black 96-well plates (n = 3 each). 25 µL of water or 25 µL of 4 ng/µL BPEI was added to each sample well (n = 3 each). The BPEI group was including to mimic “capture” of free film-released DNA. PicoGreen reagent stock was diluted 200x into PBS and 50 µL was added to each well (final PicoGreen dilution 400x, final buffer composition 0.75X PBS with 2.5 mM sodium acetate). The plate was immediately read at excitation 480 nm and emission 520 nm. The fraction of bound DNA was calculated as follows:

$$fraction\ bound\ DNA = 1 - \frac{fluorescence\ of\ film\ release\ well}{fluorescence\ of\ free\ DNA\ well}$$

4.2.9 Scanning electron microscopy (SEM) imaging of DNA multilayer films

Cells were seeded at 40,000 cells/well in a 24-well plate either directly on the DNA multilayer film or on a collagen-coated silicon chip placed at the bottom of the well. Plates were centrifuged at 100 rcf for 3 minutes to help cells settle. For collagen-coated silicon seeded cells, the DNA multilayer film was placed face down on the cells. A separate set of films was incubated in DMEM with 10% FBS. Films in media or with cells were incubated in cell culture incubators at 37°C for 24 hours. After treatment, cell culture media was removed and cells were

fixed for 1 hour at 4°C in 2% glutaraldehyde in 0.1 M sodium cacodylate. Subsequently, samples were washed three times with cold 0.1 M sodium cacodylate. The samples were then transferred to tetramethylsilane (TMS) for 20 minutes before air-drying. Dried samples were coated with gold in a Denton Sputter Coater and analyzed with a Zeiss Crossbeam 540 scanning electron microscope, operated at 5 kV, in the Peterson (1957) Nanotechnology Materials Core Facility.

4.2.10 In vitro transfection with DNA multilayer films

HEK 293T cells were seeded at 10000 cells/well in 96-well, 20000 cells/well in 48-well, or 40,000 cells/well in 24-well tissue culture plates the day before transfection. Culture medium was changed to fresh complete media prior to treatment. Transwell transfection proceeded by placing a 0.5 x 0.5 cm^2 film in the transwell insert such that the film and the cell monolayer in the bottom chamber were both immersed in media. For DNA film contact transfection, DNA films were placed directly in the cell culture wells, with the film in contact with the cell layer. Media was changed every 2 days until analysis. In order to capture free film-released DNA in the cell culture media, Mirus TransIT-X2 (X2) was diluted in OptiMEM and added to the media. X2 was dosed at a 2 µL reagent:1 µg DNA ratio assuming 100 ng, 200 ng, or 500 ng DNA per well for a 96, 48, and 24 well plate, respectively. As a positive transfection control, Mirus TransIT-X2 (X2) or LT1 was mixed with pGFP diluted in OptiMEM at a 2:1 ratio, incubated at room temperature for 20 minutes, and administered to cells.

Transfection efficiency was quantified by measuring the fraction of treated cells that successfully took up and expressed the delivered GFP plasmid. 2, 4, or 7 days after film treatment was initiated, cells were trypsinized and resuspended in warm media before centrifuging at 300 rcf for 5 minutes. Harvested cells were resuspended in PBS with ZombieViolet Viability Dye diluted 1:500 and incubated protected from light for 15 minutes. Resuspended cells were transferred to 96-well V bottom plates, centrifuged at 300 rcf for 5 minutes, and resuspended in PBS with 1% FBS. Cells were analyzed on a BD FACSCelesta

Cell Analyzer. ZombieViolet was read with a 405nm laser and 450/40 filter set, GFP fluorescence with a 488nm laser and 530/30 filter set, Cy3 labelled DNA with a 561nm laser and 586/15 filter set, and BPEI-Atto647N with the 561nm laser and 670/30 filter set. Flow cytometry data was analyzed using Flow Jo. Data was first gated to isolate single cells negative for the viability stain and then gated for DNA Cy3 fluorescence, indicating cellular association or uptake of DNA, BPEI-Atto647N fluorescence, indicating cell association or uptake of BPEI, and for GFP expression, indicating expression of delivered plasmid DNA. The fraction of single cells that were GFP positive (% GFP positive) was taken as a measure of transfection efficiency.

4.2.11 Subcellular localization of DNA film-released DNA

The subcellular localization of polyplex and film delivered DNA was examined using immunofluorescence. Cells were plated in LabTek chamber slides or directly on DNA nanolayer-coated microscope slides. At the desired timepoints, cells were fixed for 15 minutes using 4% formaldehyde. After three washes with ice cold PBS, blocking buffer containing 0.05% normal goat serum and 0.025% saponin (for permeabilization) in PBS was added to cells for 1 hour. Cells were washed 3 times with PBS before adding primary antibodies diluted in antibody diluent buffer (1% bovine serum albumin, 0.025% saponin in PBS). Rabbit monoclonal antibodies against Rab5 (1:800 dilution), Rab7 (1:600 dilution), and LAMP1 (1:800 dilution) were used to stain for early endosomes, late endosomes, and lysosomes, respectively. Cells were incubated in primary antibody solution overnight at 4°C. The next day, cells were washed 3 times with PBS before adding secondary antibody, anti-rabbit IgG Fab (1:400 dilution in antibody diluent buffer), for 2 hours. Nuclei were counterstained with Hoechst 33342. After washing the cells, a coverslip was mounted using Prolong Antifade Diamond Mountant without DAPI. Slides were stored in the dark at 4°C until confocal imaging. Immunofluorescence imaging was conducted using an Olympus FV1200 laser scanning confocal microscope. A 60x silicone oil objective was used. Image processing and analysis were performed in ImageJ (Fiji).

4.3 Results and Discussion

4.3.1 Subcellular localization of PBAE multilayer film released DNA

Based on PBAE/DNA film transfection data presented in Chapter 3, film-released DNA was not able to traffic to the nucleus to initiate transcription and gene expression without the aid of external transfection reagents. The cell membrane and endosomal entrapment are significant obstacles to intracellular delivery of DNA.[8,19,20] We examined the cellular localization of film-released DNA using immunofluorescence staining. PBAE and plasmid DNA (20 wt% Cy5-labelled) were assembled in an LbL film on a glass microscope slide. Cells treated for two days with films carrying Cy5-labelled DNA were fixed and stained for the nuclear and endosomal compartments in order to examine subcellular localization of film-delivered DNA with confocal microscopy. **Figure 4.1** shows cells treated with (PBAE/pHIV-eGFP) films for 2 days. The red Cy5-DNA localized primarily to aggregates on the cell surface and in bright spots within the green endosomal membrane staining (**Figure 4.1A**). These images suggested that film-delivered DNA was becoming trapped at the cell surface or within endosomes. Cell membrane and endosomal localization of film-released DNA combined with the lack of transfection activity suggest that film-associated DNA is either unable to enter the cell or unable to leave the endosome after internalization (**Figure 4.1B**). While the PBAE is an effective transfection reagent in pre-formed polyplexes of defined composition, the PBAE released from films was not sufficient for intracellular delivery and endosomal escape of DNA cargo.

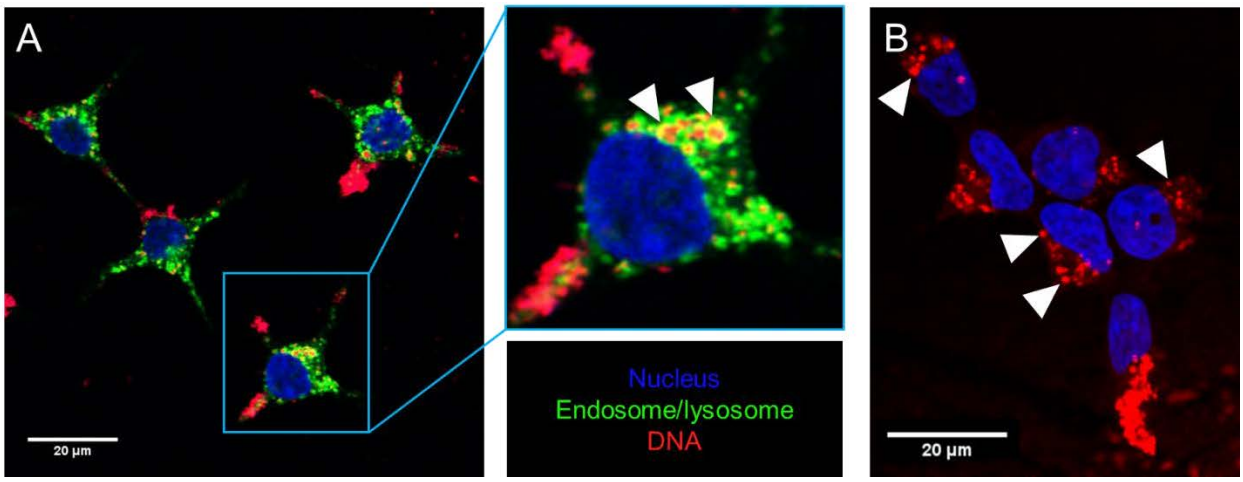

Figure 4.1 Fluorescence imaging of HEK 293T cells treated with PBAE/DNA films for 48 hours *(A) Blue indicates Hoechst nuclear stain, green is Rab5, Rab7, LAMP1 endolysosomal staining, and red is Cy5-DNA. White arrows indicate bright spots of DNA aggregated within endosomal compartments (B) Film-treated cells with green endolysosomal staining omitted for clarity.*

4.3.2 Addition of transfection reagent in solution to film-treated cells captures free DNA and facilitates delivery

Based on kinetic release studies of (PBAE/pGFP) films in PBS, the DNA dose cells encountered during film treatment was 5 to 10 times the required dose for PBAE polyplex transfection efficacy of 60-70% (discussed in Chapter 3). Little to no GFP expression in film-treated cells with more than sufficient DNA doses suggested that insufficient polycation carrier could explain low DNA delivery efficacy. This prompted us to perform the film treatment with addition of transfection reagent in solution to capture free plasmid (**Figure 4.2A**). When cells were exposed to (PBAE/pGFP) films alone, low transfection efficiency was observed. Adding branched PEI to the cell culture media improved transfection to 9.0% ± 5.1%. Adding Mirus TransIT-X2 further enhanced transfection to 53% ± 2.6% (**Figure 4.2B**). Based on this functional data, (PBAE/pGFP) films likely released free plasmid DNA that could be captured and effectively delivered by externally introduced PEI and X2 transfection reagents. As PBAE in the multilayered film degrades and the film disassembles in physiological buffers, the polycation loses positive charge density and also loses DNA binding affinity. Additionally, the pKa of the

PBAE is around pH 7.[17] As such, at pH 7.4, tertiary nitrogens on film-released PBAE are largely deprotonated and the polymer is uncharged and thus unable to re-bind free DNA.

Addition of free PEI and other polycations after DNA polyplex transfection has been shown to improve transfection efficiency. As discussed in Chapter 2, the excess polycation may supplement endosomal escape of internalized polyplexes.[21–24] In the case of (PBAE/DNA) films, however, DNA is likely released with small amounts or no PBAE complexed, resulting in limited cellular uptake and endosomal escape of DNA. Addition of free PEI and commercial reagent X2 can thus bind the uncomplexed DNA to promote intracellular delivery.

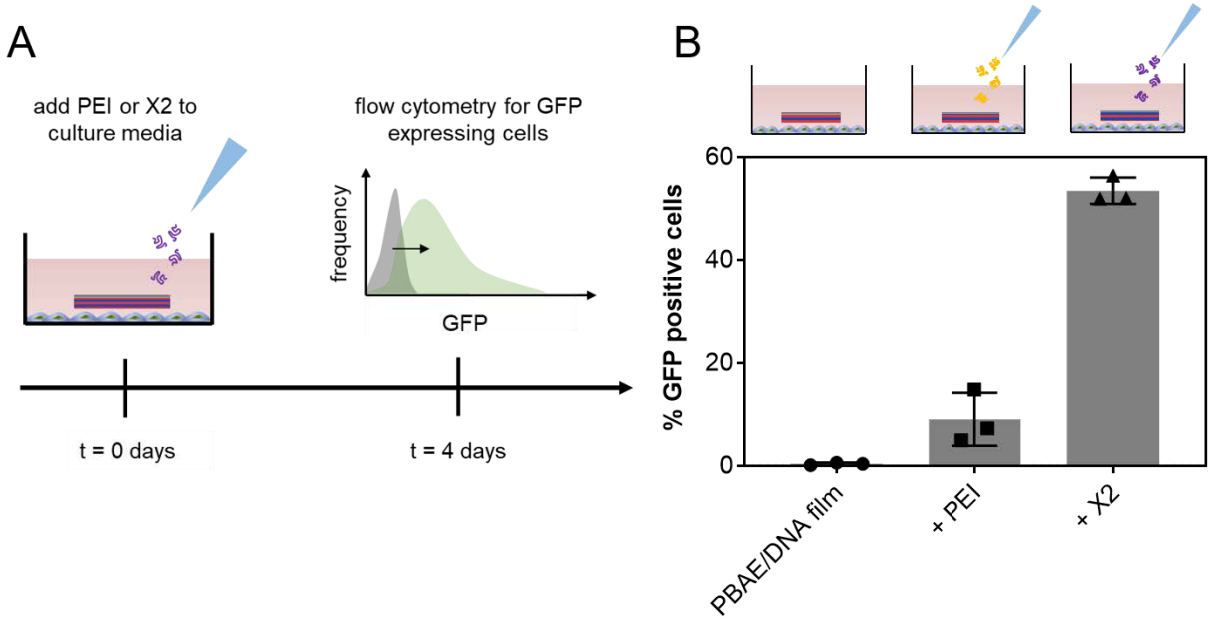

Figure 4.2 DNA film treatment of HEK 293T cells with external transfection reagent *(A) Schematic of cell treatment (B) Transfection efficiency of PBAE/DNA film and with added PEI or X2 in the culture medium.*

4.3.3 Composite poly(beta-amino ester) and polyethyleneimine DNA films exhibit improved film-mediated transfection

Based on the observation that (PBAE/DNA) film-associated transfection could be improved by adding an external transfection enhancer, we asked whether introducing polyethyleneimine as a film component might improve film-mediated transfection activity.

Polyethyleneimine was selected for its high positive charge density, nondegradability, availability in multiple molecular weights, and well-documented nucleic acid delivery activity.[25–27] However, due to BPEI's high positive charge density, it has been often associated with toxicity at higher molecular weights and higher doses. BPEI was thus incorporated along with PBAE in a hybrid film in order to leverage the transfection activity of BPEI while relying on PBAE for hydrolysis-driven film degradation and DNA release. We reasoned that complexing DNA and PEI directly and incorporating the PBAE in a degradable baselayer would best enable release of complexed PEI and DNA. Polyacrylic acid (PAA) was selected as the layering partner for PBAE because its carboxylic acids become deprotonated at pH 7.4, resulting in film swelling and interchain repulsion that can drive film dissolution.[28,29] PAA has previously been introduced to DNA multilayer films in a tetralayer architecture,[28] (PBAE/PAA/PBAE/DNA), to promote more rapid film dissociation, shortening the duration of DNA release from 5 days to 1 day.

PEI-PBAE/DNA films were constructed with the architecture: (PBAE/PAA)10 (BPEI/DNA)20 (**Figure 4.3A)**. Film contact transfection of HEK 293T cells with PEI-PBAE/DNA films achieved 20% GFP positive cells, without the aid of external transfection reagent, and addition of X2 did not further enhance transfection efficiency (**Figure 4.3B**). This dramatic increase in film transfection could be due to cell uptake of BPEI and DNA complexes, which enable intracellular delivery and transfection without help from X2. Additionally, the lack of transfection enhancement with added X2 suggest that available DNA is likely complexed with BPEI and is unavailable for X2 complexation. Introduction of BPEI in the hybrid block architecture PEI-PBAE/DNA film resulted in a 4-fold enhancement of film-mediated DNA transfection as compared to the best performing PBAE/DNA film (**Figure 4.3C**).

Based on these results and the hypothesized mechanism of action for the PEI-PBAE/DNA film, we present two potential scenarios for LbL film release of DNA with and without commercial reagent X2 in the media (**Figure 4.3D**). Hydrolytic degradation of the PBAE and release into cell culture media results in release of free or minimally complexed DNA that can be

captured and effectively delivered by soluble X2. In contrast, PBAE degradation and PAA-mediated swelling drive PEI-PBAE/DNA film dissolution into BPEI/DNA complexes that can transfect cells. Bound DNA is inaccessible to added X2. Leveraging knowledge of physicochemical characteristics of polyelectrolytes and design requirements for effective DNA delivery systems, we presented rational design of an improved LbL self-assembled DNA nanolayered thin film that enhanced film transfection efficiency by 4-fold.

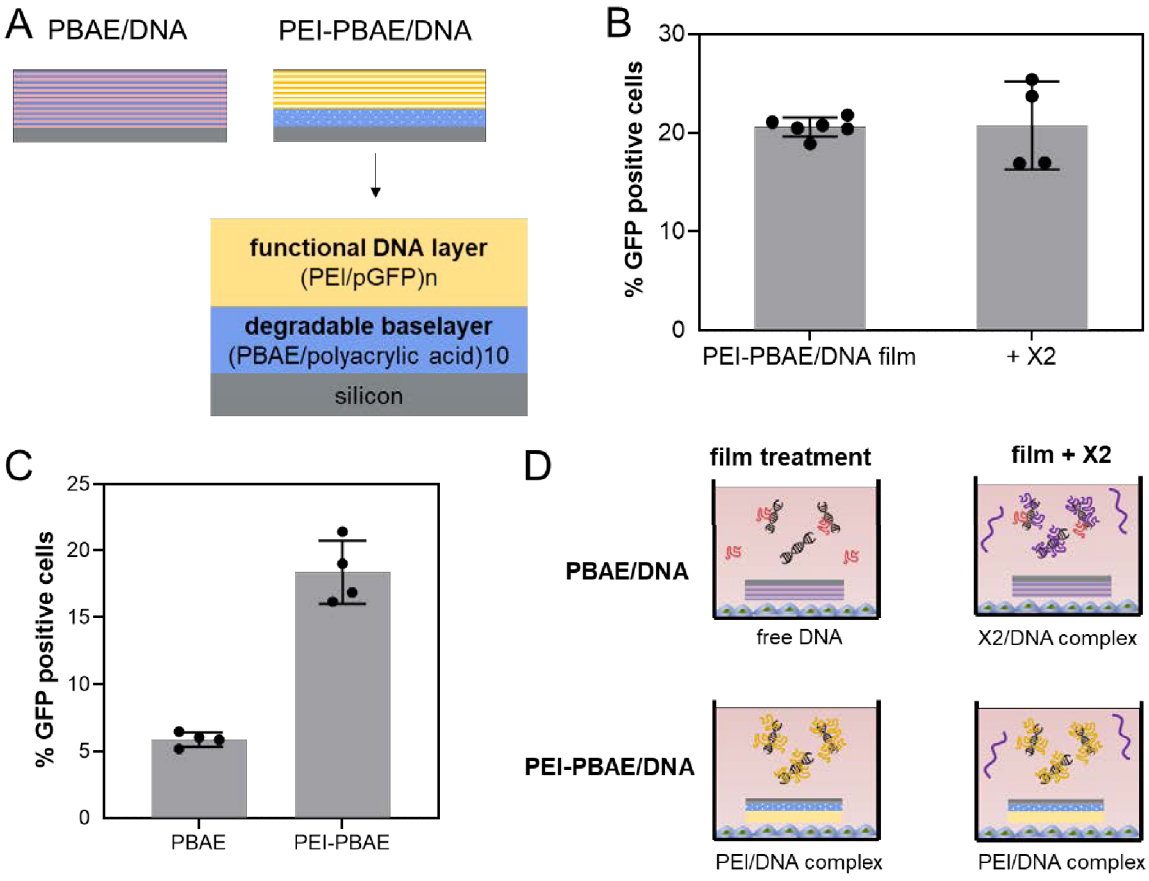

Figure 4.3 PBAE/DNA and PEI-PBAE/DNA film in vitro transfection *(A) Schematic of film architectures (B) Transfection efficiency of PEI-PBAE/DNA film and with added X2 (C) Side-by-side comparison of PBAE/DNA and PEI-PBAE/DNA film transfection (D) Proposed DNA release mechanisms in cell culture conditions.*

4.3.4 In vitro LbL film treatment mode impacts DNA delivery efficacy

PBAE/DNA films placed on 0.2 μm transwell membrane inserts failed to transfect cells in the bottom cell culture chamber. Transwell setup involved seeded cells in a monolayer in the

bottom chamber and placing the film-coated silicon in the transwell insert and placing this in the well. Fluorescence microscopy revealed that cells treated in this manner did not express detectable levels of GFP. Cells treated with PBAE/DNA film release media collected at various timepoints also did not effectively transfect cells. GFP expressing cells indicative of successful transfection were only detected when films were placed directly in contact with cells, either below or above the cell monolayer (**Figure 4.4**). Direct cell-film contact was important for PBAE/DNA film transfection.

Notably, by placing cells directly on top of or under PBAE films enabled transfection in cells touching the film, particularly along the periphery of the film (**Figure 4.4**). This suggests that cell-film interactions or close proximity are important to DNA delivery. DNA uptake by cells touching or close to the film could proceed by active cellular remodeling of the film or by uptake of film-released DNA particles that are highly concentrated in the vicinity of the film.

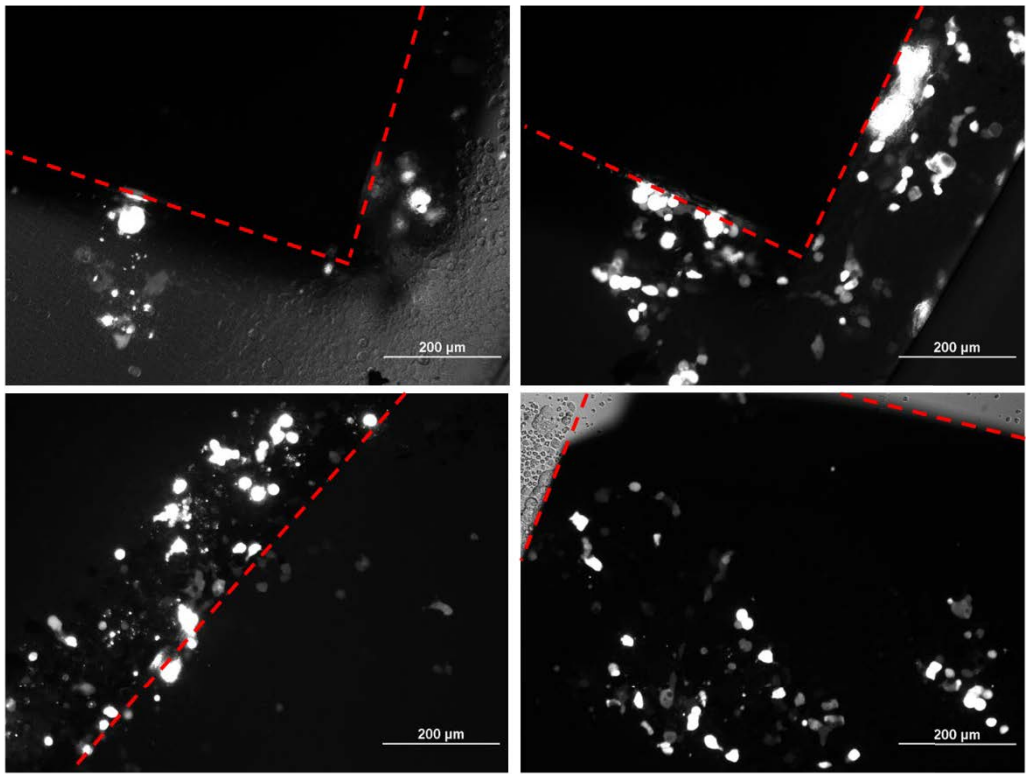

Figure 4.4 Fluorescent microscope images of HEK 293T cells treated with pGFP nanolayer films *Red dashed lines mark the edges of the film-coated silicon chip placed film-side down on the cell monolayer.*

Other groups have also observed that DNA multilayer films require close cell contact to enable effective transfection.[25,30–32] Jessel et al. (2006) embedded plasmid DNA and cationic cyclodextrin as its transfection carrier in LbL-assembled poly(L-glutamic acid) (PLE) and poly(L-lysine) (PLK) films. COS-1 cells grown on top of the films were successfully transfected and expressed the embedded plasmid DNA encoding a nuclear transcription factor and cytoplasmic GFP.[32] Treatment with supernatants from the DNA multilayers did not transfect cells, suggesting that the presence of the cells on the film was necessary. They postulated that local enzymatic degradation induced by cells in contact with the film drove DNA uptake from the films.[32] Tracking of passive release of fluorescein-labeled DNA from films incubated in cell culture media indicated that no significant DNA release from the (PLE/PLK) films occurred. These results further support that DNA availability to cells is not through uptake after passive release into solution but due to cellular uptake of DNA complexes from LbL film surfaces.

4.3.5 PBAE/DNA bilayer films release free DNA or partially complexed DNA

Successful complexation and charge neutralization of DNA can be demonstrated via DNA gel shift assay. Free plasmid DNA migrates based on charge and conformation through agarose gels. When increasing amounts of polycation are bound to DNA, migration of the DNA band is impeded. When DNA is fully complexed and when DNA's negative charge is neutralized, no migration from the loading well is observed.[33–35] Increasing PBAE or PEI doses in DNA polyplexes impede migration of DNA along the gel (**Figure 4.5**). At the same polymer:DNA mass ratios, PBAE complexes DNA to a lesser extent than PEI, due to its lower charge density per polymer mass. Converting to N/P ratio, PEI achieves full DNA complexation at N/P 4, which requires a PBAE:DNA mass ratio of 3:1.

PBAE/DNA bilayer films release primarily free DNA, which appears as a single band with similar migration to relaxed plasmid DNA (**Figure 4.5A**). A faint smear was also observed in the film releasate lane, indicating populations of DNA partially complexed with PBAE. PEI-PBAE/DNA composite films release some free DNA with a population of complexed DNA as well (**Figure 4.5B**). When free BPEI polymer was added to the film releasate at a 2:1 mass ratio, BPEI effectively captured and complexed film-released DNA and impeded DNA band migration down the gel. DNA gel electrophoresis results indicate that PBAE/DNA and PEI-PBAE/DNA films release a large population of free DNA as well as some partially and fully complexed DNA. We then sought to quantify the extent of DNA complexation and polymer:DNA ratio in film releasate.

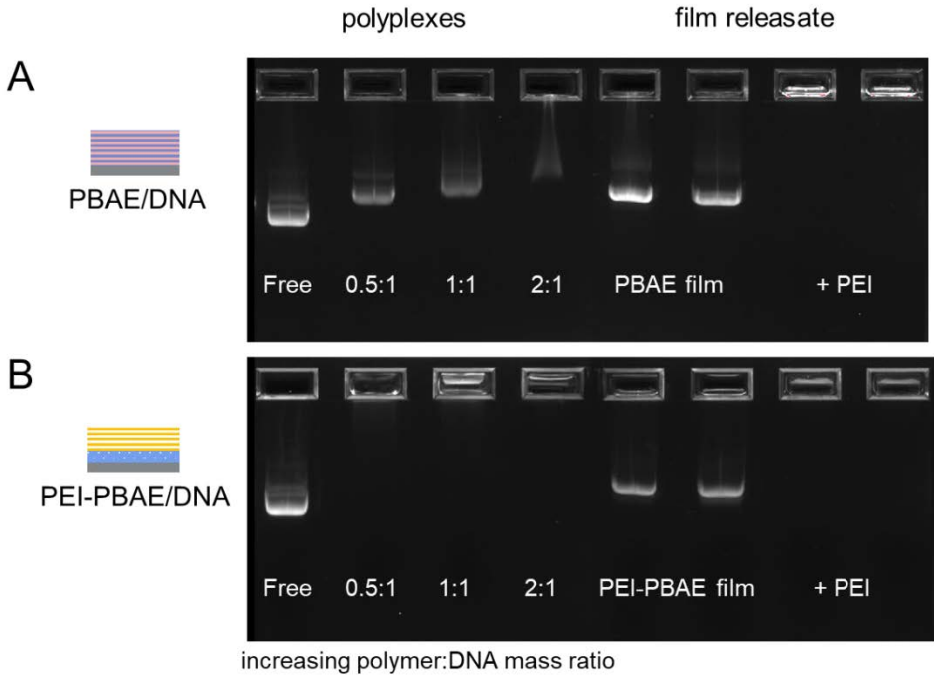

Figure 4.5 Agarose gel electrophoresis of DNA polyplexes and LbL film releasate *(A) PBAE polyplexes and PBAE/DNA film releasate (B) PEI polyplexes and PEI-PBAE/DNA film releasate.*

4.3.6 DNA-binding dye assays estimate the extent of polycation-DNA binding upon release

PicoGreen is an intercalating dye used to quantify DNA in solution with high sensitivity. The fluorescence yield of PicoGreen is enhanced by >1000-fold upon intercalation into the DNA

backbone. Exclusion of PicoGreen due to electrostatic binding between polycation and DNA can be correlated with extent of binding. A calibration curve of PicoGreen fluorescence vs. polymer:DNA ratio can be constructed (**Figure 4.6A**) and compared with LbL film releasate to estimate fraction of bound DNA and average polymer:DNA mass ratio of the released material (**Figure 4.6B**). The extent of DNA binding in film releasate differed in PBAE/DNA vs. PEI-PBAE/DNA films. PBAE films assembled with varied PBAE concentrations released DNA that was 30% complexed and PEI-PBAE films assembled with varied PEI concentrations released DNA that was 80-100% complexed (**Figure 4.6C**). Increasing the PBAE or PEI assembly concentration did not affect the extent of DNA binding upon film release into solution. Film releasate polymer:DNA mass ratios and N/P ratios were calculated from sigmoidal curve fits of PBAE and PEI-DNA binding curves (**Figure 4.6D**). PBAE films assembled with 1.5 mg/mL and 3 mg/mL PBAE released DNA with an average polymer:DNA mass ratio (N/P) of 0.6:1 (0.61) and 0.4:1 (0.45), respectively. PEI-PBAE films assembled with 0.25, 0.5, 1, and 2 mg/mL of PEI released particles with polymer:DNA mass ratios (N/P) of 0.30:1 (2.3), 0.28:1 (2.1) and 2:1 (15). While the polymer:DNA mass ratio was similar between PBAE and PEI-PBAE/DNA groups, the N/P ratio was higher in the PEI containing film releasate. At the N/P ratios > 2 calculated for PEI-PBAE/DNA film releasate, DNA is fully complexed according to agarose gel images shown in **Figure 4.5B**. In contrast, PBAE film releasates exhibited N/P ratios ~0.5, at which DNA is only partially complexed by PBAE (**Figure 4.5A**).

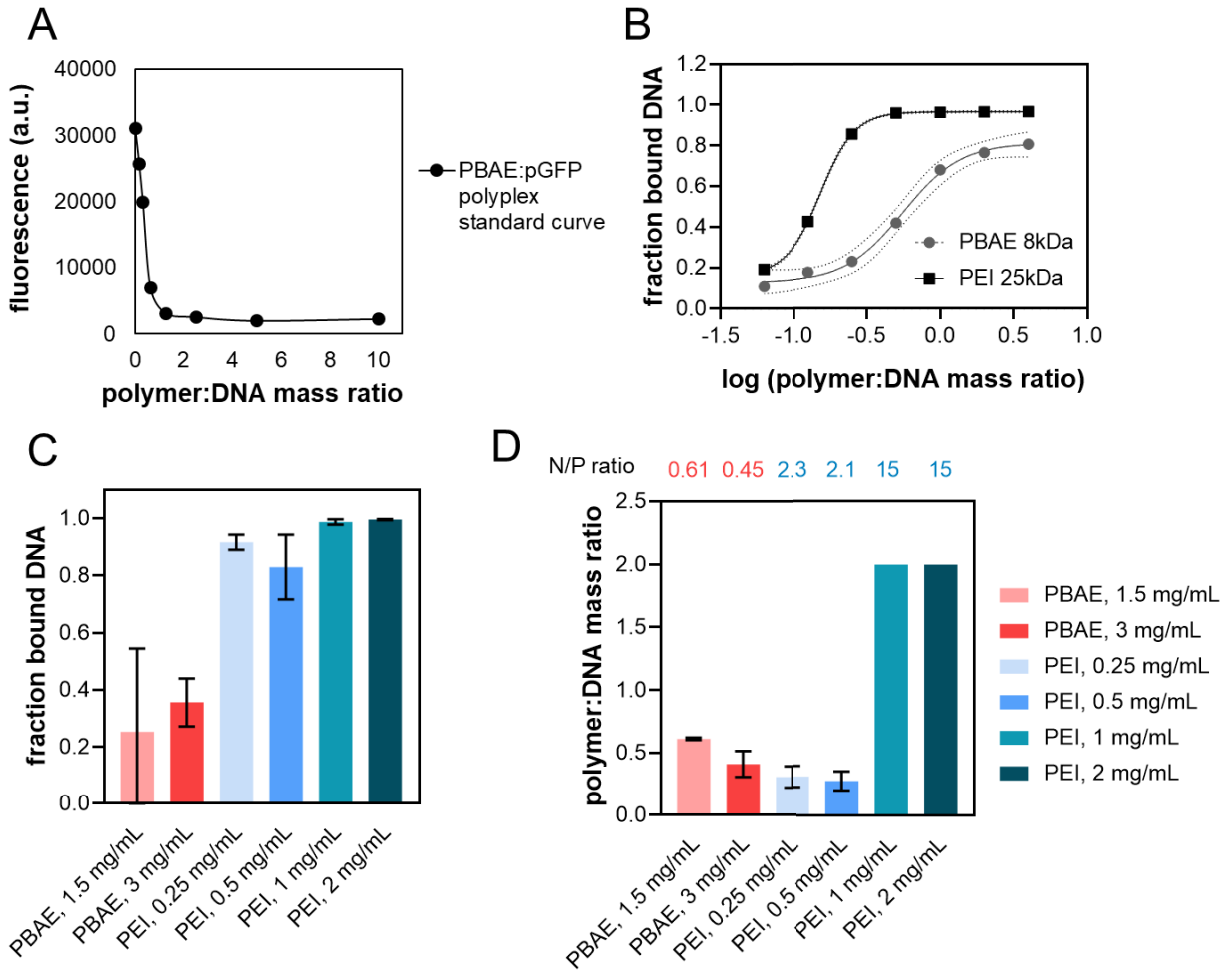

Figure 4.6 PicoGreen dye exclusion assay of LbL film released DNA *(A) Calibration curve of fluorescence vs. PBAE:DNA mass ratio (B) pmaxGFP polymer binding curves sigmoidal curve fit, dotted lines indicate 95% confidence bands (C) Fraction of bound DNA in releasate from PBAE and PEI-PBAE films, polycation dipping concentration indicated in x-axis labels (D) Polymer:DNA mass ratio of film releasate with N/P ratio conversion indicated.*

4.3.7 LbL-assembled DNA films release negatively charged nanoscale aggregates

Film releasate solutions were characterized using dynamic light scattering and zeta potential measurements. Polyplexes require a threshold polymer:DNA ratio to fully complex DNA and enable transfection, as discussed in Chapter 2. DNA multilayer films are hypothesized to have a similar threshold polymer:DNA mass ratio requirement. As such for the PBAE/DNA and PEI-PBAE/DNA architectures, the polycation concentration was varied in an attempt to modulate the total polymer content in the DNA film. Films were incubated in PBS for 24 hours

and the supernatant was analyzed using DLS before 10-fold dilution to obtain a 0.1x PBS concentration for zeta potential measurements.

PBAE/DNA films released particles with negative average zeta potential while PEI-PBAE/DNA films released slightly negative or neutral particles (**Figure 4.7A**). The number average diameter of film-released particles is shown in **Figure 4.7B**. Particle size distributions for the film releasates were quite broad, so the average zeta potential and average diameters reported here represent a subset of film-releasate particles. PBAE films released negatively charged particles with diameters of 384 ± 23.9 nm (1.5 mg/mL PBAE) and 483 ± 42.4 nm (3 mg/mL PBAE). These results suggest that PBAE films may release free DNA or DNA partially bound with polymer, consistent with gel electrophoresis and PicoGreen exclusion assay results discussed previously. Incomplete complexation of PBAE and DNA upon release from LbL films contribute to the low transfection efficiency of PBAE/DNA films.

PEI-PBAE films released slightly smaller particles with diameters of 329 ± 65.3 nm (0.25 mg/mL PEI) and 243 ± 35.2 nm (0.5 mg/mL PEI) (**Figure 4.7B**). The neutral ensemble average zeta potentials indicate that negatively and positively charged particles were both present in the PEI-PBAE film releasate, with sufficient colloidal stabilization to form 200-300 nm particles. Because PEI-PBAE films contain anionic DNA and PAA and cationic PEI and PBAE, the average surface charge of film-released particles could be attributed any combination of the four components and the exact composition is unclear. Future studies could use fluorescently-labelled polymers and DNA to probe the specific components in film-released particles.

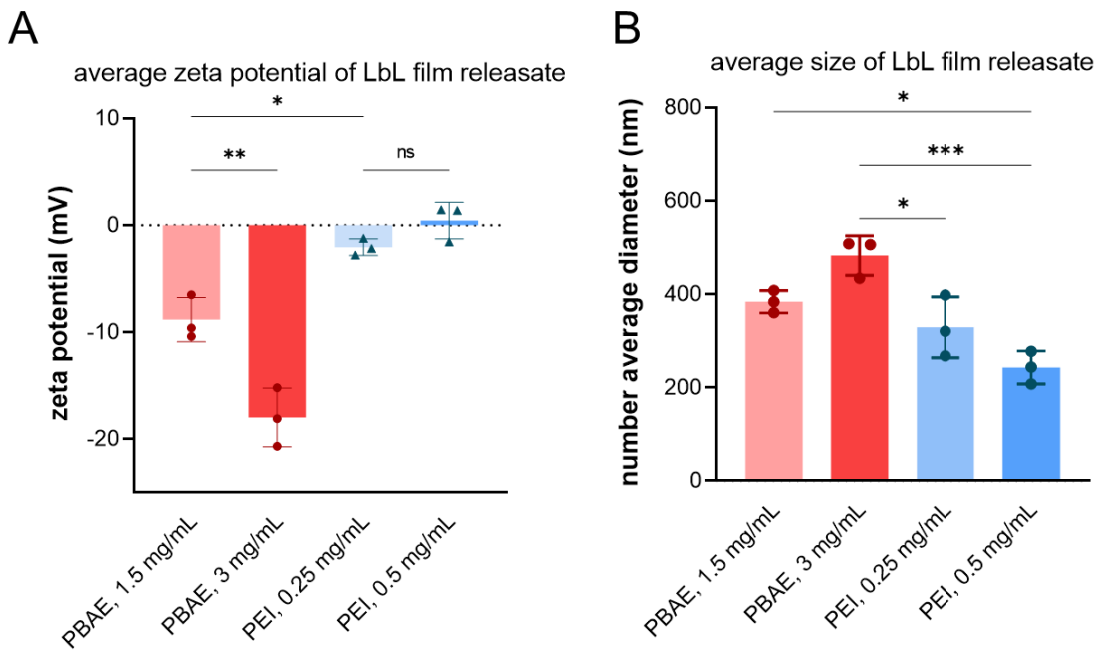

Figure 4.7 Size and charge characterization of LbL film releaseate *(A) Average zeta potential measured in 0.1x PBS (B) Average diameter of film released particles measured in 1x PBS using DLS.*

4.3.8 Scanning electron microscopy analysis of cell and DNA film interactions

Previous studies of LbL film mediated DNA delivery have incorporated underlying precursor baselayers beneath the (PBAE/DNA) functional layers to create a uniform surface charge for LbL assembly.[1,15] By selecting degradable or charge-shifting polymers for the baselayer, it becomes possible to modify the morphology and release behavior of overlying DNA layers. We incorporated protamine sulfate/poly(styrene-sulfonate) (PrS/SPS) precursor layers underneath PBAE/DNA layers. Protamine is a naturally-derived nucleic acid condensing peptide composed largely of arginine residues[36–38] and poly(styrene-sulfonate) is a strong polyanion. This baselayer combination has previously been used with PBAE/DNA functional layers to coat microneedles with plasmid DNA for intradermal DNA vaccine application.[1] The low molecular weight and bulky secondary structure of protamine in LbL can contribute to destabilization of the film and promote more rapid release.

(PrS/SPS) (PBAE/DNA) and (PBAE/PAA) (PEI/DNA) films incubated in cell media or with HEK 293T cells for 24 hours were analyzed by scanning electron microscopy (SEM) (**Figure 4.8**). **Figure 4.8A, D** depict the film surface after incubation in serum-containing media. Particles of average diameter 400-500 nm appear on the surface of both films, which is consistent with previous observations that DNA films rearrange upon incubation in PBS to present particles.[5,15] There is also a striking difference in the degrading particle morphology between the two film architectures. Individual particles or aggregates with a textured, rough appearance nucleate across the surface of the (PrS/SPS) (PBAE/DNA) film (**Figure 4.8A**). On the other hand, web-like sheets of film shed from the surface of the PEI-PBAE/DNA films, which appear to be in the process of rearranging into very spherical particles (**Figure 4.8D**). Because the baselayer templates LbL assembly and can dictate film dissolution mechanism, a PBAE/DNA film without baselayers would likely exhibit different morphologies than those depicted in **Figure 4.8A-C**.

Figure 4.8B, C depict HEK 293T cells grown directly on the (PrS/SPS) (PBAE/DNA) film surface. Cells attached to the PBAE/DNA film surface and particles were observed localized along filopodial protusions. These findings are consistent with previous observations in HeLa cells of PEI polyplex and lipoplex recruitment and internalization via actin-rich filopodia.[11,12] Internalized particles around 1000 nm in diameter were observed (**Figure 4.8B**). These are likely aggregates of smaller particles released from the film that were clustered together during uptake or brought together after endocytosis via vesicle fusion. HEK 293T cells seeded on a collagen-coated silicon surface were treated for 24 hours by placing a (PBAE/PAA) (PEI/DNA) film face down on the cells (**Figure 4.8E, F**). Filopodia extended 2-5 μm from the main cell body. Spherical particles shed by the film were deposited on the substrate, on the cell surface, and localized around filopodia. Internalized particles 500 to 1000 nm in diameter were observed in addition to similar size pits in the cell surface, where a particle may have been and was washed away during sample processing (**Figure 4.8E**).

Together, these findings suggest that an important mechanism of uptake from DNA multilayers is cell-mediated exploration and interaction with their microenvironment. The SEM images supplement the physical characterizations discussed thus far in this chapter, providing evidence of a general mechanism for initial cellular interactions with LbL-assembled DNA films. Upon immersion in physiological solutions, infiltration of water and salts into the film trigger rearrangement of the smooth polymer layers into particles. Whether cells are seeded on top of the film (**Figure 4.8B, C**) or the film is applied on top of a cell monolayer (**Figure 4.8E, F**), adherent cells filopodia to explore and capture film-associated particles. Retraction of filopodia into the cell body[12] is followed by endocytosis and intracellular processing of polymer and DNA complexes,[39] which have been thoroughly investigated previously.

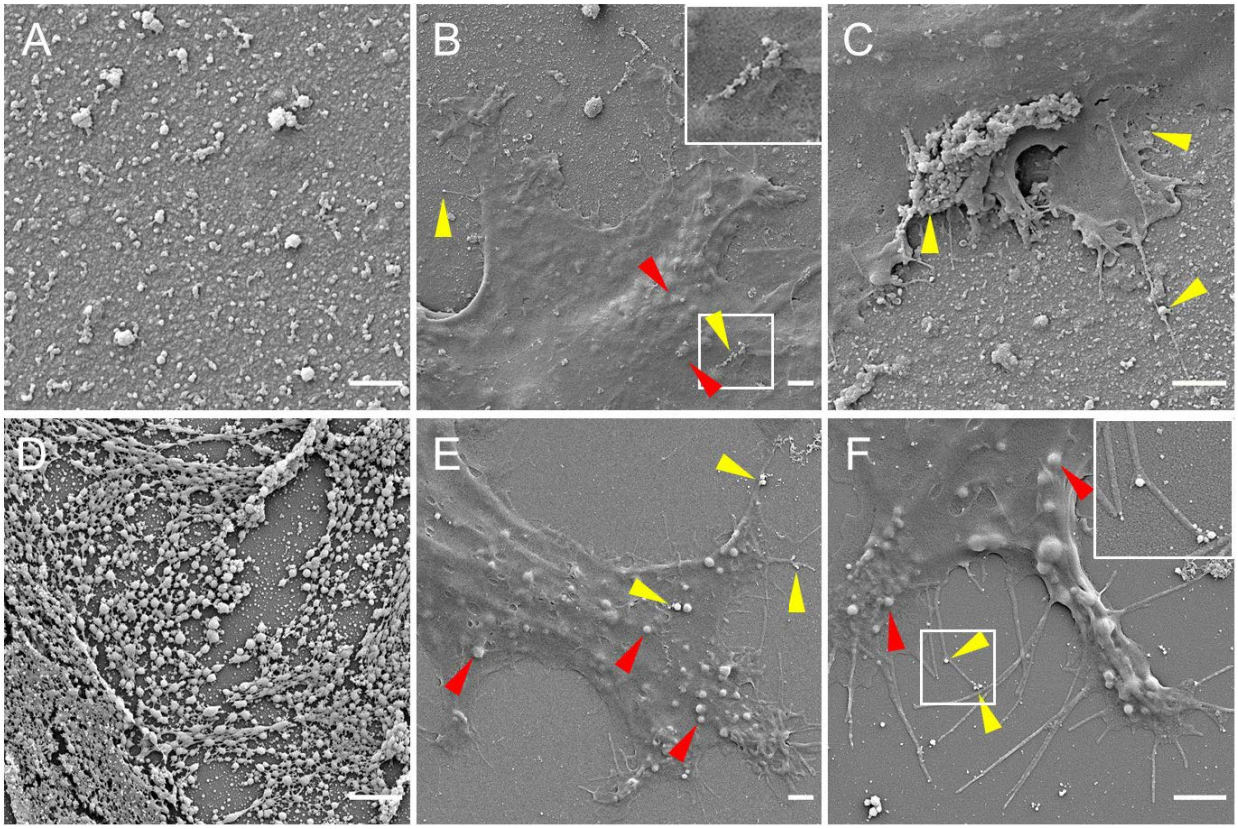

Figure 4.8 SEM imaging of DNA multilayer film disassembly and cell interaction *(A)-(C) (PrS/SPS) (PBAE/DNA) films (D)-(F) PEI-PBAE/DNA films. A, D show films after 24 hr incubation in serum-containing media; B shows a cell grown on the film and E shows a cell after film application above the cell. C, F are higher magnification frames of B, E. Red arrows mark internalized particles and yellow arrows indicate particles adsorbed to cell surface or filopodia. Insets zoom in on filopodia-associated particles. Scale bar is 2 μm.*

4.3.9 Rapid dissolution of DNA multilayer films enabled improved transfection in vitro

Effective transfection with DNA polyelectrolyte films requires release of complexed polymer and DNA with sufficient polymer to condense and enable cellular uptake of DNA. As such, film destabilization enabling concurrent release of both polycation and DNA could be expected to improve transfection efficiency. Yu, et al. (2015) incorporated polyacrylic acid (PAA), a weak polyanion, into PBAE/DNA films to promote rapid film destabilization.[28] Tetralayer films of (PBAE/PAA/PBAE/DNA) architecture released 90% of their payload in 1 day as compared to 1 week for (PBAE/DNA) films. The films enabled rapid, contact-mediated DNA transfer both *in vitro* and *in vivo.*[28]

The PrS and PBAE baselayer films introduced in this thesis were hypothesized to function similarly, promoting dissolution of slow releasing PBAE/DNA and PEI/DNA bilayer architectures and thus enabling better DNA transfer. Release kinetics in PBS were quantified by elution over time of fluorescently-labelled DNA from PBAE/DNA bilayer films with no baselayer, protamine baselayers, and low molecular weight PBAE (1 kDa) baselayers (**Figure 4.9**). While PBAE/DNA bilayers alone exhibited sustained DNA release over a period of 2 weeks, adding (PrS/SPS) or (PBAE/PAA) baselayers between the substrate and the (PBAE/DNA) block resulted in rapid release of the DNA payload in 24 hours (**Figure 4.9A**). The rapidly destabilizing baselayer (PBAE/DNA) films enabled substantially greater transfection efficiency in cells treated for 4 days (**Figure 4.9B**).

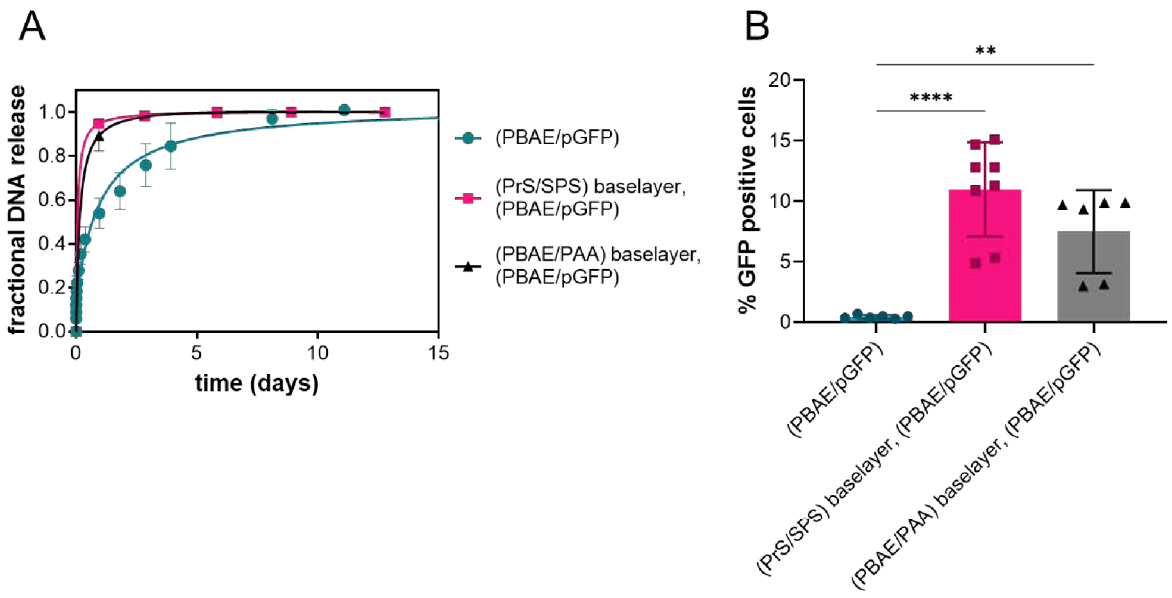

Figure 4.9 PBAE/DNA film release and transfection are enhanced by destabilizing baselayers
*(A) Cumulative DNA release over time as a fraction of total DNA loading (B) Transfection efficiency of PBAE/DNA films with and without baselayers. **p<0.01, ****p<0.0001 by one-way ANOVA with Tukey's multiple comparisons test.*

For PEI/DNA films constructed on (PBAE/PAA) baselayers, the rate of film dissolution was dependent on the molecular weight of PBAE incorporated in the baselayer. (PBAE/PAA) (PEI/DNA) films were constructed with 2 different PBAE molecular weights: 1 kDa and 8 kDa

(**Figure 4.10A**). The 1 kDa fast release film displayed more rapid release kinetics than the 8 kDa slow release film (**Figure 4.10B**). Importantly, not only was DNA release more rapid, release of fluorescently-labelled PEI was also much faster (**Figure 4.10C**). Tracking of released PEI and DNA mass ratio over time revealed that fast release PBAE baselayer films released at mass ratios around 4:1 (N/P 30) and slow release baselayer films released at mass ratios <1:1 (N/P 4). BPEI likely is released in complex with DNA based on PicoGreen assay results in section 4.3.6. Accordingly, the fast release films enabled much higher transfection efficiency (21.2% ± 7.15% GFP positive cells) than slow release films (**Figure 4.10D**).

In the context of *in vitro* transfection, which typically is studied for 2 to 7 days, rapidly destabilizing DNA multilayer films are advantageous for transfection due to concurrent release of both polycation and DNA. For *in vivo* applications, sustained release of polymer-complexed DNA is desirable due to the short half-life of released material caused by rapid clearance of released particles by immune cells, circulation of biological fluids in the implant site, and regular cellular turnover introducing new, untransfected cells.[8,40] To ensure that DNA is released with sufficient polycation, films containing alternating blocks of “release” layers that promote film disassembly and “functional” layers that contain DNA and its polycation carrier.

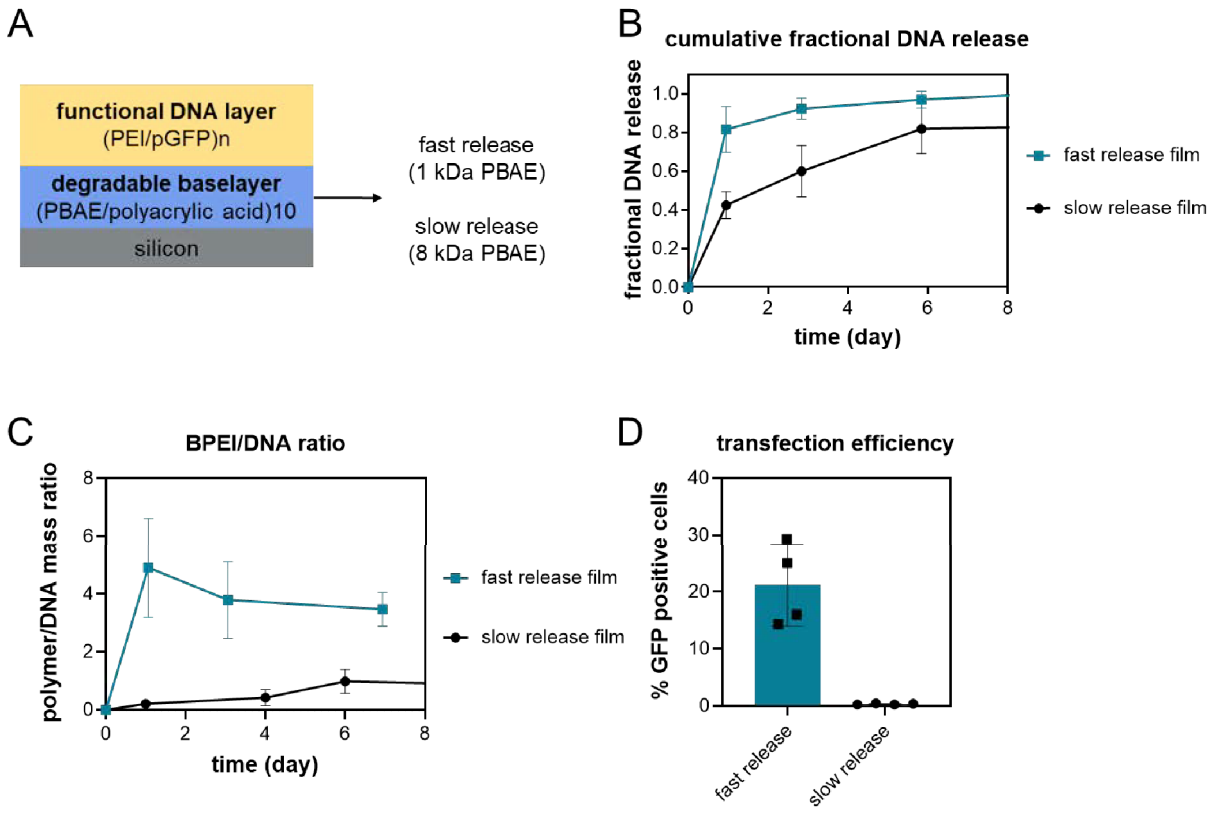

Figure 4.10 (PEI/DNA) films with low or high molecular weight PBAE baselayers exhibit different release behaviors and DNA transfection efficiencies *(A) Schematic of (PBAE/PAA) (PEI/DNA) film architecture (B) Cumulative DNA release over time as a fraction of total DNA loading (C) Ratio of BPEI-Atto647N to DNA-Cy3 over time (D) Transfection efficiency of fast and slow release PEI/DNA films.*

4.4 Conclusions

This chapter investigated the composition of DNA multilayer films and their corresponding releasate to elucidate a mechanism for cellular interaction with LbL self-assembled DNA films. We found that film treatment of cells enabled low levels of transfection and that addition of an external transfection reagent enhanced transfection activity significantly. Attributing this observation to release of uncomplexed DNA from PBAE/DNA films, we introduced PEI in a composite film architecture and demonstrated improved film-mediated transfection. Characterization of DNA complexation state, film releasate size and charge, polycation and DNA release kinetics, and imaging of cell-film interactions allowed formulation of a potential mechanism describing initial cellular interactions with DNA multilayer films. DNA

films rearrange to present DNA particles at their surface, which are recognized by cellular filopodial protrusions and recruited to the main cell body for endocytosis and intracellular processing. Complexation of polycation and DNA upon release from the film is crucial to transfection efficacy and *in vitro,* film design for rapid disassembly enabled release of bound polymer and DNA and thus high transfection efficiency. The findings presented here contribute to fundamental understanding of how cells interact with DNA multilayer films and how LbL film composition affects film-mediate nucleic acid delivery. Future studies building on the work presented here will contribute to general principles for LbL assembly of films delivering other nucleic acids, such as mRNA and siRNA, and enable rational design of effective DNA thin film coatings for biomedical implants in various nucleic acid therapy applications.

4.5 References

(1) DeMuth, P. C.; Min, Y.; Huang, B.; Kramer, J. A.; Miller, A. D.; Barouch, D. H.; Hammond, P. T.; Irvine, D. J. Polymer Multilayer Tattooing for Enhanced DNA Vaccination. *Nat. Mater.* **2013**, *12*, 367–376.

(2) Bechler, S. L.; Si, Y.; Yu, Y.; Ren, J.; Liu, B.; Lynn, D. M. Reduction of Intimal Hyperplasia in Injured Rat Arteries Promoted by Catheter Balloons Coated with Polyelectrolyte Multilayers That Contain Plasmid DNA Encoding PKCδ. *Biomaterials* **2013**, *34*, 226–236.

(3) Castleberry, S. A.; Almquist, B. D.; Li, W.; Reis, T.; Chow, J.; Mayner, S.; Hammond, P. T. Self-Assembled Wound Dressings Silence MMP-9 and Improve Diabetic Wound Healing in Vivo. *Adv. Mater.* **2016**, *28*, 1809–1817.

(4) Ogier, J. LbL-Based Gene Delivery: Challenges and Promises. In *Layer-by-Layer Films for Biomedical Applications*; Wiley-VCH Verlag GmbH & Co. KGaA: Weinheim, Germany, 2015; pp. 195–206.

(5) Wang, X.; Sun, J.; Ji, J. PH Modulated Layer-by-Layer Assembly as a New Approach to Tunable Formulating of DNA within Multilayer Coating. *React. Funct. Polym.* **2011**, *71*, 254–260.

(6) Lachelt, U.; Wagner, E.; Lächelt, U.; Wagner, E. Nucleic Acid Therapeutics Using Polyplexes: A Journey of 50 Years (and Beyond). *Chem. Rev.* **2015**, *115*, 11043–11078.

(7) Vercauteren, D.; Rejman, J.; Martens, T. F.; Demeester, J.; De Smedt, S. C.; Braeckmans, K. On the Cellular Processing of Non-Viral Nanomedicines for Nucleic Acid Delivery: Mechanisms and Methods. *J. Control. Release* **2012**, *161*, 566–581.

(8) Nelson, C. E.; Duvall, C. L.; Prokop, A.; Gersbach, C. A.; Davidson, J. M. Gene Delivery into Cells and Tissues. In *Principles of Tissue Engineering*; Elsevier, 2020; pp. 519–554.

(9) Malek, A.; Merkel, O.; Fink, L.; Czubayko, F.; Kissel, T.; Aigner, A. In Vivo Pharmacokinetics, Tissue Distribution and Underlying Mechanisms of Various PEI(–PEG)/SiRNA Complexes. *Toxicol. Appl. Pharmacol.* **2009**, *236*, 97–108.

(10) Seo, S. J.; Chen, M.; Wang, H.; Kang, M. S.; Leong, K. W.; Kim, H. W. Extra- and Intra-Cellular Fate of Nanocarriers under Dynamic Interactions with Biology. *Nano Today* **2017**, *14*, 84–99.

(11) Ingle, N. P.; Hexum, J. K.; Reineke, T. M. Polyplexes Are Endocytosed by and Trafficked within Filopodia. *Biomacromolecules* **2020**, *21*, 1379–1392.

(12) Rehman, Z. U.; Sjollema, K. A.; Kuipers, J.; Hoekstra, D.; Zuhorn, I. S. Nonviral Gene Delivery Vectors Use Syndecan-Dependent Transport Mechanisms in Filopodia to Reach the Cell Surface. *ACS Nano* **2012**, *6*, 7521–7532.

(13) Silva, J. M.; Caridade, S. G.; Costa, R. R.; Alves, N. M.; Groth, T.; Picart, C.; Reis, R. L.; Mano, J. F. PH Responsiveness of Multilayered Films and Membranes Made of Polysaccharides. *Langmuir* **2015**, *31*, 11318–11328.

(14) Benbow, N. L.; Webber, J. L.; Karpiniec, S.; Krasowska, M.; Ferri, J. K.; Beattie, D. A. The Influence of Polyanion Molecular Weight on Polyelectrolyte Multilayers at Surfaces: Protein Adsorption and Protein-Polysaccharide Complexation/Stripping on Natural Polysaccharide Films on Solid Supports. *Phys. Chem. Chem. Phys.* **2017**, *19*, 23790–23801.

(15) Jewell, C. M.; Zhang, J.; Fredin, N. J.; Lynn, D. M. Multilayered Polyelectrolyte Films Promote the Direct and Localized Delivery of DNA to Cells. *J. Control. Release* **2005**, *106*, 214–223.

(16) Lynn, D. M.; Langer, R. Degradable Poly(β-Amino Esters): Synthesis, Characterization, and Self-Assembly with Plasmid DNA. *J. Am. Chem. Soc.* **2000**, *122*, 10761–10768.

(17) Chou, J. J.; Berger, A. G.; Jalili-Firoozinezhad, S.; Hammond, P. T. A Design Approach for Layer-by-Layer Surface-Mediated SiRNA Delivery. *Acta Biomater.* **2021**, *135*, 331–341.

(18) Min, J.; Braatz, R. D.; Hammond, P. T. Tunable Staged Release of Therapeutics from Layer-by-Layer Coatings with Clay Interlayer Barrier. *Biomaterials* **2014**, *35*, 2507–2517.
(19) Sahay, G.; Alakhova, D. Y.; Kabanov, A. V. Endocytosis of Nanomedicines. *J. Control. Release* **2010**, *145*, 182–195.
(20) Medina-Kauwe, L. K.; Xie, J.; Hamm-Alvarez, S. Intracellular Trafficking of Nonviral Vectors. *Gene Ther.* **2005**, *12*, 1734–1751.
(21) Clamme, J. P.; Azoulay, J.; Mély, Y. Monitoring of the Formation and Dissociation of Polyethylenimine/DNA Complexes by Two Photon Fluorescence Correlation Spectroscopy. *Biophys. J.* **2003**, *84*, 1960–1968.
(22) Boeckle, S.; Gersdorff, K. von; Piepen, S. van der; Culmsee, C.; Wagner, E.; Ogris, M.; von Gersdorff, K.; van der Piepen, S.; Culmsee, C.; Wagner, E.; *et al.* Purification of Polyethylenimine Polyplexes Highlights the Role of Free Polycations in Gene Transfer. *J. Gene Med.* **2004**, *6*, 1102–1111.
(23) Klauber, T. C. B.; Søndergaard, R. V.; Sawant, R. R.; Torchilin, V. P.; Andresen, T. L. Elucidating the Role of Free Polycations in Gene Knockdown by SiRNA Polyplexes. *Acta Biomater.* **2016**, *35*, 248–259.
(24) Dai, Z.; Gjetting, T.; Mattebjerg, M. A.; Wu, C.; Andresen, T. L. Elucidating the Interplay between DNA-Condensing and Free Polycations in Gene Transfection through a Mechanistic Study of Linear and Branched PEI. *Biomaterials* **2011**, *32*, 8626–8634.
(25) Bengali, Z.; Rea, J. C.; Gibly, R. F.; Shea, L. D. Efficacy of Immobilized Polyplexes and Lipoplexes for Substrate-Mediated Gene Delivery. *Biotechnol. Bioeng.* **2009**, *102*, 1679–1691.
(26) Von Harpe, A.; Petersen, H.; Li, Y.; Kissel, T. Characterization of Commercially Available and Synthesized Polyethylenimines for Gene Delivery. *J. Control. Release* **2000**, *69*, 309–322.
(27) Boussif, O.; Lezoualc'ht, F.; Zanta, M. A.; Mergnyt, D.; Schermant, D.; Demeneixt, B.; Behr, J.-P. A Versatile Vector for Gene and Oligonucleotide Transfer into Cells in Culture and in Vivo: Polyethylenimine. *Biochemistry* **1995**, *92*, 7297–7301.
(28) Yu, Y.; Si, Y.; Bechler, S. L.; Liu, B.; Lynn, D. M. Polymer Multilayers That Promote the Rapid Release and Contact Transfer of DNA. *Biomacromolecules* **2015**, *16*, 2998–3007.
(29) Schönhoff, M.; Bieker, P. Linear and Exponential Growth Regimes of Multilayers of Weak Polyelectrolytes in Dependence on PH. *Macromolecules* **2010**, *43*, 5052–5059.
(30) Bengali, Z.; Pannier, A. K.; Segura, T.; Anderson, B. C.; Jang, J. H.; Mustoe, T. A.; Shea, L. D. Gene Delivery through Cell Culture Substrate Adsorbed DNA Complexes. *Biotechnol. Bioeng.* **2005**, *90*, 290–302.
(31) Truong, N. F.; Segura, T. Sustained Transgene Expression via Hydrogel-Mediated Gene Transfer Results from Multiple Transfection Events. *ACS Biomater. Sci. Eng.* **2018**, *4*, 981–987.
(32) Jessel, N.; Oulad-Abdelghani, M.; Meyer, F.; Lavalle, P.; Haîkel, Y.; Schaaf, P.; Voegel, J. C. Multiple and Time-Scheduled in Situ DNA Delivery Mediated by β-Cyclodextrin Embedded in a Polyelectrolyte Multilayer. *Proc. Natl. Acad. Sci. U. S. A.* **2006**, *103*, 8618.
(33) Saurer, E. M.; Yamanouchi, D.; Liu, B.; Lynn, D. M. Delivery of Plasmid DNA to Vascular Tissue in Vivo Using Catheter Balloons Coated with Polyelectrolyte Multilayers. *Biomaterials* **2011**, *32*, 610–618.
(34) Lynn, D. M.; Langer, R. Degradable Poly(Beta-Amino Esters): Synthesis, Characterization, and Self-Assembly with Plasmid DNA. *J. Am. Chem. Soc.* **2000**, *122*, 10761–10768.
(35) Zhang, J.; Chua, L. S.; Lynn, D. M. Multilayered Thin Films That Sustain the Release of Functional DNA under Physiological Conditions. *Langmuir* **2004**, *20*, 8015–8021.
(36) Chang, H.; Ren, K. F.; Wang, J. L.; Zhang, H.; Wang, B. L.; Zheng, S. M.; Zhou, Y. Y.; Ji, J. Surface-Mediated Functional Gene Delivery: An Effective Strategy for Enhancing

Competitiveness of Endothelial Cells over Smooth Muscle Cells. *Biomaterials* **2013**, *34*, 3345–3354.
(37) Mello, M. L. S.; Vidal, B. C. Changes in the Infrared Microspectroscopic Characteristics of DNA Caused by Cationic Elements, Different Base Richness and Single-Stranded Form. *PLoS One* **2012**, *7*, 1–12.
(38) Chang, H.; Ren, K. F.; Zhang, H.; Wang, J. L.; Wang, B. L.; Ji, J. The (PrS/HGF-PDNA) Multilayer Films for Gene-Eluting Stent Coating: Gene-Protecting, Anticoagulation, Antibacterial Properties, and in Vivo Antirestenosis Evaluation. *J. Biomed. Mater. Res. - Part B Appl. Biomater.* **2015**, *103*, 430–439.
(39) Monnery, B. D. Polycation-Mediated Transfection: Mechanisms of Internalization and Intracellular Trafficking. *Biomacromolecules* **2021**, *22*, 4060–4083.
(40) Sender, R.; Milo, R. The Distribution of Cellular Turnover in the Human Body. *Nat. Med.* **2021**, *27*, 45–48.

Chapter 5. Bone morphogenetic protein-2 plasmid DNA delivery from self-assembled polymer coatings in a critical size rabbit mandibular defect model

5.1 Introduction

Craniomaxillofacial (CMF) bone defects have a high incidence, with an estimated 7.5 million facial fractures occurring worldwide in a single year,[1] over 200,000 US children born annually with craniofacial defects,[2] and craniofacial bone grafts comprising 6% of the total US bone graft burden.[3] The clinical gold standard for cranial defect repair is the autologous bone graft, sourcing donor bone from a distant site on the patient's body.[4] This approach is limited by insufficient donor bone availability, donor site morbidity, and additional time and expense associated with bone harvest procedures.[3–6] Allografts taken from donors or cadavers, on the other hand, are associated with risk of disease transmission and immunogenicity.[7,8] In light of the limitations of current clinical cranial repair strategies, alternative materials and technologies are being explored to promote more rapid and complete regeneration of healthy bone tissue. Materials for bone repair that mimic and integrate with native bone can reduce the need for revision surgeries and promote a better long-term outcome.

Synthetic implants are a promising alternative solution for bone regeneration that can be designed for biocompatibility, osteoconductivity, mechanical strength, porosity, and degradation rate complementary to bone healing rate.[9–12] These materials can be supplemented with osteogenic molecules, such as growth factor proteins, to enhance the bone healing process. Bone morphogenetic protein-2 (BMP-2) is a promising osteoinductive biologic widely used both in bone regeneration research and in clinical products for the treatment of bone defects.[12–14]

Although systems have been developed to protect the bioactivity of recombinant proteins, they remain limited by instability to long-term storage, potential immunogenicity, and lack of native post-translational modifications.[15,16] Evidence of increased occurrence of complications and adverse events in patients receiving rhBMP-2 in spinal fusion procedures also motivates the search for alternative agents to induce bone formation.[13,17] Introduction of the

genes encoding target growth factors to local progenitor cells for endogenous protein expression may be a more robust and biologically regulated alternative to externally delivered recombinant protein.[18,19] This approach induces an endogenous repair response that is guided by in situ gene expression. Delivered genes can continue to produce target proteins over extended periods of time with native post-translational modification.[20] DNA is also more stable than most proteins and thus more amenable to storage and transport. These advantages have motivated several studies on the effect of delivery of BMP-2 DNA to progenitor cells on bone formation in orthopedic defect repair.[21–25] Viral and synthetic vectors have been investigated for gene delivery to cells for stem cell implantation therapies. Systems for delivery of genes to directly transfect cells in the defect site for endogenous osteogenic growth factor production have been less extensively studied.

Many preclinical studies investigate CMF bone regeneration in the rat calvarial defect model because of its reliability and cost efficiency.[26] However, proper assessment of clinical viability of bone regeneration systems requires testing in larger animal models with more challenging defects. For CMF defects specifically, it is also important to consider potential bone implants that have the appropriate mechanical strength for load-bearing defect locations, such as the jaw, and that can be customized to better mimic native bone structure for individual patients.[27–29] Layer-by-layer (LbL) self-assembly of thin film coatings is a versatile technique to modulate the surface properties of an implant to enable localized therapeutic release.[30,31] *In vivo* and *ex vivo* BMP-2 DNA therapy have both previously been shown in to promote bone healing.[21–24] While our specific LbL formulation of BMP-2 DNA has yet to be evaluated in this small animal setting, we sought to examine therapeutic efficacy of BMP-2 plasmid DNA-eluting LbL films in a critical size rabbit mandibular defect.

In this work, we formulated layer-by-layer (LbL) films that deliver plasmid DNA encoding human BMP-2 under the control of a ubiquitous CMV promoter. 3D-printed polycaprolactone were coated with these films and represent a customizable, defect-relevant substrate for the

mandibular bone defect. The two LbL film architectures evaluated in this study exhibited differential transfection efficacy *in vitro*, with the PEI-PBAE/DNA film releasing DNA faster and with improved transfection activity as compared with the PBAE/DNA film (see Chapter 4). These coated scaffolds were implanted into full-thickness, critical size rabbit mandibular defects to evaluate *in vivo* bone formation stimulated by BMP-2 plasmid DNA-coated scaffolds.

At the midpoint of the study, we found that there were not statistically significant differences in bone volume or bone mineral density between groups treated with the two BMP-2 plasmid DNA formulations. After the 12-week endpoint of the study, we observed that while some animals from each plasmid DNA-treated group exhibited enhanced bone growth in the defect compared to animals in the uncoated scaffold group, there were no significant differences in bone volume or BMD in the plasmid DNA formulations compared with uncoated scaffold. Through examination of bone growth within the defect volume, we discuss that the slow-degrading PCL scaffold hindered bone formation within the defect by occupying the defect volume and preventing bone ingrowth into the implant itself. Histological analyses of mandibles implanted with DNA-coated scaffolds will be performed to better understand the biological and inflammation response to the implants. In addition, in this challenging model for gene delivery, optimization of transfection efficiency and transgene expression is a critical next step to improve the potential of plasmid DNA-coated implants for bone regeneration applications.

5.2 Methods

5.2.1 Materials

BMP-2 cDNA ORF clone (pCMV3-BMP2) was purchased from Sino Biological, catalog #: HG10426-UT (Beijing, China). Research-grade plasmid preparation was performed by GenScript (Piscataway, NJ) and plasmid DNA was stored at -20°C in TE buffer at 1 mg/mL until use. Poly (beta-amino ester) (PBAE) was synthesized using 1,6-hexanediol diacrylate (Alfa Aesar) and 4,4'-trimethylenedipiperidine (Sigma-Aldrich) according to previously published methods.[32,33] Recombinant human bone morphogenetic protein-2 (BMP-2) was kindly donated

by Dr. Howard Seeherman at Bioventus. Dextran sulfate (M_r 100,000) was purchased from Fluka BioChemika. Laponite XLG was purchased from Southern Clay Products (now BYK Additives, Inc). All other materials were obtained from Millipore Sigma (St. Louis, MO) unless otherwise specified. Linear polyethyleneimine (25 kDa LPEI) was obtained from Polysciences (Warrington, PA). Phosphate buffered saline (PBS) was purchased from Lonza (Morristown, NJ). Accublue Broad and High Sensitivity dsDNA Quantitation kits were obtained from Biotium (Fremont, CA). Precast 0.8% and EX 1% agarose E-gels were obtained from ThermoFisher Scientific (Waltham, MA). Polycaprolactone OsteoplugTM (Osteoplug) implants were purchased from OsteoporeTM at a discounted price, with custom dimensions of 10 mm diameter, 5 mm thickness to match the rabbit mandibular defect dimensions.

5.2.2 Preparation of polyelectrolyte solutions

All polymer and buffer solutions were sterile-filtered through 0.2 μm cellulose acetate syringe filters. MilliQ water used for all buffers was autoclaved on liquid cycle at 350°F for 60 minutes before use. BMP-2 plasmid DNA was diluted with sterile-filtered pH 5, 10 mM sodium acetate without further filtration to prevent DNA loss. The MilliQ water and 10mM sodium acetate rinse baths were sterile-filtered using a 0.2 μm polyethersulfone vacuum filtration unit.

5.2.3 Layer-by-layer assembly on PCL implants

All containers and equipment used for Osteoplug dipping and spraying were either purchased pre-sterilized, or wiped three times with 70% ethanol. Dip baths were made in 12-well cell culture pre-sterilized plates at a volume of 3.5 mL per well, with one implant dipped into a single well. Osteoplug implants were oxygen plasma treated (Harrick PDC-32G) for 60 s, then soaked in the PBAE solution for at least 30 minutes. They were then alternately dipped in a Zeiss-Microm DS-50 Slide Stainer as described for each formulation below.

<u>PBAE/DNA formulations:</u> PBAE bath (10 minutes), two 10 mM sodium acetate rinse baths (30 seconds each with agitation), DNA bath (10 minutes), two 10 mM sodium acetate rinse baths (30 seconds each with agitation) to complete one cycle. This cycle was repeated 50 times for a

total of 50 bilayers. Polyelectrolyte solutions were as follows: PBAE, 2 mg/mL, 100 mM sodium acetate (pH 5.2); DNA (pCMV-BMP2), 0.5 mg/mL, 10 mM sodium acetate.

PEI-PBAE/DNA formulations: PBAE bath (5 minutes), two MilliQ water rinses (30 seconds each with agitation), PAA bath (5 minutes), two MilliQ water rinses (30 seconds each with agitation). This cycle was repeated 10 times to form the PBAE/PAA baselayer. BPEI bath (5 minutes), two 10 mM sodium acetate rinses (30 seconds each with agitation), DNA bath (10 minutes), two 10 mM sodium acetate rinses (30 seconds each with agitation) to complete one cycle. This cycle was repeated 40 times for a total of 40 BPEI/DNA layers on top of the PBAE/PAA baselayer. Polyelectrolyte solutions were as follows: PBAE, 1 mg/mL, 100 mM sodium acetate; PAA (50kDa), 1 mg/mL, 100 mM sodium acetate; BPEI (M_n 10kDa), 0.25 mg/mL, 100 mM sodium acetate; DNA (pCMV-BMP2), 0.5 mg/mL, 10 mM sodium acetate.

BMP-2 protein formulation:[34] PBAE bath (5 minutes), two DI water rinses (30 seconds each with agitation), dextran sulfate bath (5 minutes), two DI water rinses (30 seconds each with agitation), 10 μg/mL rhBMP-2 (5 minutes), two DI water rinses (30 seconds each with agitation), dextran sulfate bath (5 minutes), two DI water rinses (30 seconds each with agitation) to complete one tetralayer. This cycle was repeated ten times for a total of ten tetralayers. The Osteoplug implants were allowed to air-dry overnight before barrier layer deposition. The (chitosan/laponite) barrier layer was assembled using spray LbL as follows: chitosan was sprayed at a rate of 0.25 mL/s for 2 seconds, followed by a 30-second nitrogen gas spray. The laponite solution was sprayed at a rate of 0.22 mL/s for 2 seconds, followed by a 30-second nitrogen spray. This was repeated ten times for a total of ten bilayers.

Coated Osteoplug implants were allowed to air-dry overnight before placing in a sealed autoclave pouch. Coated implants were constructed 7-10 days before implantation, stored in a sealed autoclave pouch with desiccant during shipping from MIT to the UT Health Science Center at Houston, and kept sealed and dry until implantation.

5.2.4 In vivo rabbit mandibular defect

Animal studies were performed in compliance with University of Texas Health Science Center at Houston Institutional Animal Care and Use Committee. and were performed on protocol # AWC-20-0083, PI Professor Simon Young.

Surgeries were performed as described in Shah et al.[28] Briefly, skeletally mature male and female New Zealand White Rabbits, approximately 6 months of age (3.5-4.5 kg) were obtained from Charles River Laboratory and allowed to acclimate for at least 7 days. Studies contained 5-6 rabbits per treatment group with rabbits randomly assigned. 3 rabbits in the empty defect group received titanium fixation plates to prevent post-operative jaw fracture. It was determined that post-operative plate fixation was not required and thus was not implemented in subsequent surgeries.

Prior to surgery, buprenorphine (0.02-0.03 mg/kg) was injected subcutaneously. 35-55 mg/kg ketamine and 1.25-1.75 mg/kg acepromazine were injected before surgery and isoflurane with oxygen was administered throughout the procedure to induce and maintain anesthesia. A hot water blanket was placed under the animal to maintain warmth. Heart rate, oxygen saturation, respiratory rate, temperature and nonresponse to toe-pinch reflex were monitored throughout the procedure. Lactated Ringer's solution was administered via IV catheter throughout the procedure.

With the animal in dorsal position, the incision site was shaved, scrubbed with alcohol and chlorhexidine, then draped. A subdermal injection of 0.5 mg/kg 0.25% bupivicaine was injected along the planned incision site on the inferior mandible. A scalpel was used to make a midline incision from the mentum posteriorly to the midpoint between the left and right angles of the mandible. Bovie electrocautery was used to continue dissection through the underlying fascia to the mandibular inferior border. A subperiosteal dissection was used to expose the lateral surface of the mandible from the mental foramen to the anterior border of the ramus. A 10 mm-diameter trephine bur on a contra-angle surgical handpiece with constant saline

irrigation was used to drill through the cortical plate, tooth roots, and lingual plate, removing tooth and bone fragments as they were freed to produce a full thickness, 10 mm-diameter circular defect. Care should be taken throughout the procedure to not damage the facial artery.

For the empty defect control group, no implant was used. For the treatment groups (uncoated scaffold, PBAE/DNA scaffold, PEI-PBAE/DNA scaffold, BMP-2 protein scaffold), the appropriate implant was press-fit into the defect. The muscle and fascia, then skin, were closed using 4-0 Vicryl sutures. Warm saline was used to clean the incision site of blood. After recovery, rabbits were returned to housing. 0.02-0.03 mg/kg buprenorphine was administered subcutaneously every 12 hours for 48 hours, then as-needed for analgesia.

5.2.5 In vivo C-arm X-ray imaging 6 weeks after surgery

Rabbits treated with BMP-2 plasmid DNA delivery systems were scanned 6 weeks post-op using a Toshiba Infinix VF-i/SP (INFX-8000V Type S) CT scanner to obtain a midpoint measurement of bone growth. Mid-point C-arm image data was analyzed using 3DSlicer open source software. Isosurfaces were created in the Segment Editor by setting a threshold grayscale value bounds to 60 and 160. A line was drawn spanning the diameter of the defect area using the markups tool. 33 mm in Slicer was found to be equivalent to 10 mm actual diameter of the defect. Using the circular scissors tool, a cylindrical ROI of 33 mm diameter was made to isolate the defect, and then the mean grayscale value and bone volume were quantified. Slicer volume was converted to actual bone volume using the same scaling factor. The grayscale value was used to calculate bone mineral density (BMD) using a calibration curve, obtained by scanning hydroxyapatite phantoms of known BMD and quantifying their grayscale value. Quantification was performed twice per sample by drawing the ROI two separate times and obtaining the corresponding mean grayscale values and bone volumes.

5.2.6 Euthanasia, mandible harvest and fixation

After 12 weeks, the rabbits were sedated with 35-55 mg/kg ketamine and 1.25-1.75 mg/kg acepromazine subcutaneously and then euthanized with 1 mL of phenobarbital solution

administered to the ear vein. Absence of cardiovascular function was verified. The entire mandible from incisors to mandibular condyles was exposed using a scalpel. Shears were used to separate the mandible in the midline between the incisors and the mandibular condyle was disarticulated to remove the mandible. Harvested mandibles were fixed in 10% non-buffered formalin for 48 hours, rinsed thoroughly in water, and then placed in 70% ethanol in water until further analysis.

5.2.7 Ex vivo microCT imaging of excised mandibles 12 weeks post-op

After fixation and before decalcification, excised mandibles were scanned using a Bruker Skyscan 1276 microCT with the following scan parameters: 85 kV source voltage, 200 μA source current, 20.1 μm image pixel size, 0.5-degree rotation step over 180 degrees total, 2x2 camera binning, and 1 mm aluminum filter. Scans were reconstructed in NRecon software and exported to analyze using MicroView open source software. Qualitative isosurfaces were created using the isosurface function, with a threshold value set to 20,000. Bone growth was quantified using the bone analysis function and a cylindrical ROI with 10 mm diameter and 10 mm thickness, slightly larger than the mandibular thickness to ensure all bone growth into the defect was included in the analysis. The bone analysis threshold was set to 20,000. Bone mineral density was determined by use of microCT hydroxyapatite phantoms, which were used to create a standard curve of bone mineral density to grayscale value measured. The average grayscale value measured in the ROI was compared to the standard curve to calculate a bone mineral density (BMD, mg hydroxyapatite/cm^3).

5.2.8 Statistical analyses

Statistical analysis was performed using GraphPad Prism 9 software, with n=5 animals per treatment group: uncoated PCL scaffold control, PBAE/DNA-coated scaffolds, and PEI-PBAE/DNA-coated scaffold. Ordinary one-way ANOVA with Tukey's multiple comparison's test was used to analyze mid-point *in vivo* CT and endpoint *ex vivo* microCT bone volume and BMD

measurements. Asterisks indicate significance levels: *p≤0.05, **p≤0.01, ***p≤0.001, ****p≤0.0001.

5.3 Results and Discussion

5.3.1 Selection of polycaprolactone 3D-printed scaffold

The scaffold was selected based on several bone defect model-specific criteria: degradation rate around 12-16 weeks to match the timescale of the *in vivo* study, appropriate dimensions for the bone defect animal model, mechanical strength due to the load-bearing nature of the defect, sufficient porosity to allow for cell infiltration, simple fabrication or accessibility from a vendor, biocompatible, and made of a material that could be easily differentiated from bone in a microCT scan was desirable. The Osteoplug™ 3D-printed polycaprolactone scaffold was selected because it met all of the above specifications, with the exception of degradation rate, which was much slower than desired: 18-24 months[35] as compared with the target 12-16 weeks. 3D-printed PCL scaffolds have been previously used in human patients and received FDA approval.[35]

5.3.2 LbL assembly of plasmid DNA coatings on scaffolds

The PBAE/DNA and PEI-PBAE/DNA film architectures were based off of previously developed formulations discussed in Chapter 3 and 4 of this thesis and were selected for their differential GFP plasmid transfection activity *in vitro*. The PEI-PBAE/DNA film formulation exhibited 2 to 5-fold increased transfection efficiency over PBAE/DNA films *in vitro* and was hypothesized to enable greater BMP-2 plasmid DNA delivery and bone growth *in vivo*. Polyelectrolyte concentrations and film thickness was modified to obtain total BMP-2 protein loading of 14 μg and DNA loadings of approximately 450 μg. The total loadings of (PBAE/pBMP2)50 and (PBAE/PAA)10(BPEI/pBMP2)40 coated scaffolds were 459 μg ± 42.4 μg and 427 μg ± 26.5 μg (mean ± SD) plasmid DNA per Osteoplug (**Figure 5.1A**). The DNA release kinetics from film-coated scaffolds are shown in **Figure 5.1B**. The PEI-PBAE/DNA film formulation released 100% of DNA content in 5 days in PBS while PBAE/DNA films released

100% of DNA in 10 days, consistent with results discussed in Chapter 4. Compared to the 12-week duration of this animal study, these release rates are relatively fast. Fast DNA release combined with the short half-life of foreign DNA *in vivo* and the transient nature of plasmid DNA therapy, BMP2 production and bone growth stimulated by pBMP2-delivering scaffolds was expected to occur during the first 3-4 weeks of the study. As such, potential differences in bone growth would most likely be observed during the first 3-4 weeks and become less apparent by the 12-week endpoint of our study.

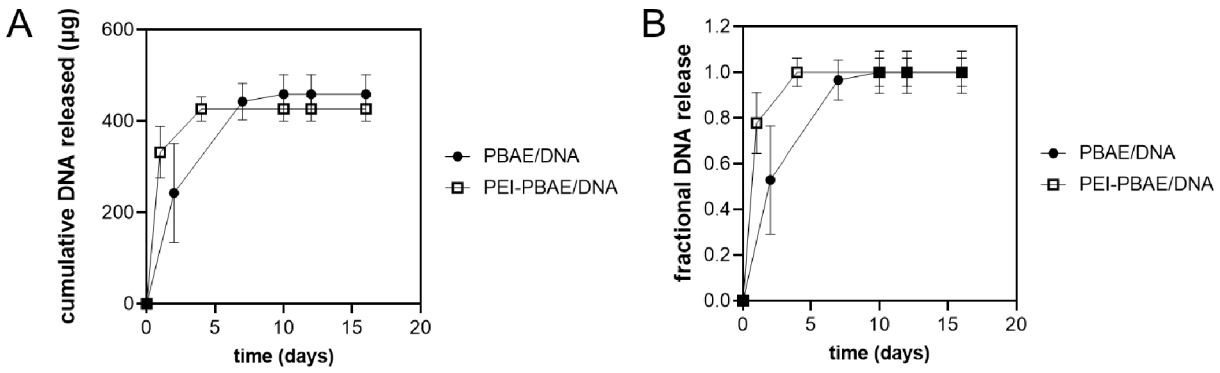

Figure 5.1 Cumulative and fractional BMP-2 plasmid DNA release kinetics from DNA film-coated PCL implants *(A) Cumulative DNA released in PBS at 37°C (B) DNA release profile normalized to total DNA content.*

5.3.3 CT analysis of bone growth in BMP-2 protein and DNA-treated groups at 6 weeks

In vivo CT scans at the study midpoint provided early measurements of bone regeneration and were used to supplement endpoint microCT quantification of bone volume. BMP-2 protein (n = 6), PBAE/DNA (n = 5), and PEI-PBAE/DNA-coated (n = 5) scaffolds were implanted in rabbit mandible defects with the surgeon (SY) blinded to the treatment group. In the BMP-2 protein group, full bridging of the defect with bone was observed in 4 of 6 animals (**Figure 5.2A**). None of the PBAE/pBMP2 scaffold-treated animals had fully bridged defects at 6 weeks, but bone deposits along the border of the defect can be seen in 3 of 6 animals (**Figure 5.2A**). The bone void actually appeared to grow in 1 of the 6 PBAE/pBMP2 treated animals. Of the PEI-PBAE/pBMP2 treated animals, 2 of 6 animals exhibited partial bridging of the defect

and the other 3 animals had disconnected bone deposits along the defect border. Quantification of bone volume from the CT scans indicated that BMP-2 protein treated animals had the greatest bone volume in the defect region of interest (ROI), followed by PEI-PBAE/DNA treated animals, and then PBAE/DNA treated animals (**Figure 5.2B**). Normalization of the bone volume measurements by total defect volume also showed the same trend, although the difference between BMP-2 protein treatment and PEI-PBAE/DNA treatment was not significant (**Figure 5.2B**). Bone mineral density (BMD, mg hydroxyapatite/cubic centimeter) was calculated by constructing a standard curve of CT scan mean grayscale intensity vs. known hydroxyapatite content of CT phantoms. The bone mineral densities of all three treatment groups were similar (**Figure 5.2C**). The variation among animals of the same group were quite large, especially in the PBAE/DNA treatment group. Because we did not have 6-week CT scan data for uncoated scaffold control animals, it is difficult to draw conclusions about enhancement of bone regeneration in treatment groups vs. control. However, a clear difference can be observed between BMP-2 protein, PEI-PBAE/pBMP2 and PBAE/pBMP2 scaffold treatment groups qualitatively in **Figure 5.2A** and quantitatively in **Figure 5.2B and C**. Greater bone volume and defect bridging occurred in the BMP-2 protein and PEI-PBAE/pBMP2 scaffold groups than in the PBAE/DNA group. BMP-2 protein is a strongly osteoinductive molecule that has been shown to maintain its bioactivity throughout LbL self-assembly.[36–41] These results indicate that 14.5 μg BMP-2 coated scaffolds could induce bone growth within the mandibular defects.

Bone repair activity of DNA-coated scaffolds relies on effective intracellular uptake of released plasmid DNA, nuclear localization, transcription, translation, and ultimately production of bioactive BMP-2.[42–45] With bone volume and bone mineral density as the primary quantitative output, this study did not allow detailed investigation of intermediate cellular uptake, DNA processing, and gene expression steps that determine efficacy of DNA delivery. Differences in bone volume and defect bridging between the PEI-PBAE/DNA and PBAE/DNA formulations

suggest that the two formulations may have different gene delivery efficacy, which is consistent with functional differences observed in Chapter 4.

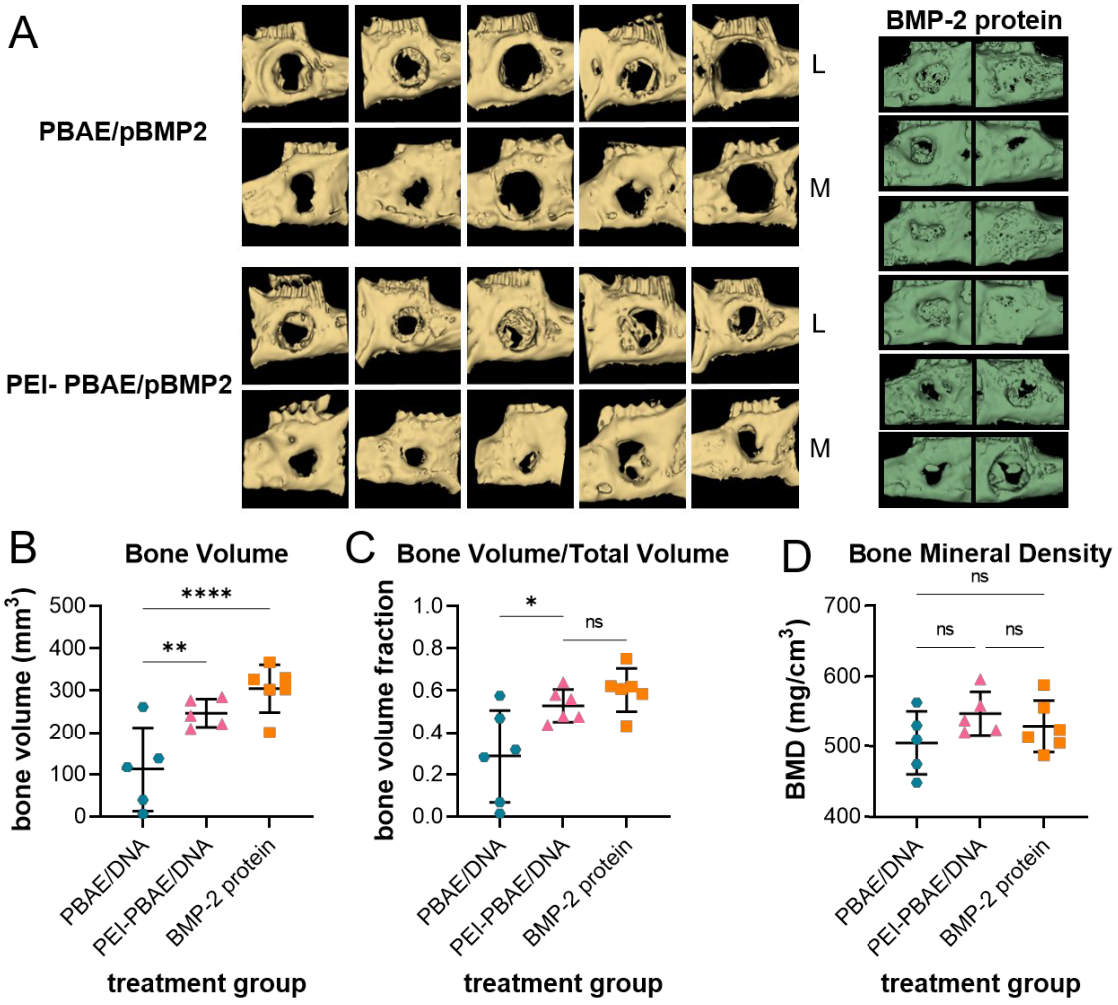

Figure 5.2 CT analysis of bone growth at 6 weeks for BMP-2 plasmid DNA and protein treatment groups *(A) Isosurfaces of CT scans generated in 3DSlicer, L = lateral, M = medial face of the mandible (B) Quantification of bone volume (C) Bone volume divided by total defect volume (D) Calculated bone mineral density. *p<0.05, **p<0.01, ****p<0.0001 by ANOVA with Tukey multiple comparisons test.*

5.3.4 microCT bone growth analysis of explanted mandibles at 12 weeks

In microCT analysis of the control groups, we found that empty defect rabbits with no scaffold implanted exhibited substantial bone growth (**Figure 5.3A**). Implantation of the uncoated PCL scaffold impaired bone growth compared to the empty defect control with significantly lower bone volume and BMD at 12 weeks (**Figure 5.3B, C**). This result was

unexpected given that the scaffold was intended to act as a colonization site for cells and support bone and tissue regeneration in the defect. BMP-2 protein-coated scaffolds slightly enhanced bone volume and BMD compared to blank scaffold, but not significantly. These observations suggested that the PCL scaffold interfered with bone growth in this setting.

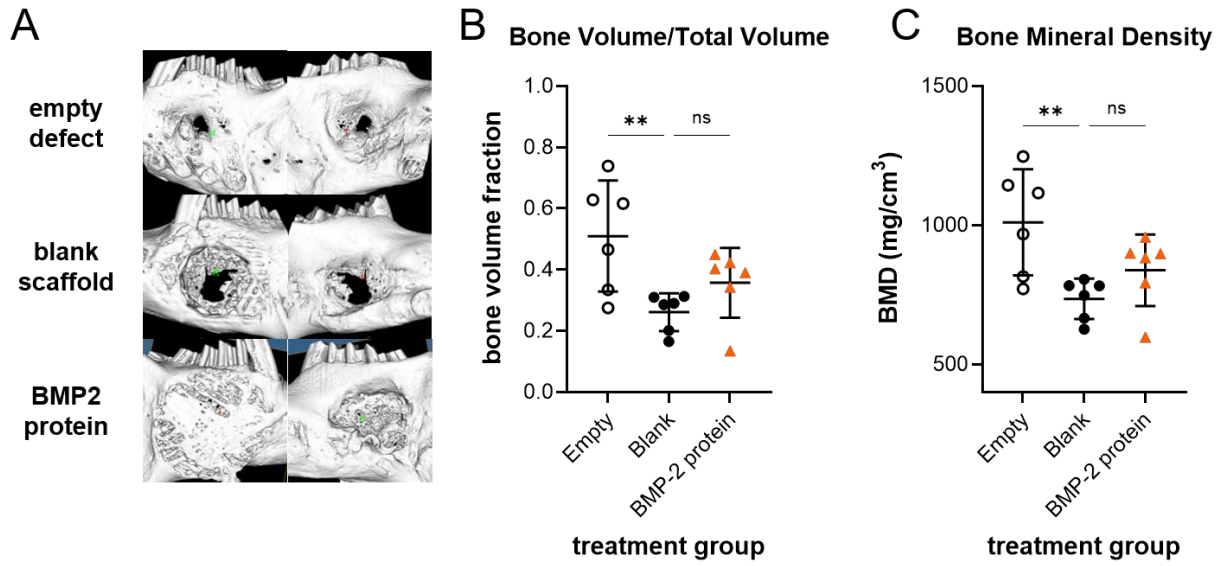

Figure 5.3 12-week microCT analysis of explants from control and BMP-2 protein treatment groups *(A) Isosurfaces of CT scans generated in MicroView (B) Bone volume divided by total defect volume (D) Calculated bone mineral density. *p<0.05, **p<0.01 by ANOVA with Tukey multiple comparisons test.*

To further explore this hypothesis, we compared cross-sectional microCT slices from rabbit mandibles containing empty defect, uncoated scaffold, and BMP-2 protein scaffold (**Figure 5.4**). Bone growth in the empty defect was observed throughout the defect volume with a continuous, close-packed appearance (**Figure 5.4A**). In contrast, bone growth in defects containing uncoated scaffold and BMP-2 protein scaffold was fragmented, occurring in small spicules of bone (**Figure 5.4B, C**). From the 3D reconstructions, the waffle pattern of the 3D-printed PCL scaffold is also apparent in Figure 5.4B and C. In scaffold-treated groups, bone formation occurred along the surface and around the struts of the scaffold. Comparison of bone growth patterns in the empty defect and scaffold-implanted defects indicate that the PCL scaffold may act as a void filler and impede bone formation throughout the defect volume.

Polycaprolactone (PCL) implants have relatively long degradation times, ranging from 5 months to 2 years, depending on the fabrication method.[35,46–48] Various approaches have been taken to expedite the degradation of PCL in bone regeneration scaffolds including modifying pore size, scaffold permeability, surface porosity, and creating composite materials. In general, histological observations of PCL scaffolds *in vivo* demonstrated that PCL remained in the implanted area for extended periods of time, often past the endpoint of the study, and bone growth occurred around the scaffold and through pores.[46,49] Future studies could utilize PCL composite scaffolds containing more rapidly degrading polymers (e.g. poly(lactic-co-glycolic acid)) to enable degradation rates complementary to the bone healing timeline or with increased porosity to promote bone mineral infiltration and degradation.

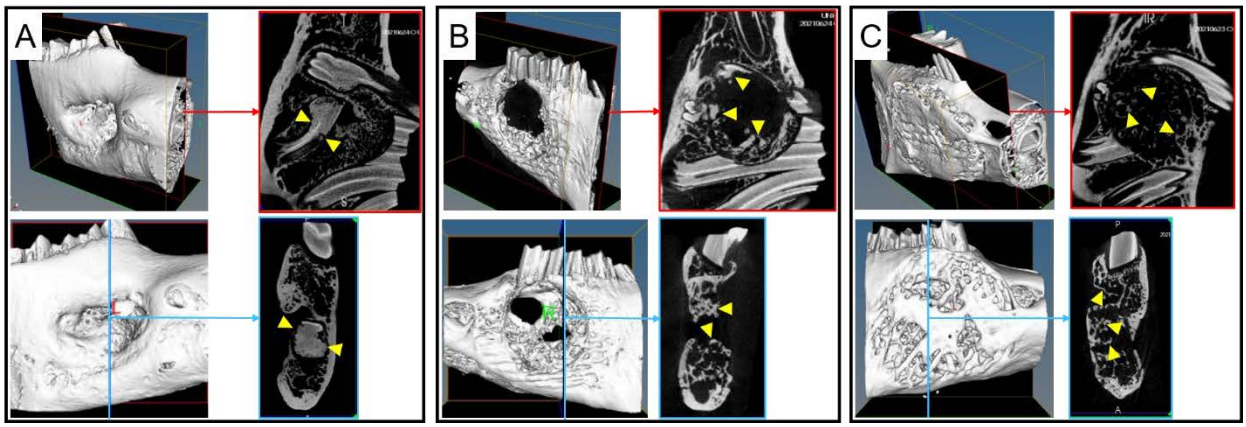

Figure 5.4 microCT cross-sections from control and BMP-2 protein treatment groups *Yellow triangles mark bone formations within the defect volume. Red arrow/box correspond to sagittal cross-section; blue arrow/box correspond to coronal cross-sectional view (A) Empty defect (B) uncoated (blank) scaffold (C) BMP-2 protein-coated scaffold.*

Qualitative examination of microCT reconstructions of DNA scaffold-treated mandibles after 12 weeks (**Figure 5.5A**) revealed similar trends in bone growth to 6-week *in vivo* CT scans (**Figure 5.2A**). Visually, little further bone growth occurred between 6 and 12 weeks. The BMP-2 protein formulation released over 1 week, while the PEI-PBAE/DNA and PBAE/DNA formulations released DNA over 5 days or 10 days, respectively. Given the transient effects of plasmid DNA transfection and the short-lived duration of BMP-2 protein release, bone growth

early in the 12-week study followed by little to no further bone deposition could be expected. This finding reinforces the value of sustained therapeutic delivery to continuously supplement bone and tissue regeneration. Combining a more rapidly degrading scaffold with sustained release of BMP-2 protein or plasmid DNA at higher instantaneous doses could enable more extensive bone growth than observed in this study.

We found that there was no significant difference in bone volume or bone volume fraction between PBAE/DNA and PEI-PBAE/DNA formulations and that these films did not induce additional bone regeneration compared to the blank scaffold control (**Figure 5.4 B, C**). BMP-2 protein coated scaffolds induced the most bone growth, with full bridging of the defect in 4 of 6 animals, but quantitative analysis of bone volume did not reveal a significant difference from blank scaffold treated defects. Due to different instrument resolutions and reconstruction methods for the 6-week *in vivo* CT and the 12-week *ex vivo* microCT results, bone volume fraction and BMD values cannot be compared directly between the two timepoints. As previously observed in **Figure 5.2** *in vivo* CT results, BMD was similar among the treatment groups (**Figure 5.5D**). Two of 5 PBAE/DNA scaffold treated animals had low bone volume and BMD and the defect volume appeared to increase in these animals. Histological analyses could reveal potential biological processes responsible for this unexpected result, such as inflammation or foreign body response.[50–52] Immunohistochemical staining for human BMP-2 protein may also reveal differences in BMP-2 expression around the defect site.

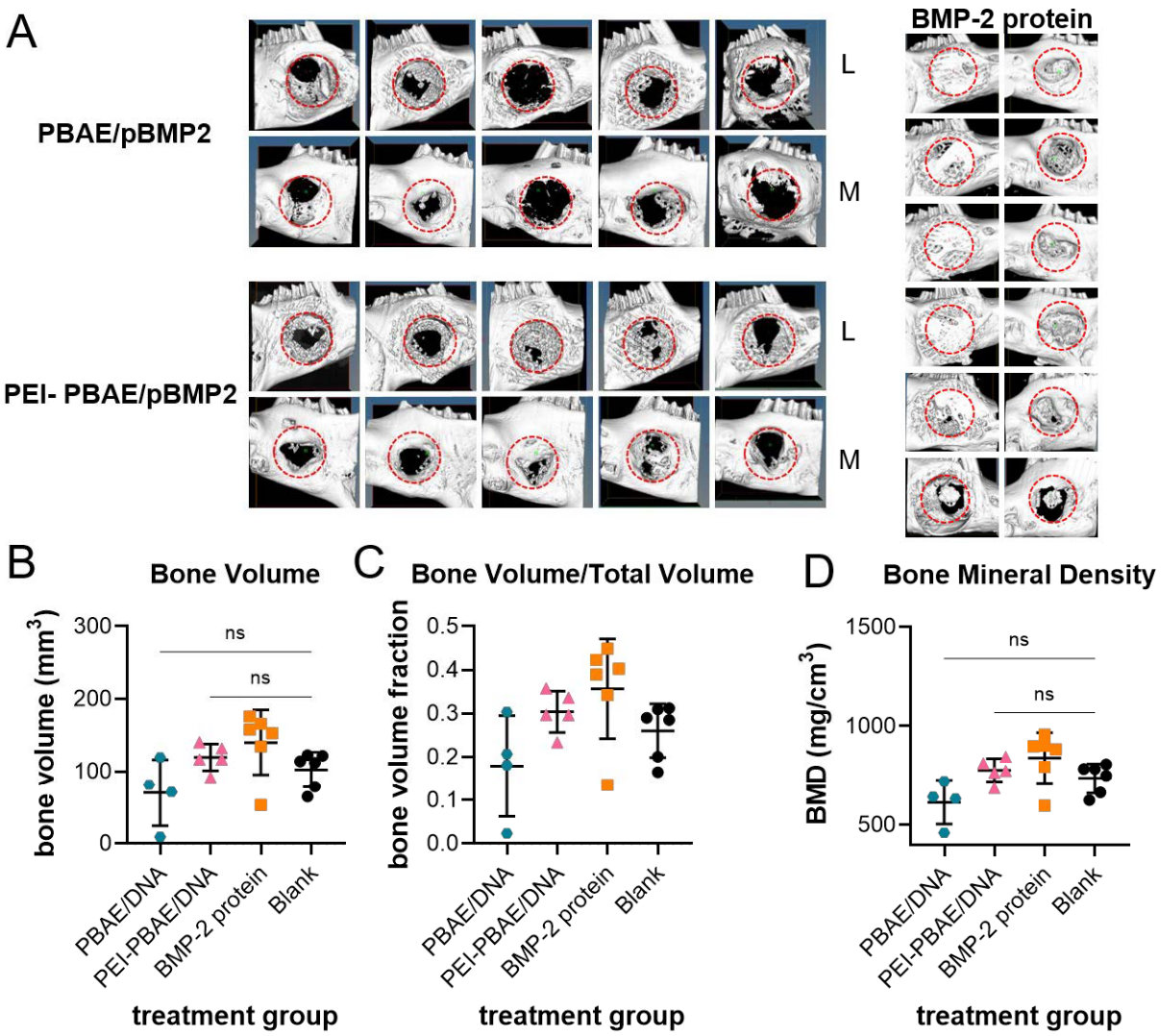

Figure 5.5 microCT analysis of explanted mandibles at 12 weeks *(A) Isosurfaces of CT scans generated in MicroView. Red circles indicate ROI used for quantification. L = lateral, M = medial face of the mandible (B) Quantification of bone volume (C) Bone volume divided by total defect volume (D) Calculated bone mineral density.*

5.4 Conclusions

In this study, we developed layer-by-layer films delivering osteogenic BMP-2 plasmid DNA. These films were coated on the surface of mechanically robust, 3D-printed PCL scaffolds, which were chosen to meet many of the criteria for our craniomaxillofacial bone defect application. Scaffolds coated with BMP-2 plasmid DNA-eluting formulations were implanted into load-bearing rabbit mandibular defects to investigate the effect of BMP-2 plasmid DNA delivery

in this injury model. We found that BMP-2 plasmid DNA coated scaffolds did not consistently affect bone formation at 6 or 12 weeks. We proposed that the underlying scaffold degraded too slowly for the timeline of this study, inhibiting bone regeneration at the experimental timepoints. The LbL assembled DNA films discussed here could be applied to a faster degrading or otherwise optimized scaffold for future investigation in a rabbit mandibular defect model. DNA nanolayered film design could also be modified to extend duration of DNA release and promote a greater extent of bone formation. *In vivo* tracking of plasmid DNA release kinetics and protein expression using plasmids encoding fluorescent or luminescent reporter proteins would provide valuable information about the how the *in vivo* environment affects DNA-eluting film behavior and kinetics of transfection. Finally, how the wound microenvironment impacts DNA release and cellular delivery from LbL-assembled scaffold coatings needs further study, for example, how the hematoma environment can affect DNA transport, what cell types and cell density occupy a healing bone defect and will mediate in situ expression of exogenously delivered nucleic acids.

5.5 References

(1) Lalloo, R.; Lucchesi, L. R.; Bisignano, C.; Castle, C. D.; Dingels, Z. V.; Fox, J. T.; Hamilton, E. B.; Liu, Z.; Roberts, N. L. S.; Sylte, D. O.; *et al.* Epidemiology of Facial Fractures: Incidence, Prevalence and Years Lived with Disability Estimates from the Global Burden of Disease 2017 Study. *Inj. Prev.* **2020**, *26*, 27–35.

(2) Zuk, P. A. Tissue Engineering Craniofacial Defects With Adult Stem Cells? Are We Ready Yet? *Pediatr. Res.* **2008**, *63*, 478–486.

(3) Gaihre, B.; Uswatta, S.; Jayasuriya, A. C. Reconstruction of Craniomaxillofacial Bone Defects Using Tissue-Engineering Strategies with Injectable and Non-Injectable Scaffolds. *J. Funct. Biomater.* **2017**, *8*, 1–19.

(4) Chenard, K. E.; Teven, C. M.; He, T.-C.; Reid, R. R. Bone Morphogenetic Proteins in Craniofacial Surgery: Current Techniques, Clinical Experiences, and the Future of Personalized Stem Cell Therapy. *J. Biomed. Biotechnol.* **2012**, *2012*, 1–14.

(5) Colazo, J. M.; Evans, B. C.; Farinas, A. F.; Al-Kassis, S.; Duvall, C. L.; Thayer, W. P. Applied Bioengineering in Tissue Reconstruction, Replacement, and Regeneration. *Tissue Engineering Part B*, 2019, *25*, 259–290.

(6) Baldwin, P.; Li, D. J.; Auston, D. A.; Mir, H. S.; Yoon, R. S.; Koval, K. J. Autograft, Allograft, and Bone Graft Substitutes: Clinical Evidence and Indications for Use in the Setting of Orthopaedic Trauma Surgery. *J. Orthop. Trauma* **2019**, *33*, 203–213.

(7) Szpalski, C.; Barr, J.; Wetterau, M.; Saadeh, P. B.; Warren, S. M. Cranial Bone Defects: Current and Future Strategies. *Neurosurg. Focus* **2010**, *29*, 1–11.

(8) Bonda, D. J.; Manjila, S.; Selman, W. R.; Dean, D. The Recent Revolution in the Design and Manufacture of Cranial Implants: Modern Advancements and Future Directions. *Neurosurgery* **2015**, *77*, 814–824.

(9) Gosain, A. K. Biomaterials for Reconstruction of the Cranial Vault. *Plast. Reconstr. Surg.* **2005**, *116*, 663–666.

(10) Dimitriou, R.; Jones, E.; McGonagle, D.; Giannoudis, P. V. Bone Regeneration: Current Concepts and Future Directions. *BMC Med.* **2011**, *9*, 1–10.

(11) Tollemar, V.; Collier, Z. J.; Mohammed, M. K.; Lee, M. J.; Ameer, G. A.; Reid, R. R. Stem Cells, Growth Factors and Scaffolds in Craniofacial Regenerative Medicine. *Genes Dis.* **2016**, *3*, 56–71.

(12) Bishop, G. B.; Einhorn, T. A. Current and Future Clinical Applications of Bone Morphogenetic Proteins in Orthopaedic Trauma Surgery. *Int. Orthop.* **2007**, *31*, 721.

(13) Benglis, D.; Wang, M. Y.; Levi, A. D. A Comprehensive Review of the Safety Profile of Bone Morphogenetic Protein in Spine Surgery. *Oper. Neurosurg.* **2008**, *62*, ONS423–ONS431.

(14) Hankenson, K. D.; Gagne, K.; Shaughnessy, M. Extracellular Signaling Molecules to Promote Fracture Healing and Bone Regeneration. *Adv. Drug Deliv. Rev.* **2015**, *94*, 3–12.

(15) Evans, C. H.; Palmer, G. D.; Pascher, A.; Porter, R.; Kwong, F. N.; Gouze, E.; Gouze, J.-N.; Liu, F.; Steinert, A.; Betz, O.; *et al.* Facilitated Endogenous Repair: Making Tissue Engineering Simple, Practical, and Economical. *Tissue Eng.* **2007**, *13*, 1987–1993.

(16) Walsh, G.; Jefferis, R. Post-Translational Modifications in the Context of Therapeutic Proteins. *Nat. Biotechnol.* **2006**, *24*, 1241–1252.

(17) Carragee, E. J.; Hurwitz, E. L.; Weiner, B. K. A Critical Review of Recombinant Human Bone Morphogenetic Protein-2 Trials in Spinal Surgery: Emerging Safety Concerns and Lessons Learned. *Spine J.* **2011**, *11*, 471–491.

(18) Evans, C. H. Gene Delivery to Bone. *Adv. Drug Deliv. Rev.* **2012**, *64*, 1331–1340.

(19) Ren, B.; Betz, V. M.; Thirion, C.; Salomon, M.; Jansson, V.; Müller, P. E.; Betz, O. B. Gene-activated Tissue Grafts for Sustained Bone Morphogenetic Protein-2 Delivery and Bone Engineering: Is Muscle with Fascia Superior to Muscle and Fat? *J. Tissue Eng. Regen. Med.* **2018**, *12*, 1002–1011.

(20) Khan, K. H. Gene Expression in Mammalian Cells and Its Applications. *Adv. Pharm. Bull.* **2013**, *3*, 257–263.
(21) Bez, M.; Sheyn, D.; Tawackoli, W.; Avalos, P.; Shapiro, G.; Giaconi, J. C.; Da, X.; David, S. Ben; Gavrity, J.; Awad, H. A.; *et al.* In Situ Bone Tissue Engineering via Ultrasound-Mediated Gene Delivery to Endogenous Progenitor Cells in Mini-Pigs. *Sci. Transl. Med.* **2017**, *9*, 1–9.
(22) Acri, T. M.; Laird, N. Z.; Jaidev, L. R.; Meyerholz, D. K.; Salem, A. K.; Shin, K. Nonviral Gene Delivery Embedded in Biomimetically Mineralized Matrices for Bone Tissue Engineering. *Tissue Eng. - Part A* **2021**, *27*, 1074–1083.
(23) Khorsand, B.; Nicholson, N.; Do, A. V.; Femino, J. E.; Martin, J. A.; Petersen, E.; Guetschow, B.; Fredericks, D. C.; Salem, A. K. Regeneration of Bone Using Nanoplex Delivery of FGF-2 and BMP-2 Genes in Diaphyseal Long Bone Radial Defects in a Diabetic Rabbit Model. *J. Control. Release* **2017**, *248*, 53–59.
(24) Raftery, R. M.; Mencía-Castaño, I.; Sperger, S.; Chen, G.; Cavanagh, B.; Feichtinger, G. A.; Redl, H.; Hacobian, A.; O'Brien, F. J. Delivery of the Improved BMP-2-Advanced Plasmid DNA within a Gene-Activated Scaffold Accelerates Mesenchymal Stem Cell Osteogenesis and Critical Size Defect Repair. *J. Control. Release* **2018**, *283*, 20–31.
(25) Kolk, A.; Boskov, M.; Haidari, S.; Tischer, T.; van Griensven, M.; Bissinger, O.; Plank, C. Comparative Analysis of Bone Regeneration Behavior Using Recombinant Human BMP-2 versus Plasmid DNA of BMP-2. *J. Biomed. Mater. Res. - Part A* **2019**, *107*, 163–173.
(26) Spicer, P. P.; Kretlow, J. D.; Young, S.; Jansen, J. A.; Kasper, F. K.; Mikos, A. G. Evaluation of Bone Regeneration Using the Rat Critical Size Calvarial Defect. *Nat. Protoc.* **2012**, *7*, 1918–1929.
(27) Young, S.; Bashoura, A. G.; Borden, T.; Baggett, L. S.; Jansen, J. A.; Wong, M.; Mikos, A. G. Development and Characterization of a Rabbit Alveolar Bone Nonhealing Defect Model. *J. Biomed. Mater. Res. - Part A* **2008**, *86*, 182–194.
(28) Shah, S. R.; Young, S.; Goldman, J. L.; Jansen, J. A.; Wong, M. E.; Mikos, A. G. A Composite Critical-Size Rabbit Mandibular Defect for Evaluation of Craniofacial Tissue Regeneration. *Nat. Protoc.* **2016**, *11*, 1989–2009.
(29) Hu, T.; Naidu, M.; Yang, Z.; Lam, W. M.; Kumarsing, R. A.; Ren, X.; Ng, F.; Wang, M.; Liu, L.; Tan, K. C.; *et al.* Bone Regeneration by Controlled Release of Bone Morphogenetic Protein-2: A Rabbit Spinal Fusion Chamber Molecular Study. *Tissue Eng. Part A* **2019**, *25*, 1356–1368.
(30) Ogier, J. LbL-Based Gene Delivery: Challenges and Promises. In *Layer-by-Layer Films for Biomedical Applications*; Wiley-VCH Verlag GmbH & Co. KGaA: Weinheim, Germany, 2015; pp. 195–206.
(31) Alkekhia, D.; Hammond, P. T.; Shukla, A. Layer-by-Layer Biomaterials for Drug Delivery. *Annu. Rev. Biomed. Eng.* **2020**, *22*, 1–24.
(32) Lynn, D. M.; Langer, R. Degradable Poly(β-Amino Esters): Synthesis, Characterization, and Self-Assembly with Plasmid DNA. *J. Am. Chem. Soc.* **2000**, *122*, 10761–10768.
(33) Chou, J. J.; Berger, A. G.; Jalili-Firoozinezhad, S.; Hammond, P. T. A Design Approach for Layer-by-Layer Surface-Mediated SiRNA Delivery. *Acta Biomater.* **2021**, *135*, 331–341.
(34) Howard, M. T. Layer-by-Layer Systems for Craniomaxillofacial Bone Repair, MIT, 2021.
(35) Teoh, S. H.; Goh, B. T.; Lim, J. Three-Dimensional Printed Polycaprolactone Scaffolds for Bone Regeneration Success and Future Perspective. *https://home.liebertpub.com/tea* **2019**, *25*, 931–935.
(36) Macdonald, M. L.; Samuel, R. E.; Shah, N. J.; Padera, R. F.; Beben, Y. M.; Hammond, P. T. Tissue Integration of Growth Factor-Eluting Layer-by-Layer Polyelectrolyte Multilayer Coated Implants. *Biomaterials* **2011**, *32*, 1446–1453.
(37) Patel, Z. S.; Young, S.; Tabata, Y.; Jansen, J. A.; Wong, M. E. K.; Mikos, A. G. Dual

Delivery of an Angiogenic and an Osteogenic Growth Factor for Bone Regeneration in a Critical Size Defect Model. *Bone* **2008**, *43*, 931–940.
(38) Shah, N. J.; Hyder, M. N.; Quadir, M. a; Dorval Courchesne, N.-M.; Seeherman, H. J.; Nevins, M.; Spector, M.; Hammond, P. T. Adaptive Growth Factor Delivery from a Polyelectrolyte Coating Promotes Synergistic Bone Tissue Repair and Reconstruction. *Proc. Natl. Acad. Sci. U. S. A.* **2014**, *111*, 12847–12852.
(39) Min, J.; Choi, K. Y.; Dreaden, E. C.; Padera, R. F.; Braatz, R. D.; Spector, M.; Hammond, P. T. Designer Dual Therapy Nanolayered Implant Coatings Eradicate Biofilms and Accelerate Bone Tissue Repair. *ACS Nano* **2016**, *10*, 4441–4450.
(40) Thorsson, V.; Gibbs, D. L.; Brown, S. D.; Wolf, D.; Bortone, D. S.; Ou Yang, T. H.; Porta-Pardo, E.; Gao, G. F.; Plaisier, C. L.; Eddy, J. A.; *et al.* The Immune Landscape of Cancer. *Immunity* **2018**, *48*, 812–830.
(41) Martin, J. R.; Howard, M. L. T.; Wang, S.; Berger, A. G.; Hammond, P. T. Oxidation-Responsive, Tunable Growth Factor Delivery from Polyelectrolyte-Coated Implants. *Adv. Healthc. Mater.* **2021**, *10*, 1–11.
(42) Raup, A.; Jérôme, V.; Freitag, R.; Synatschke, C. V.; Müller, A. H. E. Promoter, Transgene, and Cell Line Effects in the Transfection of Mammalian Cells Using PDMAEMA-Based Nano-Stars. *Biotechnol. Reports* **2016**, *11*, 53–61.
(43) Bozo, I. Y.; Deev, R. V.; Smirnov, I. V.; Fedotov, A. Y.; Popov, V. K.; Mironov, A. V.; Mironova, O. A.; Gerasimenko, A. Y.; Komlev, V. S. 3D Printed Gene-Activated Octacalcium Phosphate Implants for Large Bone Defects Engineering. *Int. J. Bioprinting* **2020**, *6*, 93–109.
(44) Durymanov, M.; Reineke, J. Non-Viral Delivery of Nucleic Acids: Insight into Mechanisms of Overcoming Intracellular Barriers. *Front. Pharmacol.* **2018**, *9*, 1–15.
(45) Wilber, A.; Frandsen, J. L.; Wangensteen, K. J.; Ekker, S. C.; Wang, X.; McIvor, R. S. Dynamic Gene Expression after Systemic Delivery of Plasmid DNA as Determined by in Vivo Bioluminescence Imaging. *Hum. Gene Ther.* **2005**, *16*, 1325–1332.
(46) Lam, C. X. F.; Hutmacher, D. W.; Schantz, J.-T.; Woodruff, M. A.; Teoh, S. H. Evaluation of Polycaprolactone Scaffold Degradation for 6 Months in Vitro and in Vivo. *J. Biomed. Mater. Res. Part A* **2009**, *90A*, 906–919.
(47) Byun, J. H.; Lee, H. A. R.; Kim, T. H.; Lee, J. H.; Oh, S. H. Effect of Porous Polycaprolactone Beads on Bone Regeneration: Preliminary in Vitro and in Vivo Studies. *Biomater. Res.* **2014**, *18*, 1–8.
(48) Dwivedi, R.; Kumar, S.; Pandey, R.; Mahajan, A.; Nandana, D.; Katti, D. S.; Mehrotra, D. Polycaprolactone as Biomaterial for Bone Scaffolds: Review of Literature. *J. Oral Biol. Craniofacial Res.* **2020**, *10*, 381–388.
(49) Sun, H.; Mei, L.; Song, C.; Cui, X.; Wang, P. The in Vivo Degradation, Absorption and Excretion of PCL-Based Implant. *Biomaterials* **2006**, *27*, 1735–1740.
(50) Shah, N. J.; Hyder, M. N.; Moskowitz, J. S.; Quadir, M. A.; Morton, S. W.; Seeherman, H. J.; Padera, R. F.; Spector, M.; Hammond, P. T. Surface-Mediated Bone Tissue Morphogenesis from Tunable Nanolayered Implant Coatings. *Sci. Transl. Med.* **2013**, *5*, 1–10.
(51) Veiseh, O.; Doloff, J. C.; Ma, M.; Vegas, A. J.; Tam, H. H.; Bader, A. R.; Li, J.; Langan, E.; Wyckoff, J.; Loo, W. S.; *et al.* Size- and Shape-Dependent Foreign Body Immune Response to Materials Implanted in Rodents and Non-Human Primates. *Nat. Mater.* **2015**, *14*, 643–651.
(52) Alhag, M.; Farrell, E.; Toner, M.; Claffey, N.; Lee, T. C.; O'Brien, F. Evaluation of Early Healing Events around Mesenchymal Stem Cell-Seeded Collagen-Glycosaminoglycan Scaffold. An Experimental Study in Wistar Rats. *Oral Maxillofac. Surg.* **2011**, *15*, 31–39.

Chapter 6. Conclusions and Future Directions

6.1 Thesis summary

Nucleic acid therapies, including DNA therapies in particular, are promising approaches to specifically and durably treat disease. This thesis presents the design and mechanistic investigation of layer-by-layer (LbL) thin films for controlled, localized delivery of plasmid DNA. We examined the impact of LbL solution conditions on DNA loading and release kinetics, elucidated potential mechanisms for DNA release and cellular uptake from polyelectrolyte multilayer films, and evaluated DNA-coated implants in a rabbit model of bone repair.

In Chapter 1, we reviewed recent preclinical and clinical progress in nucleic acid therapies. Barriers to non-viral gene delivery and nanotechnology approaches to bypass these obstacles were discussed. LbL self-assembly was introduced as a promising technique to enable controlled, localized DNA delivery.

In Chapter 2, polymer-DNA polyplexes were used as model systems to identify factors impacting polycation-mediated transfection. Polymer:DNA ratio was found to be a key determining factor for polyplex size, charge, and transfection efficiency, consistent with previous reported studies of polycation-mediated DNA delivery. The importance of free polycation chains for stabilizing polyplexes and for enhancing DNA delivery efficacy was discussed. Plasmid size and cell type were also found to impact DNA polyplex transfection efficiency. Shorter plasmids were more effectively delivered and expressed and greater transfection was achieved in rapidly dividing cells.

In Chapter 3, we investigated the impact of different LbL assembly parameters on robust DNA loading, release kinetics, and polymer/DNA composition in (PBAE/DNA) bilayer architecture films. We determined the effects of DNA concentration, assembly pH, ionic strength, and number of film bilayers on the composition and release behavior of DNA nanolayer films assembled on silicon chips. (PBAE/DNA) films degraded via surface erosion and the duration of DNA release could be tuned by varying the number of bilayers. We also

demonstrated that assembly conditions could be used to tune the polymer:DNA ratio in films, a key factor determining pre-formed polyplex DNA delivery efficacy.

In Chapter 4, we elucidated the composition of DNA multilayer films and their corresponding releasate and related these findings to LbL film-mediated DNA transfection efficacy. We found that (PBAE/DNA) films enabled low levels of transfection that were augmented by addition of an external transfection reagent. We introduced PEI into DNA film architectures to more stably complex DNA and demonstrated improved film-mediated transfection. Characterization of film releasate and imaging of cell-film interactions allowed formation of a potential mechanism describing initial cellular interactions with DNA multilayer films. Cellular uptake of film-associated DNA was proposed to proceed as follows: DNA films rearranged to present particles at the surface, which are recruited by filopodia to cell bodies for endocytosis and intracellular processing. Film design for rapid disassembly was demonstrated to promote release of polymer-DNA complexes, enabling high transfection efficiency.

In Chapter 5, we applied LbL-assembled DNA films in an *in vivo* efficacy study, evaluating bone formation in rabbit mandibular defects treated with BMP-2 pDNA-coated implants. Six-week and 12-week CT scans revealed that some animals from each treatment group exhibited enhanced bone growth, but differences in bone volume and bone mineral density were not statistically significant. We discussed scaffold selection and hypothesized that the slow-degrading PCL scaffold hindered bone formation within the defect. Histological analyses of mandibles implanted with DNA-coated scaffolds are underway to better understand the biological response to the implants.

6.2 Future directions

6.2.1 LbL incorporation of multiple DNAs for staggered release

In this thesis, we have demonstrated that the (PBAE/DNA) two-component architecture is a tunable and effective local DNA delivery system. The bilayer architecture could be further modulated to shorten or further extend duration of DNA release and to enable sequential

release of multiple DNAs by introducing diffusion barrier layers, which have been applied for staged protein and antibiotic delivery. Delivery of multiple therapeutic nucleic acids from LbL films would have broad applications in modulating tissue morphogenesis (e.g., bone and wound regeneration) which involve temporally-defined protein signaling cascades.

6.2.2 Kinetic studies of DNA film disassembly and cellular interaction with the film

In Chapter 4, we primarily examined cellular association with films and characterized film releasate at single timepoints. While our findings provide important clues about how DNA multilayer films mediate transfection, time course studies would provide valuable information about dynamics of film rearrangement, filopodial exploration of the cell microenvironment, and the process of film-released particle uptake by cells. Building films with fluorescently-labelled polyelectrolytes would allow real-time confocal imaging of films incubated with and without cells. SEM imaging of earlier and later timepoints in film release and cell treatment would also contribute to a more complete picture of LbL film-mediated DNA delivery.

6.2.3 Addressing tissue and cell targeting to minimize off-target effects

While nanoparticles can be modified with targeting ligands to direct trafficking to certain cell types, the random nature of DNA release from LbL films makes targeting more challenging. Antibodies, antibody fragments, or peptides could be conjugated to the polycation to help polymer-DNA complexes target desired cells. In addition, regulatory sequences in the nucleic acid can help direct gene expression only within target cells, specifically cell or tissue-specific promoters. Tissue targeting is critical, particularly in permanent gene editing applications, because off-target transfection could have deleterious or mutagenic effects.

6.2.4 In vitro and in vivo examination of biological responses to DNA multilayer films

In this thesis, the primary metric of DNA film function was transfection efficiency, defined as expression of the protein encoded by the plasmid DNA. The *in vitro* studies presented were primarily concerned with film release and cellular uptake of DNA, without detailed study of cytoplasmic trafficking, nuclear entry, polyplex unpacking, and transcription. These intermediate

steps between cellular uptake and protein expression represent additional obstacles to DNA delivery. The progression of film releasate through these steps may be tracked using fluorescently-labelled polycation and DNA. Overcoming cellular barriers to DNA delivery can be accomplished by incorporating designer polycations other than the basic PBAE and PEI applied in this work into LbL DNA films to enhance transfection activity.

Future studies should also investigate immune responses to DNA multilayer films, which can affect biocompatibility and safety of these delivery systems. Histological analysis of rabbit mandible samples is underway and tissues will be examined for inflammatory cell infiltration and the presence of a fibrous capsule that typically indicates foreign body response.[1,2] Immunogenic response to implanted materials may be evaluated *in vitro* focusing on immune cell viability, maturation, and activation.[3] Activation studies will allow broad profiling of inflammatory markers at the protein and RNA level to assess immune rejection or tolerance of biomaterials.[4] *In vitro* analysis of immune response will provide a wealth of biocompatibility and safety information about DNA multilayer films.

6.3 References

(1) Shah, N. J.; Hyder, M. N.; Moskowitz, J. S.; Quadir, M. A.; Morton, S. W.; Seeherman, H. J.; Padera, R. F.; Spector, M.; Hammond, P. T. Surface-Mediated Bone Tissue Morphogenesis from Tunable Nanolayered Implant Coatings. *Sci. Transl. Med.* **2013**, *5*, 1–10.

(2) Jhunjhunwala, S. Neutrophils at the Biological-Material Interface. *ACS Biomater. Sci. Eng.* **2018**, *4*, 1128–1136.

(3) Andorko, J. I.; Hess, K. L.; Pineault, K. G.; Jewell, C. M. Intrinsic Immunogenicity of Rapidly-Degradable Polymers Evolves during Degradation. *Acta Biomater.* **2016**, *32*, 24–34.

(4) Lock, A.; Cornish, J.; Musson, D. S. The Role of In Vitro Immune Response Assessment for Biomaterials. *J. Funct. Biomater.* **2019**, *10*, 1–15.